

Sensitivity and probabilistic slope stability analyses to understand sources of geotechnical
uncertainty in Open Pit Mining

by

Gustavo Adolfo Velarde Herencia

A thesis submitted in partial fulfillment of the requirements for the degree of

Master of Science

in

Geotechnical Engineering

Department of Civil and Environmental Engineering
University of Alberta

Abstract

The open pit mining industry is an essential sector around the globe, playing a crucial role in energy production and the development of renewable energy technologies. To this end, open pit mining is increasing efforts to implement best engineering practices to develop sustainable mining that aims to balance economic benefits with safety and environmental aspects. This balance is currently assessed through open pit slope design that seeks to implement reliable, cost-effective, and safe slopes that meet the needs of the operator and other stakeholders. Current practice of open pit slope design encompasses slope stability analyses and the adoption of Design Acceptance Criteria (DAC). The results of the slope stability analysis are compared against the selected DAC to decide whether the slope design can be implemented or if modifications are required to meet the selected DAC. Furthermore, this decision-making process is influenced by uncertainties, both epistemic and aleatoric, that can potentially lead to an increased risk for the operator.

Different sources of uncertainties associated with the design of open pit slopes have been identified and classified in geotechnical literature. In a reliability-oriented approach, these sources of uncertainties are formally managed by adopting sophisticated monitoring technologies, modelling techniques, and leveraging enhanced knowledge derived from experience in the open pit operation.

This approach outlines the reliability level in slope design to be leveraged or increased for future design phases. Consequently, reliability analyses are becoming increasingly important in slope designs, which also requires the adoption of design acceptance criteria that accurately reflect the reliability level. To this end, Reliability-Based Design Acceptance Criteria (RBDAC) were proposed by Macciotta et al. (2020). The 2020 RBDAC adopt the concepts of reliability and slope stability approaches to meet the economic risk appetite in slope design. However, the 2020 RBDAC need testing against different reliability levels to validate the assumptions behind these. This thesis aims to test assumptions behind the developed 2020 RBDAC and to demonstrate its practicability and flexibility through analyses conducted in an open mine sector under specific site conditions.

The thesis is structured as a paper-based thesis. An introductory chapter presents the knowledge gaps and objectives of the thesis. A succinct literature review is then presented to cover materials essential for understanding the work in the following chapters but avoiding repetition with the literature review in the subsequent paper-chapters. The research then followed with a parametric study to characterize the uncertainty of the rock mass strength properties and of the geological discontinuities under three scenarios with different reliability levels targeting the 2020 RBDAC. The research also focuses on uncertainty associated with modelling geological discontinuities for different reliability levels. The uncertainty of the rock mass strength properties was defined by Probability Density Functions (PDFs) while the uncertainty of the geological structures was defined through kinematic analysis. These were input parameters for performing probabilistic slope stability analyses using 2-dimensional Limit Equilibrium (LE) method and Monte Carlo technique. The results obtained from the three scenarios in terms of Factor of Safety (FoS), Probability of Failure (PoF), and the associated Coefficient of Variation (COV) of the resultant FoS (COV_{FoS}) match the ranges defined in the 2020 RBDAC. The flexibility of the 2020 RBDAC is also demonstrated with a slope design that compares a proposed pushback leveraging the information analyzed and compared with a design that targets the current DAC proposed by Read and Stacey (2009). The results show a decrease in mining additional volume while adopting a safe design.

The other aspect of the work was to investigate the impact of uncertainty associated with fracture normal stiffness. To this end, sensitivity analyses were performed using a continuum model and discontinuum model that test the epistemic uncertainty and its impact on the slope design. This impact is observed in the results of FoS or Strength Reduction Factor (SRF), suggesting that the fracture normal stiffness may act as possible trigger for progressive failure by decreasing the magnitude as a result of the inherent excavation process and low stress environment generated by the excavation process. The probabilistic and sensitivity analyses constitute powerful design tools for managing

uncertainties and implementing reliable slope designs. These tools can be leveraged in the slope design process along with the 2020 RBDAC.

Preface

A version of Chapter 3 from this thesis has been published in the journal of Geotechnical and Geological Engineering with the following citation:

Velarde, G. and Macciotta, R. (2024). Adopting Reliability-Based Design Acceptance Criteria in Probabilistic Open Pit Slope Analysis: A Parametric Study. Geotechnical and Geological Engineering 2024. <https://doi.org/10.1007/s10706-024-02749-w>

A version of Chapter 4 from this thesis is being prepared for submission to the Engineering Geology Journal with the following citation:

Velarde, G., Macciotta, R., and Martin, C.D. (2024). Effect of uncertainty in fracture normal stiffness on pit slope stability calculations. University of Alberta Geotechnical Centre [Unpublished].

Acknowledgement

I want to express my profound gratitude to my supervisor, Dr. Renato Macciotta, for having faith in me and providing invaluable support throughout my studies and research work at the University of Alberta. His wise guidance, advice, extensive knowledge, encouragement, and patience were indispensable in completing this thesis. I will always be indebted.

My gratitude is also extended to the Large Open Pit members, with special thanks to Ashley Creighton from Rio Tinto and Phil de Graaf from De Beers Group for their insightful and valuable technical comments. Their contribution added extra value to my research work, for which I will always be grateful.

I would like to extend my sincere gratitude to Dr. Derek Martin. His time spent in our discussions and for teaching and guiding me in key aspects covered in this research work are greatly appreciated. I am grateful to have met one of the leading figures in rock mechanics and geotechnical engineering and to have had the opportunity to learn from him. I am also thankful to all my professors and other faculty members at the department of Civil and Environmental Engineering who have contributed to my education and professional growth.

Special thanks for my beloved family: my mother Carmen, my father Pablo, my brother Rodrigo, and my relatives, for their love and constant support. Thanks for believing in me.

Finally, thank God for always giving me strength, perseverance, courage and helping me to accomplish my dreams.

Table of Contents

1.0	Introduction.....	1
1.1	Problem statement.....	4
1.2	Research objectives.....	5
1.3	Methodology.....	5
1.4	Outline of thesis.....	7
2.0	Literature review.....	8
2.1	Open pit slope design.....	8
2.2	Design acceptance criteria for inter-ramp and overall scale.....	8
2.3	Slope Stability methods.....	12
2.3.1	Limit Equilibrium (LE).....	12
2.3.2	Shear Strength Reduction (SSR).....	16
2.4	Uncertainty in geotechnical engineering.....	17
2.5	Deterministic analysis.....	20
2.6	Probabilistic analysis.....	21
2.6.1	First Order Second Moment (FOSM).....	22
2.6.2	Point estimate method.....	22
2.6.3	Monte Carlo.....	23
3.0	Adopting Reliability-Based Design Acceptance Criteria in Probabilistic open pit slope analysis: A parametric study.....	25
3.1	Introduction.....	26
3.2	Basis for the open pit configuration and geology.....	29
3.2.1	Location and Geologic Setting.....	29
3.3	Uncertainty in rock strength.....	32
3.4	Methodology.....	35
3.4.1	Uncertainty associated with structure.....	39
3.5	Results and discussion.....	42

3.5.1	First Scenario: limited information at pre-mining phase.	42
3.5.2	Second scenario: increased design reliability	52
3.5.3	Third scenario: Very high design reliability at mature phase of operations.....	60
3.6	Reliability-Based DAC	67
3.7	Use of the RBDAC for Design.....	69
3.8	Conclusions	74
4.0	Effect of uncertainty in fracture normal stiffness on pit slope stability calculations.....	76
4.1	Introduction	76
4.2	Fracture Normal Stiffness	78
4.3	Methodology	85
4.3.1	Open Pit Slope configurations and material parameters	85
4.3.2	Continuum model setup with RS2: Case one.....	90
4.3.3	Discontinuum model setup with Slope Model: Case one	92
4.3.4	Discontinuum model setup with Slope Model: Case two	94
4.4	Results and discussion.....	95
4.4.1	Displacement and stresses.....	95
4.4.2	The effect of normal stiffness on Strength Reduction Factor (SRF).....	105
4.5	Conclusions	115
5.0	General conclusions and future research work	116
5.1	Conclusion.....	116
5.2	Recommended Future Research Work	117
6.0	References.....	119

List of Tables

Table 2-1: Summarized FoS and PoF values adopted in different acceptability criteria in existent literature for Inter-ramp and Overall Slopes	10
Table 3-1: Coefficient of Variation of intact rock parameters from a subset of previous studies	33
Table 3-2: Summary of Hoek-Brown parameters and Mohr-Coulomb parameters for the rock mass assumed in scenario 1	46
Table 3-3: Orientation of principal large-scale structures, scenario 1	49
Table 3-4: Summary of Hoek-Brown parameters and Mohr-Coulomb parameters assumed in scenario 2	54
Table 3-5: Orientation of principal large-scale structures, scenario 2.	57
Table 3-6: Calibrated rock mass strength properties assumed in scenario 3, from Valdivia and Lorig (2000).....	61
Table 3-7: Orientation of principal large-scale structures, scenario 3	62
Table 3-8: Summary of FoS-PoF pairs and COV_{FoS} obtained from three scenarios evaluated	68
Table 3-9: Summary of the limit equilibrium analysis for the design proposed for the next pushback	72
Table 4-1: Summary of fracture normal stiffness from a subset of previous studies.....	83
Table 4-2: Rock mass parameters adopted in the sensitivity analysis for Case 1	86
Table 4-3: Pairs of fracture normal-shear stiffness evaluated.....	87
Table 4-4: Intact rock parameters adopted in the sensitivity analysis for Case 2	89
Table 4-5: Results of calculated Strength Reduction Factor (SRF) for variations of fracture normal stiffness. Continuum model results in RS2	107

List of Figures

Figure 1-1: 2020 RBDAC matrix in terms of a) FoS and b) PoF for different levels of design reliability and economic consequence category. FoS values follow established relationships between FoS-PoF, following Lognormal distribution and Normal distribution indicated in parentheses. (adapted from Macciotta et al., 2000).....	4
Figure 2-1: Generalized open pit slope configuration and terminology	8
Figure 2-2: Slope failure mechanisms (adapted from Martin and Stacey 2018)	14
Figure 2-3: Large scale pit slope failure involving different failure mechanism (Hoek et al., 2000)	15
Figure 2-4: Definition directional strength that considers a) definition of shear strength according to the orientations of discontinuities, and subsequent b) slope stability analysis (adapted from Read and Stacey 2009)	16
Figure 3-1: Region where the base case study inspiring the model in this work is located	29
Figure 3-2: a) Geological map of the base case used to inform this study (after Padilla et al. 2001) and b) a typical cross section (A-A') looking north.....	31
Figure 3-3: Workflow adopted for the probabilistic analyses to test the reliability-based DAC	36
Figure 3-4: Information used for the three scenarios to account for aleatoric and epistemic uncertainty	41
Figure 3-5: Relationship between UCS and m_i for the five porphyry copper deposits in the region	43
Figure 3-6: Process for the development of PDFs of dependent parameters (UCS and m_i). The flow illustrates how 2 sets of correlated Normal distributions are built and then scaled to the parameter distributions.....	44
Figure 3-7: Calculated equivalent Mohr-Coulomb parameters and goodness of fit assumed in scenario 1: a) PDFs for cohesion, b) PDFs for friction angle, c) the Q-Q plot for Cohesion, d) the Q-Q plot for Friction angle	46
Figure 3-8: Limit equilibrium analysis result for rock mass strength failure, scenario 1	47

Figure 3-9: a) Calculated distribution of FoS for scenario 1 considering failure through the rock mass. b) The Q-Q plot of the Lognormal distribution fit	48
Figure 3-10: Scenario 1: a) Main structural orientation of large-scale structures. b) Structural orientation of Planar/Wedge-type structures. OSA is the overall slope angle and orientation	50
Figure 3-11: Limit equilibrium analysis result for structurally controlled failure, scenario 1	51
Figure 3-12: a) Calculated distribution of FoS for scenario 1 considering structurally controlled failure. b) The Q-Q plot of the distribution fitted.....	52
Figure 3-13: PDFs of equivalent Mohr-Coulomb parameters for granodiorite unit assumed in scenario 2: a) Cohesion and b) Friction angle. The Q-Q plots for: c) cohesion and d) friction angle	53
Figure 3-14: PDFs of equivalent Mohr-Coulomb parameters for andesite unit assumed in scenario 2: a) cohesion and b) friction angle. The Q-Q plots: c) cohesion and d) friction angle	54
Figure 3-15: Limit equilibrium analysis result for rock mass strength failure, scenario 2	55
Figure 3-16: Calculated distribution of FoS for scenario 2 considering rock mass strength failure for: a) Overall slope, b) Lower Inter-ramp slope, and c) Upper Inter-ramp slope. The Q-Q plot of the distribution fitted for each Monte Carlo simulation: d) Overall slope, e) Lower Inter-ramp slope, and f) Upper Inter-ramp slope.....	56
Figure 3-17: Scenario 2: a) Main structural orientation of large-scale structures and b) Structural orientation of Planar/Wedge-type structures.....	58
Figure 3-18: Limit equilibrium analysis results for structurally controlled failure, scenario 2	59
Figure 3-19: a) Calculated distribution of FoS distribution for scenario 2 considering structurally controlled failure for a) Overall slope, b) lower Inter-ramp slope, c) upper Inter-ramp slope. The Q-Q plot of the distribution fitted for each PDF d) Overall slope, e) lower Inter-ramp slope, f) upper Inter-ramp slope	60
Figure 3-20: Scenario 3: a) Main structural orientation of large-scale structures and b) structural orientation of Planar/Wedge-type structures	63

Figure 3-21: Limit equilibrium results of back analysis considering large-scale structures implicitly, scenario 3.....	64
Figure 3-22: a) Calculated distribution of FoS for scenario 3 considering large-scale structures implicitly. b) The Q-Q plot of the distribution fitted.....	65
Figure 3-23: Limit equilibrium results of back analysis considering large-scale structures explicitly, scenario 3.....	66
Figure 3-24: a) Calculated distribution of FoS for scenario 3 considering large-scale structures explicitly. b) The Q-Q plot of the distribution fitted.....	66
Figure 3-25: a) PDFs for overall scale of rock mass strength failure. b) PDFs for Overall slope of structurally controlled failure.....	67
Figure 3-26: Plot of $COV_{FoS-FoS/PoF}$ results in the 2020 RBDAC (modified from Macciotta et al. 2020)	69
Figure 3-27: Limit equilibrium analysis results for the next pushback targeting the 2020 RBDAC	71
Figure 3-28: Limit equilibrium analysis results for the next pushback targeting the 2009 DAC	73
Figure 3-29: Slope design configurations for the next pushback targeting both the 2020 RBDAC and the 2009 DAC	74
Figure 4-1: Distribution of types of rock faults and schematic cross-section through shear zones at different depths of crust (Passchier and Trouw, 2005).....	80
Figure 4-2: Stress-displacement characteristic of discontinuities under both a) normal loading and precompressed conditions (modified from Hungr and Coates 1983); and under b) repeated loading cycles (modified from Bandis et al. 1983).....	82
Figure 4-3: Dimensions of the open pit slope analyzed for Case 1	86
Figure 4-4: Dimensions of the open pit slope analyzed for Case 2	88
Figure 4-5: Stereographic projection of structural data considered for the Case 2.....	89
Figure 4-6: RS2 finite element model used for the sensitivity analysis.....	91

Figure 4-7: Location of history points and horizontal extensometer	92
Figure 4-8: Representation of the lattice formulation as a) an assembly of nodes connected by springs and b) stiffness components of each spring. (Macciotta and Martin 2016)	93
Figure 4-9: Model setup in Slope model for Case 1	94
Figure 4-10: Model setup in Slope model for Case 2	95
Figure 4-11: Horizontal displacements	96
Figure 4-12: Vertical displacement	97
Figure 4-13: Minimum principal stress changes through the excavation sequence for: a) History Point A, b) History Point B, and c) History Point C	98
Figure 4-14: Displacement recorded by the three history points in the a) horizontal direction and b) vertical direction	99
Figure 4-15: Horizontal displacement contours for different fracture normal stiffness values. Case one	100
Figure 4-16: Vertical displacement contours for different fracture normal stiffness values. Case one	101
Figure 4-17: Displacement recorded by the three history points in the a) horizontal direction and b) vertical direction adopting a normal stiffness of 1000 MPa/m	102
Figure 4-18: Displacement recorded by the three history points in the a) horizontal direction and b) vertical direction adopting a normal stiffness of 500 MPa/m	102
Figure 4-19: Displacement recorded by the three history points in the a) horizontal direction and b) vertical direction adopting a normal stiffness of 100 MPa/m	103
Figure 4-20: Horizontal displacement contours for different fracture normal stiffness values. Case two	104
Figure 4-21: Vertical displacement contours for different fracture normal stiffness values. Case two	105

Figure 4-22: Calculated Strength Reduction Factor at different discontinuity normal stiffness values.	
Continuum model results in RS2	106
Figure 4-23: Variation of calculated SRF with fracture normal stiffness	108
Figure 4-24: Variation of SRF with the ratio between fracture shear to normal stiffness	108
Figure 4-25: Contours of Factor of Safety for the different models analyzed at different fracture normal stiffness. Discontinuum model for Case one.....	110
Figure 4-26: Rock breakage generated through the course of excavation sequence. Discontinuum model for Case one	112
Figure 4-27: SRF results using RS2 and Slope Model at different fracture normal stiffness.....	113
Figure 4-28: Contours of Factor of Safety for the different models analyzed at different fracture normal stiffness. Discontinuum model for Case two	114
Figure 4-29: Rock breakage generated through the course of excavation sequence. Discontinuum model for Case two	114

List of Abbreviations

ASTM	American Society for Testing and Materials
COV	Coefficient of Variation
COV _{FoS}	Coefficient of Variation of FoS
COV _{mi}	Coefficient of Variation of m_i
COV _{UCS}	Coefficient of Variation of UCS
D	Disturbance factor
DAC	Design Acceptance Criteria
DFN	Discrete Fracture Network
FE	Finite Element
FJM	Flat Joint Model
FoS	Factor of Safety
FOSM	First Order Second Moment
GSI	Geological Strength Index
ISA	Inter-ramp Slope Angle
ISRM	International Society of Rock Mechanics
LE	Limit Equilibrium
LOP	Large Open Pit
NPV	Net Present Value
OMS	Ordinary Method of Slices
OSA	Overall Slope Angle
PDF	Probability Density Function
PoF	Probability of Failure
Q-Q	Quantile-Quantile
RBDAC	Reliability Based Design Acceptance Criteria
RMR	Rock Mass Rating
SJM	Smooth Joint Model
SRF	Strength Reduction Factor
SSR	Shear Strength Reduction
TARP	Trigger Action Response Plan

UCS	Uniaxial Compressive Strength
UDEC	Universal Distinct Element Code
VMS	Volcanic Massive Sulphides

List of symbols

a	Hoek-Brown material constant for rock mass
β	Slope angle
c	Cohesion
E_i	Elastic modulus of intact rock
E_{rm}	Elastic modulus of rock mass
H	Height of slope
k_n	Fracture normal stiffness
k_s	Fracture shear stiffness
m_b	Hoek-Brown material constant for rock mass
m_i	Hoek-Brown parameter for intact rock
s	Hoek-Brown material constant for rock mass
μ	Mean
γ	Unit weight
φ	Friction angle
δ_{ij}	Pearson correlation coefficient
σ_1	Major Principal stress
σ_3	Minor Principal stress
σ_{ci}	Uniaxial compressive strength of intact rock

1.0 Introduction

The open pit mining industry, essential to the transition towards renewable energy technologies, is increasingly adopting best engineering practices to develop sustainable mining. A key element in the engineering practice of open pit mining is the slope design process, which aims to achieve an optimum configuration that is both economically viable and safe (Hoek and Bray, 1981). Generally, the optimal balance between economics and safety is achieved by minimizing the volume excavation for a given likelihood of slope failure, while ensuring safety through sound procedures such as robust monitoring programs and TARPs (Trigger Action Response Plans). An imbalance due to an increased likelihood of failure can lead to operational delays and ore dilution, therefore reducing the profitability of the mine through the Net Present Value (NPV) or cash flow. For these reasons, achieving such an optimal balance in open pit slope design has been the focus of significant research efforts over the years.

One of the key components in the formulation of open pit slope design (Read and Stacey, 2009) is the slope stability analysis at every scale, from bench to the overall slope. This analysis is further required for risk and cost-benefit assessments. As part of the open pit slope design framework, the slope stability analysis needs to meet slope design criteria that satisfy the economic needs of the operation. The fundamental approach of slope stability analysis is to calculate a safety index for a given slope that can be expressed either as the Factor of Safety (FoS) or the Strength Reduction Factor (SRF). The FoS/SRF is defined as the ratio of the geotechnical capacity and the external demand imposed (Wesseloo and Read, 2009). This approach is routinely performed and updated based on the level of engineering efforts achieved through various stages (e.g., Pre-feasibility, Feasibility) of the development of the open pit mine. On the other hand, Performance-based Design (e.g. Martin and Stacey, 2018; Macciotta et al., 2020, Kafash et al., 2022) is an approach that is becoming popular in current geotechnical practice. With increasing adoption of advanced numerical modelling to assess the stress-strain behaviour of slopes, along with ongoing observation and monitoring of slope performance (e.g., displacement monitoring, reconciliation programs, pore pressure drawdowns), Performance-based

design aims to predict the performance of the geotechnical structures based on incorporating numerical modelling predictions to match observed performance (Kafash et al., 2022). This can lead to more robust, reliable, and more economic slope designs, thereby enhancing the decision-making process.

Another component added to the formulation of open pit slope design is the definition of the intended level of performance established according to the tolerable economic risk. The adoption of tolerable levels varies based on the potential consequences of the slope which is outlined by the Design Acceptance Criteria (DAC). Traditionally, the level of slope performance is supported by the slope stability assessments under both deterministic and probabilistic approach. As such, the DAC define allowable or minimum FoS and maximum Probability of Failure (PoF) for different tolerable risk levels. DAC considering different consequence levels, and therefore different target FoS and PoF have been published by various authors (e.g. Hoek and Bray, 1981; Priest and Brown, 1983; Swan and Sepulveda, 2000). Their extensive work and contribution of practitioners experience worldwide resulted in a comprehensive and generalized DAC developed by the Large Open Pit project in 2009. The 2009 DAC provide minimum acceptable FoS and maximum PoF for a given level of consequence and slope scale (Bench, Inter-ramp, Overall) to be used in a comparative basis. Current practice encompasses carrying out slope stability analysis and comparison of the calculated FoS-PoF against the 2009 DAC. Thus, depending on whether the slope stability results meet the selected DAC, the slope design is either implemented or modified until the selected DAC is achieved.

The slope design formulation is not straightforward as it is subjected to significant sources of uncertainties. These can potentially create an imbalance in the economic and operational viability (Read and Stacey, 2009). Understanding, identifying, incorporating, and reporting uncertainties is essential to define both current reliability level and target reliability levels in open pit slope design. In light of uncertainty, the role of the FoS in slope design has played a crucial role and emphasised widely in geotechnical literature (e.g., Abramson et al., 2002; El-Ramly, 2001; Martin and Stacey, 2018). The FoS serves to balance the uncertainty in geotechnical knowledge with the potential consequences of a slope

failure. Although, uncertainty can be addressed through stochastic methods such as sensitivity analysis or probabilistic analysis deriving to a PoF. Consequently, the acceptability of a specific slope design is determined by the evaluation of the FoS in conjunction with the PoF.

It has been identified that the 2009 DAC, expressed in terms of pairs of FoS-PoF, do not adequately reflect aspects such as the reliability level and economic consequence level. Hence, they do not represent consistent levels of risk (Adams, 2015; Macciotta et al., 2020). These can lead to overly conservative criteria and may prevent the evaluation of opportunities for adopting flexible slope design with higher economic outcomes. To this end, Macciotta et al. (2020) identified that open pit slope design has been evolving in different ways. These include a better understanding of uncertainties within a performance-based risk-informed approach, increased capacity of well-implemented slope instability management plans, the adoption of flexible designs that balance design confidence and risk tolerance, and the use more sophisticated tools for designing and monitoring slope performance. These considerations have led to the need to adopt flexible DAC that consider the reliability levels of the slope design and reflect tolerable risk, performance requirements, and the level of consequences. An example of reliability-based approach to DAC was described by Gaida et al. (2021). They developed an in-house DAC based on level of design reliability and level of consequences. Adopting these in-house DAC, they identified an opportunity to optimize a slope design sector by choosing less conservative DAC than those described in the 2009 guidelines. The results outlined the risk-reward benefit obtained by steepening the slope, allowing to maximize the profitability of the mine. This outcome highlights the importance of reliability-based risk-informed DAC.

In this regard, Macciotta et al. (2020) proposed Reliability-based DAC (RBDAC) that include a double entry matrix in terms of FoS-PoF defined for different reliability levels and economic consequence categories, see Figure 1-1. The 2020 RBDAC aim to address limitations of previous DAC, and its formulation is based on a robust mathematical approach to define FoS-PoF pairs, previous adopted criteria, levels of confidence, and levels of consequences focused on economic risks.

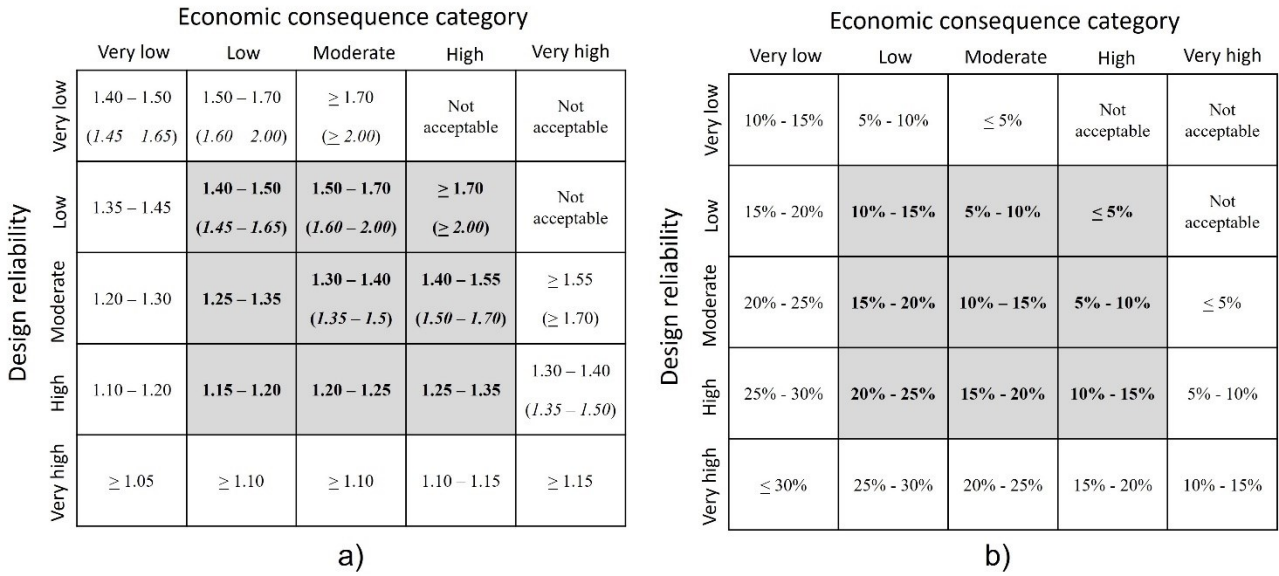


Figure 1-1: 2020 RBDAC matrix in terms of **a) FoS** and **b) PoF** for different levels of design reliability and economic consequence category. FoS values follow established relationships between FoS-PoF, following Lognormal distribution and Normal distribution indicated in parentheses. (adapted from Macciotta et al., 2020 with permission)

1.1 Problem statement

Due to the steady increase in size, depth, mining rates of open pit mines (Sharon and Eberhardt, 2020) and in view of depletion of current ore bodies (Creighton et al., 2022), the mining industry requires adoption of more flexible and strategic mine plans that takes advantage of the greater improvement of the slope design process. Adopting the 2020 RBDAC can result in a more profitable and sustainable business by achieving reliable and safe open pit slope designs. In this regard, industry adoption requires testing of the hypothesis behind the development of the defined FoS-PoF pairs in the 2020 RBDAC matrix for the different levels of design reliability and economic consequences, as well as testing the applicability of the 2020 RBDAC to provide opportunities for slope design optimization. Furthermore, this requires understanding of the impact of different sources of uncertainties on the calculated FoS and PoF values.

This will lead to explore potential benefits to optimize slope designs or to manage instabilities in a more robust way by developing consistent mitigative plans without impacting the economic business.

1.2 Research objectives

The general objective of this research is to conduct a stochastic analysis, including both probabilistic and sensitivity analyses. The aim is to test the assumption of COV_{FoS} behind the 2020 RBDAC for the different reliability levels, the PDF of resulting FoS, and the practicability of its use. These analyses will consider the primary sources of geotechnical uncertainties related to open pit slope design. This includes evaluating the influence of uncertainties associated with selection of fracture normal stiffness in slope modelling, which is recognized as one of the more uncertain input parameters in this context. The specific objectives of the research are to:

1. Review and synthesize existing literature on geotechnical parameter uncertainty for different rock types and for different levels of design reliability associated with different levels of engineering effort in investigation, characterization, and testing. This review will serve as input for the abroad adoption of the 2020 RBDAC.
2. Perform probabilistic slope stability analyses to test the FoS-PoF pairs under different scenarios of reliability level. The outcomes will validate or lead to modification to the 2020 RBDAC matrix.
3. Illustrate the practical applicability and versatility of the 2020 RBDAC by proposing an open pit slope design.
4. Conduct sensitivity analysis to evaluate the influence of fracture normal stiffness on the calculated stability of open pit slope design. The objective is to understand the impact of this specific source of uncertainty and to provide guidance on the models adopted for evaluation against the 2020 RBDAC.

1.3 Methodology

The methodology adopted to meet the research objectives is described as follows:

- Characterize uncertainty of the geomechanical parameters of particular rock mass units that are distributed in an open pit mine sector. This characterization is based on literature review of values adopted in similar lithology and site-specific data. Selected information encompasses statistical moments of material parameter values such as mean, standard deviation, and coefficient of variation (COV) to measure dispersion and to further quantify parameter uncertainty. These data are used as input parameters for slope stability analyses, following a defined Probability Density Functions (PDFs) to establish reliability level. Additionally, variability of the geological structural information was assessed through stereographic projections, which can be included in stochastic analysis, to gain insight into the effect of epistemic uncertainty associated with structure geometry.
- Conduct stochastic stability analyses using the 2-dimensional Limit Equilibrium (LE) Method and a probabilistic approach based on the information obtained. The probabilistic slope stability analysis aims to track the design reliability in terms of the COV of the resulting FoS and the associated PDF of the propagation of uncertainty through the FoS. The analysis is carried out under two approaches: isotropic analysis and anisotropic approach. The former assumes a homogeneous rock mass strength while the latter assumes heterogeneous rock mass strength governed by strength of the rock mass and the structural component. These considerations accounts for structural controlled failures which are commonly observed in open pit slopes. The outcomes of the analyses are then evaluated against the 2020 RBDAC to assess compatibility.
- Develop a pit slope geometry design utilizing the material parameters for the highest design reliability category. Two slope stability analysis are performed, assuming a same level of consequence to target both the 2009 DAC and the 2020 RBDAC. The two designs aim to be consistent with current industry practices. A comparison between two slope designs is then performed in terms of volume excavation, the achieved overall slope angle, and the integration into mine plans.

- A compilation of deformability parameters, specifically the normal stiffness of fractures (e.g. joints, faults) encountered in rock mass, is summarized from a literature review. The uncertainty of this parameter, which is a stress-dependant parameter, cannot be assessed by traditional methods such as the LE method. Therefore, a stress-strain analysis is adopted to formally address this stress-dependant parameter. Typical open pit configurations with specific fracture network are analyzed using a continuum model and discontinuum model, in conjunction with sensitivity analysis. The results aim to provide insight into the reduction of epistemic uncertainty, leading to achieve greater reliability in the slope design process.

A more detailed explanation of the methodology is included in the next chapters.

1.4 Outline of thesis

This thesis is structured into five main chapters. Chapter 1 provides an introduction, problem statement, research objectives, methodology, and the outline of the thesis. Chapter 2 introduces a literature review of open pit slope stability assessments, uncertainties in geotechnical engineering, and design acceptance criteria. Chapter 3 presents the methodology developed for characterizing parameters associated with geomechanical uncertainty and illustrates how these input parameters serve as inputs for conducting probabilistic slope stability analysis. The chapter evaluates three scenarios at distinct reliability levels to test the assumptions behind the 2020 RBDAC and to evaluate potential gains associated with its adoption. Chapter 4 presents the results of the effect of fracture normal stiffness on the calculated FoS to support the definition of target reliability level by reducing epistemic uncertainty. Chapter 5 presents general conclusions of the research and recommendations for future research.

2.0 Literature review

2.1 Open pit slope design

Open pit slope design aims to define the mining boundaries, location, and slope geometries. The slope geometrical configuration comprises of three scales: Bench, Inter-ramp, and Overall. Bench scale is the basic unit in the slope design, and its geometry depends mainly on geological structures, mining techniques, and mining capabilities (e.g. equipment). Inter-ramp scale consists of a stack of benches located between hauls roads or step-outs, whereas the Overall scale comprises of various inter-ramp slopes or simply extends from the lowest bench (pit floor) to the highest bench (pit crest). Figure 2-1 shows the terminology used to describe the slope geometrical configuration of the three scales.

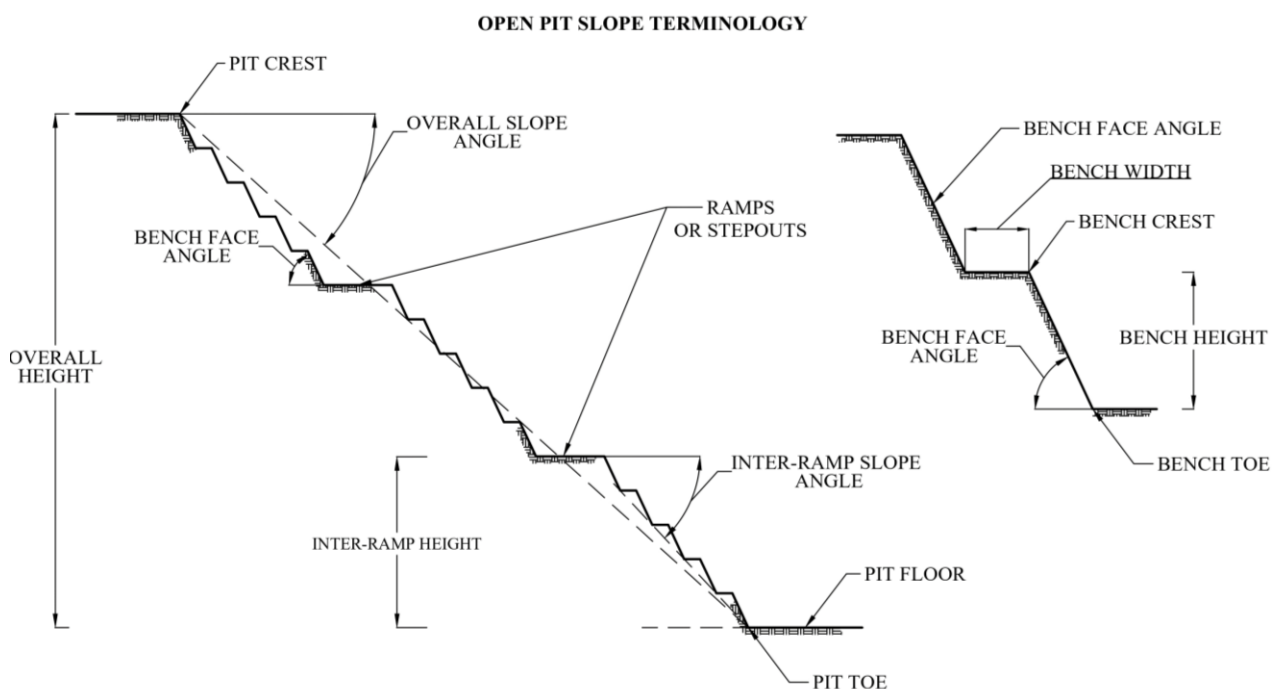


Figure 2-1: Generalized open pit slope configuration and terminology

2.2 Design acceptance criteria for inter-ramp and overall scale

Acceptability criteria of open pit slope design have been discussed extensively and have evolved over time. These criteria aim to establish a comparative basis between the calculated FoS/PoF and the

required performance level of the slope. Different aspects have been considered in defining the acceptability criteria such as design life, including short-term and long-term slopes (Hoek and Bray, 1981; Swan and Sepulveda, 2000; Department of Minerals and Energy, 1999), the consequences of slope failure, and importance of the slope.

It has been recognized that the larger the scale of the slope (from individual benches to overall slopes), the higher the risks associated with a potential slope failure. For instance, Priest and Brown (1983) defined three categories of slope consequences (not serious, moderately serious, and very serious) based on the slope height. Consequently, the acceptability criteria in terms of FoS tend to increase with the scale of the slope, while the acceptability criteria in terms of PoF decrease with the increase of slope scale. The importance of the slope is to some extent related to the operational factors of slope design, such as proximity to critical infrastructure (e.g., crusher, haul road) inherently carrying higher risk (Hoek and Bray, 1981; Department of Minerals and Energy, 1999; Swan and Sepulveda, 2000).

Sullivan (2006) conducted a review of the practice of slope design, focusing on the acceptability criteria or standards adopted by operators. The author presented a table of acceptability criteria in terms of FoS considering both geotechnical conditions and operational factors. Geotechnical conditions basically are used to express the uncertainty of the complexity of the geological and geotechnical aspects. This review highlighted on a notable gap between early design phases and operational stages, where the volume and quality of data influence the design process. It suggests that, in situations of greater the uncertainty, a more conservative acceptability level is adopted.

The acceptability criteria, as noted by many authors, rely heavily on engineering judgement and experience (Priest and Brown, 1983; Swan and Sepulveda, 2000; Department of Minerals and Energy, 1999). Later on, Read and Stacey (2009) presented a DAC that consist of a range of typical values of FoS and PoF. These values are derived from previous criteria, practitioner experience, and relevant

literature review. The 2009 DAC is formulated for a different slope scale (bench, Interramp and overall), and for different level of consequence of failure. These DAC have been widely accepted and adopted by many practitioners.

However, Adams (2015) and Macciotta et al. (2020, 2021, 2022) recognized that formulation of DAC should consider the risks, calculated FoS and PoF, and an adequate risk model that incorporates levels of design reliability. Adams (2015) presented a methodology for selection of DAC based on key factors such as uncertainty levels, consequence levels, and design life of the slope. This methodology relies on a semi-quantitatively assessment, emphasizing the importance of these factors for selecting of DAC in order to provide a more consistent level of risk management. Recently, Macciotta et al. (2020, 2021, 2022) proposed a RBDAC matrix that are based on reliability levels, and consequences of failure. The 2020 RBDAC matrix poses a strong mathematical background to define pairs of FoS-PoF. The 2020 RBDAC are robust and cover important aspects outlined in previous acceptability criteria. The advantages of adopting reliability-based DAC were described by Gaida et al. (2021). They conducted a quantitative assessment of the geotechnical model adopting in-house DAC that couple reliability levels and consequence of failure. These in-house DAC were tested in a slope stability analysis to optimize a design sector, where the results adopting lower DAC increased the business outcome by increasing the reliability of the geotechnical model. The adoption of DAC based on reliability approach provides advantages and has defensible aspects than previous DAC defined subjectively. A further discussion on the adoption of 2020 RBDAC was presented by Creighton et al. (2022). Table 2-1 summarizes the acceptability criteria that were proposed by many authors over the years.

Table 2-1: Summarized FoS and PoF values adopted in different acceptability criteria in existent literature for Inter-ramp and Overall Slopes

FoS	PoF (%)	Slope Design	Comments	Author
1.3	-	Short-term slope	Short-term and long-term slopes and	Hoek and Bray (1981)

1.5	-	Long-term slope carrying haul road	operational factors	
1.6-2	0.3-1	Slopes with height greater than 50 m	Consequences of failure and operational factors	Priest and Brown (1983)
1.2-2	0.3-10	Pit wall (Interramp or overall)	Consequences of failure and operational factors	Department of Minerals and Energy (1999)
>1.2	15-30	Interramp Slope	Operational factors: Expansion and final wall	Swan and Sepulveda (2000)
>1.3	8-15	Overall slope	Scale of failed volume	
1.2-1.3	1-3	Interramp or Overall	Based on Geotechnical conditions and operational factors	Sullivan (2006)
1.2-1.5	<1	Slope near important structure		
1.15-1.3	10-25	Interramp Slope	Consequences of failure	Read and Stacey (2009)
1.2-1.5	5-20	Overall slope		
-	1-5	Interramp Slope	Consequences of failure and operational factors	Gibson (2011)
-	1-2	Overall slope		
1.2-1.6	2-30	Slope design based on design life	Consequences of failure, levels of confidence	Adams (2015)
1.15-1.5	-	Overall slope	Consequences of failure, reliability	Gaida (2021)
1.10-2	5-30	Interramp and Overall Slope	Reliability level and consequence of failure.	Macciotta et al. (2020, 2021, 2022)

2.3 Slope Stability methods

2.3.1 Limit Equilibrium (LE)

Slope stability assessment is a fundamental component in geotechnical engineering for both civil and mining applications. The slope stability analysis is carried out for three principal purposes (Alzoubi, 2009): to investigate a failed slope through back-analysis, to design a slope by investigating potential modes of failure, and to predict the slope behaviour. Among the various methods employed for slope stability analysis, the LE method is the most common and widely implemented for soil and rock engineering applications.

The LE method is based on the calculation of factor index that is known as the FoS. The FoS relates the available shear strength and the state of stress of the postulated failure surface. A FoS of 1 implies a condition on the verge of equilibrium whereas a FoS above 1 implies stability. The calculation of FoS requires three components: shear strength properties of the materials, postulated slip surface based on the failure mechanism to be investigated, and the chosen method of analysis based on static equations. There are two methods of analysis for LE analysis: single free body and the method of slices. The latter is the most popular approach which consists of dividing the soil or rock mass into slices above the postulated slip surface. At each of these slices, equilibrium equations are applied to determine the interslice shear and normal forces.

The LE method should satisfy three static conditions: (i) equilibrium of forces in vertical direction, (ii) equilibrium of forces in horizontal direction, and (iii) equilibrium of moments at any point. While some LE methods offer simplicity by partially satisfying these static conditions, others are rigorous to satisfy the three conditions. For example, the Ordinary Method of Slices (OMS) and simplified Bishop provide simplicity but only satisfy some of these conditions, resulting in reduced confidence on the results. In contrast, rigorous methods that satisfy all the static equations include Janbu generalized, Spencer, Morgenstern-Price, and Sarma. However, they require other specific

assumptions and considerations which are not statically determined. Understanding the assumptions and limitations of each method are essential on slope stability analysis. A more detail and explanation can be found in Abramson et al. (2002) and Duncan et al. (2014), the authors discussed extensively the assumptions, mathematical background, and limitations of the different methods.

The choice of the method depends highly on the geometry of the slip surface and type of failure mechanism being analyzed. Selecting the incorrect failure mechanism invalidates the stability analysis (Hoek and Bray, 1981). The geometry of the slip surface can be categorized as circular and no-circular surface (Abramson et al., 2002; Duncan et al., 2014). Circular slip surfaces are commonly assumed in the analysis of homogeneous materials and heavily fractured rock masses (Hoek and Bray, 1981; Priest and Brown, 1983). However, non-circular or irregular slip surfaces are more realistic in complex geological environments or heterogeneous materials (e.g. faults, stratification, shear zones) which should be examined in more detail (Abramson et al., 2002).

The type of failure mechanism in rock slopes has been investigated extensively by many authors (e.g., Sjoberg, 1996; Hoek et al., 2000; Read and Stacey, 2009) and classified based on the description of kinematics of failures (Hoek and Bray, 1981; Martin and Kaiser, 1984). Martin and Kaiser (1984) provided valuable insight about failure mechanisms. They categorized three classes of failure considering the influence of the internal geology on the failure mechanism (Figure 2-2).

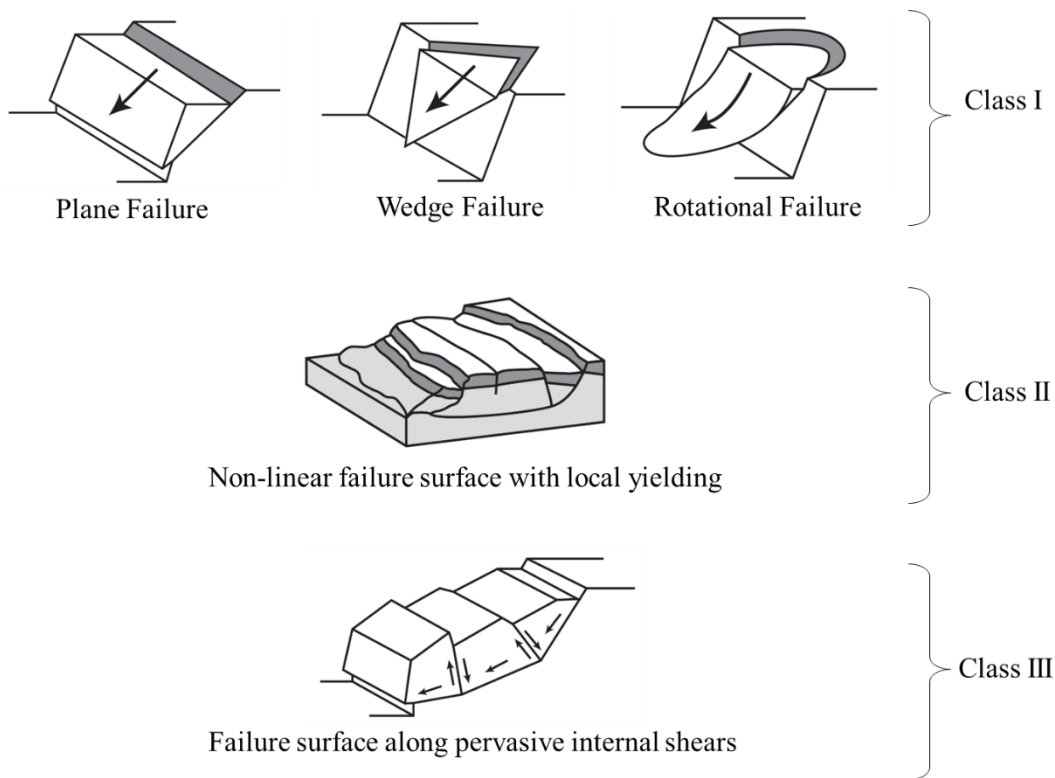


Figure 2-2: Slope failure mechanisms (adapted from Martin and Stacey 2018, with permission from CSIRO publishing)

The class I includes rock slope failure with rigid motion along a through-going discontinuity or known as plane shear sliding mode (Alzoubi, 2009). The class II includes local yielding of the rock mass to allow motion along a non-circular slip surface. The class II involves local yielding of the rock mass through pervasive internal shear surfaces to allow motion through an irregular, non-circular basal plane. Moreover, the authors pointed out that traditional LE method is suitable for class I and class II. However, Martin and Kaiser (1984) used the Sarma method to analyze class III. They performed a parametric study to determine the factors that influence the solution and to compare the results with the Morgenstern-Price method. They found that internal shear orientation (using Sarma) affects the calculated FoS and differs from the Morgenstern-Price results. They emphasized the great significance of the methods and the internal shear surfaces considered in slope stability analysis and in back analysis as some methods can over- or under- estimate the mobilized shear strength.

When analyzing a slope failure mechanism in open pit slopes that are governed by large-scale discontinuities (see Figure 2-3) or in combination with discontinuities (such as step-path), one technique for addressing the complexity of these failure types using LE method involves using a directional strength approach (Swan and Sepulveda, 2000; Read and Stacey, 2009). The directional strength consists of defining the shear strength of the rock mass and the shear strength of the structures (e.g. Mohr Coulomb) based on their respective direction, as shown in Figure 2-4. This approach is particularly useful for analyzing non-daylighting structures and step-path failures.

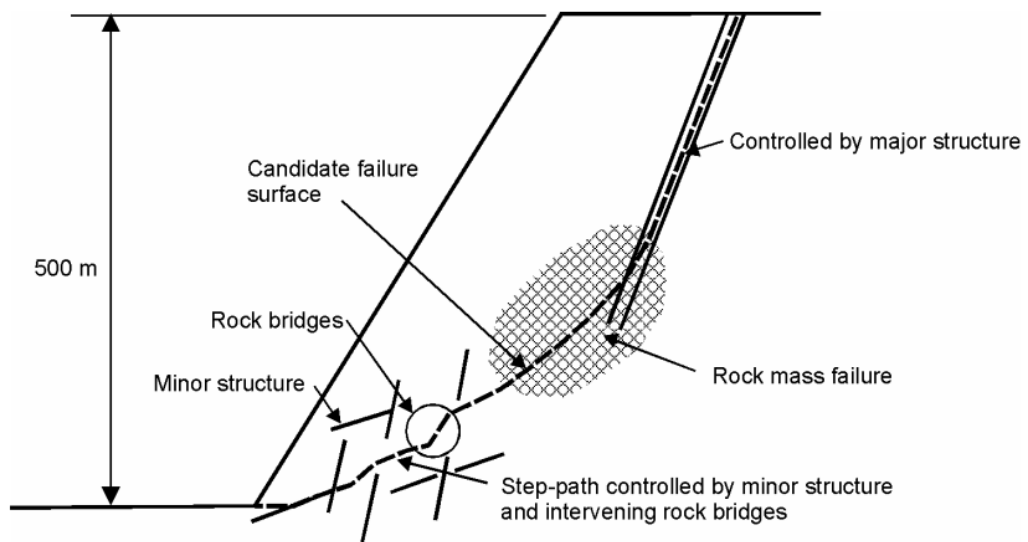


Figure 2-3: Large scale pit slope failure involving different failure mechanism (Hoek et al., 2000 with permission)

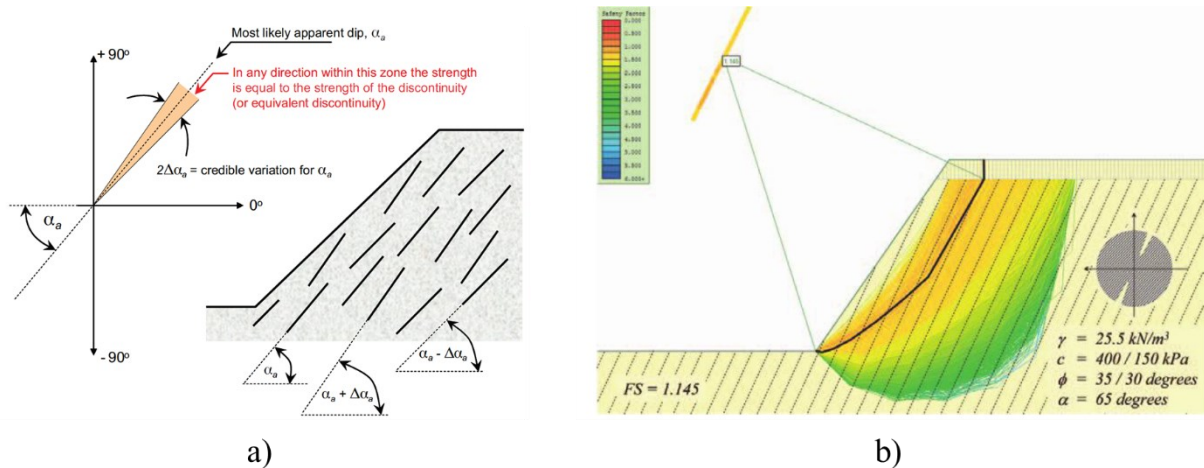


Figure 2-4: Definition directional strength that considers a) definition of shear strength according to the orientations of discontinuities, and subsequent b) slope stability analysis (adapted from Read and Stacey 2009, with permission from CSIRO publishing)

2.3.2 Shear Strength Reduction (SSR)

Evaluation of Slope stability can be done using a numerical approach and the Shear Reduction Strength (SSR) method (Zienkiewicz et al., 1975; Dawson et al., 1999; Griffiths and Lane, 1999). This method is used to evaluate stress-strain behaviour of the geomaterials and complex failure mechanisms. It involves an iterative process that reduces progressively the shear strength properties of the soil and rock mass (e.g., cohesion, friction angle) in a series of trial numerical stress-strain analyses. The factor by which the shear strength properties are reduced is known as the SRF. The systematic reduction in shear strength allows the identification of a critical failure surface that is marked for a transition from numerical convergence to divergence. Some advantages of SSR over LE method include that it provides realistic representation of potential failure surfaces, accounts for complex material behaviour such as strain-softening behaviour (e.g., Conte et al., 2010; Rafiei Renani and Martin, 2020b), and can be combined with monitoring data to yield higher confidence in back-analyses and in predictive models (Sharon and Eberhardt, 2020). Therefore, the SSR method is widely employed in geotechnical engineering to enhance the understanding of failure mechanisms and to improve accuracy of slope stability calculations.

2.4 Uncertainty in geotechnical engineering

Uncertainty in Geotechnical engineering refers to inherent variability of the soil and rock masses, investigation error and biases, and the lack of knowledge about the ground conditions, having implications on the decision-making process. Uncertainties has been further categorized in three broad categories (Baecher and Christian, 2003): (i) natural variability, (ii) knowledge uncertainty or epistemic uncertainty, and (iii) operational uncertainties. The natural variability is associated to the natural processes both spatial and temporal that led to the formation of soil and rock mass. The knowledge or epistemic uncertainty is associated to the lack of understanding and/or lack of evidence. Furthermore, Baecher and Christian (2003) subdivided the epistemic uncertainty into three sub-categories: site characterisation uncertainty, model uncertainty, and parameter uncertainty. The decision and model uncertainty comprises operational uncertainties (e.g. excavation, construction, monitoring performance) which are not accounted explicitly in the models adopted, and the decision uncertainties (e.g. social objectives, economic business, social aversion) that impact the development of a project. Uncertainty arises from different sources which have been described in Geotechnical literature (Giani, 1992; Wenner and Harrison, 1996; Whitman, 2000; Fookes et al., 2000; Baynes, 2010; Baecher and Christian, 2003; Hadjigeorgiou and Harrison, 2011; Phoon and Retief, 2016; Read and Stacey, 2009; Macciotta et al., 2020; Macciotta, 2023). Macciotta et al. (2020) categorized key sources of uncertainties that include the geological/hydrogeological model, spatial variability of properties, strength criterion, testing, method of analysis, and human error. Following the categorization by Macciotta et al. (2020), some of these sources of uncertainty are described as follows:

- Geological model. As recognized by Whitman (2000), Steffen (2008), Baynes (2010), Sharon and Eberhardt (2020); knowledge of the geological environment is fundamental in development of a project as it constitutes a significant source of uncertainty. This encompasses spatial distribution of geomaterials (overburden soils and rock basement), unforeseen geological features such as localised weak rock mass, fault, weak stratum as well as the spatial

distribution of geohazards like landslides and active faults. In the mining industry, the spatial distribution of such materials is unique, and it is based on the genesis of ore formation. Ore formation involves a sequence of different events such as geomorphological, magmatic, tectonic, diagenetic, climatic, among others, which occurred throughout geological history. Worldwide, various types of ore deposits have been recognized and categorized based on their orogenic features, commodities features, ore grades, and other criteria (Ridely, 2013). Similarly, Read and Stacey (2009) described the major type of ore deposits in open pit mining such as Porphyry deposits, Epithermal deposits, Kimberlites, Volcanic Massive Sulphides (VMS), Skarn deposits, and Stratabound deposits. Each deposit has unique geological characteristics such as types of alteration, rock types and structural control, thus forming the basis for a geological model. This model, in turn, is fundamental for building a geotechnical model. More details of geological models, diverse lithologies, and description of their engineering properties are given by Fookes et al. (2000) and Goodman (1993).

- Design parameters. Another source of uncertainty is related to the choice of reliable design parameters. This source of uncertainty is intrinsically linked to the challenges in data collection, sampling methods, testing methods, measurement error, and the transformation uncertainty when using empirical or correlation models (Baynes, 2010; Whitman, 2000; Hadjigeorgiou and Harrison, 2011; Phoon and Retief, 2016). Notably, following common procedures like ASTM and/or ISRM aims to reduce systematic errors and improve the accuracy of the tests or sampling. However, data collection from field surveys is often subjected to various constrains such as limited visibility, accessibility, and time (Hadjigeorgiou and Harrison, 2011). Moreover, accounting for scale effects (Wenner and Harrison, 1996) and time effects that can downscale the design parameter add more complexity, making it challenging to rely on a single design parameter. The uncertainty in design parameter depends on engineering judgement supported by statistical procedures.

- Method of analysis and analytical models. These sources of uncertainty are related to model uncertainty, which is attributed to the lack of understanding in choosing a mathematical model that accurately represents the real world (Baecher and Christian, 2003; Ceryan et al., 2018). Examples include uncertainties in selecting a postulated failure mechanism, the associated method of analysis, and the mathematical model adopted to carry out simulations such as LE or SSR (Baynes, 2010). The choice of a failure criterion (e.g. Mohr Coulomb, Hoek-Brown) also falls within these sources of uncertainty.
- Human-related. Zimmerman (2000) described causes of human-related uncertainty that are subject to interpretation based on the quantity and the quality of information. The lack of information, the ability to transform information into perceivable information, the engineering measurements, and human beliefs when developing the basis of available data are all important aspects to consider when dealing with uncertainties.

Statistical tools are extensively used in engineering practice to quantify uncertainty. These tools often involve summary statistics, which are descriptive parameters used to measure both the central tendency and the dispersion of data (Baecher and Christian, 2003). Central tendency is typically represented by mean, median, and mode, while dispersion is represented using standard deviation, range, variance, inner quartiles, and the COV. The COV, a dimensionless parameter defined as the ratio of the standard deviation to the mean, allows for the measurement of uncertainty (Macciotta et al. 2020).

In geotechnical engineering, the COV has been used to quantify uncertainties associated with design parameters. The COV of soil and rocks properties vary over wide range and can be as large as 1 (Baecher and Christian, 2003; Phoon and Retief, 2016). Higher values of COV indicate greater variability (Ruffolo and Shakoor, 2009). The COV is highly dependant on factors such as the number of tests, the specific rock or soil properties being measured (e.g., unit weight typically has a low COV, while deformability properties such as stiffness have a high COV), and the procedures or methods

adopted in laboratory programs or in situ characterization (Phoon and Chin, 2015; Phoon and Retief, 2016). The COV decreases with more consistent information, and when correlation between parameters parameter exists, it leads to the development of multivariate models (Phoon and Retief 2016).

For instance, Ruffolo and Shakoor (2009) demonstrated that the higher the COV, the greater lab tests are needed to characterize the Uniaxial Compressive Strength (UCS). Based on this work, Hadjigeorgiou and Harrison (2011) highlighted that the COV is also linked to the rock type and can increase with higher levels of anisotropy and heterogeneity of the material. Similarly, Bewick et al. (2015) observed higher COV of UCS tests on heterogeneous rock, which exhibited different failure modes during the lab testing program. This demonstrates numerically that the COV decreases with an increase in the quantity and quality of information, thereby reducing uncertainty in design parameters. Various COV values have been reported in the literature (e.g., Phoon and Chin, 2015; Phoon and Retief, 2016). Therefore, the COV has been used to establish a more defensible framework, justifying increased investment in investigation to achieve more consistent and predictable designs.

2.5 Deterministic analysis

Traditionally, the slope design has been based on FoS. The basis formulation on calculating an adequate and acceptable FoS is centered on the selection of adequate input parameters (e.g., shear strength, pore pressures, unit weight), failure mechanism, and a suitable method of analysis (e.g. LE method). This selection has been subjected to data availability, careful interpretation, and engineering judgement (Hoek and Bray, 1981; El-Ramly, 2001; Phoon and Retief, 2016). This method of calculating the FoS is commonly referred as the deterministic approach.

The role of FoS to account for uncertainties and variability of the input parameters has been recognized by many researchers (e.g. Abramson et al., 2002; Ceryan et al. 2018; Martin and Stacey, 2018). Martin and Stacey (2018) highlighted that the choice of a FoS depends on the degree of risk, which is based on accumulated experience with a particular rock and soil mass, and its magnitude

varies with performance requirements. It has also been recognized that the same value of FoS does not reflect the same level of uncertainty, and adopting higher values does not necessarily represent higher levels of safety (El-Ramly, 2001; Abramson et al., 2002).

Some limitations of the deterministic approach include the introduction of degrees of conservatism in slope design, overlooking the randomness of input parameters, and the level of uncertainty that is not considered explicitly but rather subjectively. However, sensitivity analysis can be adopted to investigate uncertainties by identifying factors that are more relevant and critical (e.g., shear strength, pore pressures, discontinuity stiffness) in a specific slope stability analysis.

2.6 Probabilistic analysis

The probabilistic approach is a framework that manages uncertainties more formally (Priest and Brown, 1983) by considering the limits of the input variables. This leads to a more comprehensive assessment of slope behaviour. Probabilistic analysis facilitates risk-informed decisions, supporting risk assessment, mitigation, and management, as well as the evaluation of design reliability (El-Ramly, 2001). The probabilistic approach is based on the principles of the deterministic approach, but it systematically incorporates the uncertainty and randomness of input variables. This integration of uncertainty is typically achieved through the quantification or estimation of uncertainty using statistical methods based on observations and measurements. In the conventional methodology of probabilistic analysis, random variables are identified and expressed through PDFs. These random variables can be classified as discrete variable and continuous random variable. Discrete variables describe cases in which uncertain variables can only take specific and distinct values, whereas a continuous random variables describe cases in which uncertain variables can occur within a continuous interval (e.g. shear strength). Examples of discrete distributions include Uniform, Binomial, Geometric, Negative Binomial, Poisson, Pascal. Examples of continuous random variables are Normal, Triangular, Lognormal, Gamma, Beta, among others. After adopting a slope stability analysis method and

analytical model, multiple realizations are performed for different sets of variables generated from the PDF of the input variables, resulting in a set of FoS values with a resultant PDF of FoS. The PoF is calculated as the area below the PDF of FoS for FoS of 1 and lower.

El-Ramly (2001), Abramson et al. (2002), Macciotta et al. (2020, 2021, 2022), and among other authors have discussed that the PoF provides a more consistent measure of safety. El-Ramly (2001) illustrated an example involving the design of a pile foundation. The initial design, due to limited information, adopted a higher FoS. However, with further integration of detailed information, the associated PoF resulted in a lower value than the initial design. The addition of more information reduced the FoS but increased the reliability level. This conclusion suggests that designs with the same degree of PoF provide a more consistent level of safety than equal FoS.

Different techniques for performing probabilistic analysis are explained in the following sections.

2.6.1 First Order Second Moment (FOSM)

The First Order Second Moment (FOSM) method is based on the Taylor series approach (Abramson et al., 2002). This method involves identifying the significant variables that can affect stability or can contribute to the uncertainty. Generally, the FOSM method consists of calculating the first two moments (mean and variance) of the variables involved. Then, the best estimate, usually the mean, is used to calculate the performance function (e.g., the FoS for slope stability analyses). Subsequently, the variance of the FoS with respect to the variables is estimated using partial derivatives. As a result, the mean and variance are estimated from the resulting values of FoS, at which the PoF can be obtained by assuming a PDF of FoS. This method requires $2N+1$ calculations, where N is the number of variables. This method offers advantages such as identifying of critical parameters in overall uncertainty evaluation. It is simple and rapid to implement, allowing its use in conjunction with numerical models.

2.6.2 Point estimate method

The point estimate method was proposed by Rosenblueth (1975). The FoS is calculated using a combination of random variables simulated by values that take one standard deviation above or below the mean. If only one random variable is considered in the calculation of FoS, only two results of FoS are obtained, the first considering a mean value minus one standard deviation, and the second considering a mean value plus one standard deviation. Thus, this method requires $2N$ calculations where N is the number of variables. From the results of calculated FoS, the mean and variance can be calculated and by assuming a PDF, the PoF can be calculated. This method requires low computation time and provides insight into overall uncertainty, facilitating its adoption in conjunction with numerical methods.

2.6.3 Monte Carlo

The previous methods do not produce a PDF of FoS and require significant assumptions on the PDF of input parameters and resulting FoS. The Monte Carlo technique is a very well-known simulation method widely applied in Geotechnical Engineering to address random sampling and uncertainty (Tamimi, 1989; Hoek, 1998, El-Ramly, 2001; Abramson et al. 2002, Baecher and Christian, 2003). This technique can handle a large number of simulations without significant computational effort in the iterative process. The technique consists of performing repeated simulations to yield a solution by entering a design equation and choosing a set of input parameters in accordance with the PDF of each input parameter. As a result, for a set of input parameters, a set of output parameter are generated along with the resulting PDF. Accuracy can improve with an increasing number of simulations to produce an adequate PDF. In slope stability analysis, the output parameters are represented as the calculated values of FoS. Thus, these calculated FoS values are analyzed to determine the shape of the PDF, the statistical moments, and the PoF. The advantages of Monte Carlo Simulation include:

- Capability of determining a final PDF based on input variables derived from any kind of distribution (e.g., Normal, Lognormal, Gamma)

- It does not offer complexity with an increase in input variables and can handle possible correlation between them.

The advantages, simplicity, and capabilities of the Monte Carlo technique in Slope Stability analysis are of great interest to practitioners. However, it becomes resource intensive for numerical models and is constrained to the LE method.

3.0 Adopting Reliability-Based Design Acceptance Criteria in Probabilistic open pit slope analysis: A parametric study

A version of this chapter has been accepted for publication in the journal of Geotechnical and Geological Engineering.

Abstract:

Design of open pit slopes is a decision-making process which aims to maximize ore recovery while minimizing the stripping ratio. Slope design will typically meet a Design Acceptance Criteria (DAC), and the current practice of designing open pit slopes adopts the industry-wide accepted Guidelines of Open Pit Slope Design published in 2009. However, designing open pit slopes is a complex process that involves inherent risks and geotechnical uncertainties. Consequently, reliability analyses have become a valuable tool in managing uncertainties. This paper presents a parametric study that considers uncertainties related to the rock mass strength properties and the slope geometric configurations, evaluated at three different design reliability levels. This parametric study adopts a reliability-based DAC (RBDAC) approach presented in 2020. The reliability assessment is carried out using probabilistic analyses adopting the 2D LE method along with Monte Carlo simulations. The input variables for the rock mass strength are defined through Probability Density Functions (PDFs) that capture the natural variability while the input variables of geological structures are defined through kinematic assessments. The PDFs of the rock mass strength properties were modelled based on the generalized Hoek-Brown criterion using the mean, coefficient of variation (COV), and correlation coefficient. Probabilistic analysis results show that most of the resultant pairs of Factor of Safety (FoS) and Probability of Failure (PoF), and associated COV of the resulting FoS (COV_{FoS}) are consistent with the RBDAC approach. This approach has significant implications for slope optimization for planned pit pushbacks.

Key words: Reliability-based Design Acceptance criteria, Probabilistic analysis, Coefficient of Variation

3.1 Introduction

The design of open pit slopes aims to extract the ore resources in a safe and efficient manner, maximizing the volume of ore recovered and minimizing overall excavation volumes. This has the objective of maximizing profit whilst maintaining safety, with the important benefit that lower overall excavated volumes decrease the carbon footprint of the mining operation. The current design practice in open pits follows the widely accepted guidelines published by the Large Open Pit (LOP) project in 2009 (Read and Stacey, 2009). The process is complex due to the nature of the orebodies, the geological settings, and the uncertainty associated with the geological environment and material properties (Read and Stacey, 2009).

Generally, the slope design is undertaken at different scales: bench, inter-ramp, and global (Overall slope). The slope design process requires a variety of slope stability analyses from empirical assessments, kinematic analyses (bench-scale design), limit equilibrium deterministic analyses, to stochastic and numerical assessments for critical sectors of the pit. The design should target a Factor of Safety (FoS) and/or Probability of Failure (PoF) for an accepted level of risk (Martin and Stacey, 2018). The minimum acceptable FoS and maximum PoF are based on industry guidelines.

The current, widely adopted DAC in open pit mining was proposed by Wesseloo and Read (2009). This DAC was informed by previous work, including that by Swan and Sepulveda (2000) where they developed DAC in terms of minimum allowable FoS and maximum PoF that considered slope type, condition (expansion or final wall), and characteristics of the instability assessed in terms of failure volume and loss of ramps. Accordingly, and to provide flexibility in its application, the 2009 DAC considers different levels of consequence (Low, Moderate, High) and the scale of the slope (Bench, Inter-ramp, Overall).

Macciotta et al. (2020, 2021) identified that although the 2009 DAC had been widely adopted by the mining industry, mature operating pits sought to justify the application of DAC on the basis of the reliability of the geotechnical design and transitioning to performance-based design (design targeting performance in terms of deformations and/or expected failure volumes based on the monitored performance of previous pushbacks). Furthermore, it was identified that the target FoS-PoF pairs proposed in the 2009 DAC for the same level of consequence and scale of the slope were not mathematically consistent in terms of the statistical relationship between FoS and PoF.

Transitioning towards performance-based design allows operations that have developed a robust geotechnical model over the years, based on extensive site investigations, model updating, monitoring and back analyses of previous slope failures; to adopt in-house DAC that are less conservative than those in the 2009 guidelines while maintaining acceptable levels of safety and managing economic risks. Macciotta et al. (2020) identified this corresponds to a real and perceived increase in the reliability in the slope stability analyses as knowledge is gained, which is better addressed explicitly through reliability-based designs that consider uncertainty in the assessments and calculation of PoF.

Adams (2015) had identified the importance of uncertainty in slope characteristics, design life and consequences of failure, in the adoption of DAC and introduced an evaluation of a “confidence” ranking of High, Medium, and Low confidence relating to the confidence in the design stability analysis.

An example of the adoption of reliability-based open pit slope design that considers DAC as a function of the reliability in slope stability analyses was presented by Gaida et al. (2021) and Creighton et al. (2022). The selection of target FoS required an evaluation of the reliability in the geotechnical models and stability analyses, and the associated consequences of slope failure within a double-entry matrix that mapped to the suggested target FoS, consistent with Macciotta et al. (2020). Reliability was assessed through five ranking scales, ranging from very low reliability to very high reliability, which depended on the quantity and quality of information, and subsequent interpretation.

The DAC for inter-ramp and overall slopes discussed in Macciotta et al. (2020, 2021, 2022) has this consideration of both the reliability in slope design and consequences of failure. Uncertainty in the components involved in the slope design process varies depending on the level of engineering effort, and the reliability in slope stability analyses can be best examined through probabilistic analyses where uncertainties can be expressed as a defined Probability Density Function (PDF) of the resultant values of FoS. Thus, the design reliability is expressed through COV_{FoS} . Macciotta et al. (2020) presented a reliability-based DAC (RBDAC) matrix that considers pairs of FoS-PoF that are mathematically associated through COV_{FoS} for different reliability levels assuming the resulting FoS are distributed following Lognormal and Normal distributions, and for different economic consequences of slope failure. An important consideration is made in Macciotta et al. (2020), where the RBDAC approach considers management of economic risks as long as safety risks are kept within tolerable levels through monitoring and Trigger Action and Response Plans (TARPs).

This paper aims at testing some of the assumptions behind the development of the 2020 RBDAC matrix. This paper presents a parametric study that adopts the geomechanical characteristics and slope configuration of an operating open pit mine, and tests the application of the RBDAC in Macciotta et al. (2020). The study adopts a probabilistic analysis using a 2-dimensional (2D) limit equilibrium method, considering that deterministic 2D limit equilibrium is the most common approach for the design of pit slopes followed by its probabilistic application considering parameter uncertainty. The analyses aim to evaluate the influence of the natural variability of the rock mass strength and the variability of the geological structures on the slope stability, the latter to gain some insight into the role of epistemic uncertainty in slope stability (in this study, associated with the geometry of discontinuities). The natural variability of the rock mass strength is addressed through simulating probabilistic input strength parameters defined by a mean value and a COV. The variability of the geological structures is evaluated through stereographic projections and incorporated into the slope stability analysis through generalized anisotropic strength (Read and Stacey, 2009; Bar et al., 2016; Nagendran and Mohamad Ismail, 2021).

Consequently, results of the calculated FoS-PoF and COV_{FoS} are compared to the RBDAC matrix in Macciotta et al. (2020). Additionally, the RBDAC is applied to the design of a pushback in the geological setting adopted from the case study.

3.2 Basis for the open pit configuration and geology

The configurations and material characteristics applied in this study are based on an open pit mining operation located in Chile, South America. The following summary was obtained from previous work by Valdivia and Lorig (2000) and Padilla et al. (2001), at the selected site.

3.2.1 Location and Geologic Setting

The operation is located in a large porphyry copper deposit, one of a number of large operations located in northern Chile (Figure 3-1). It has a topographical elevation of 3100 (masl).

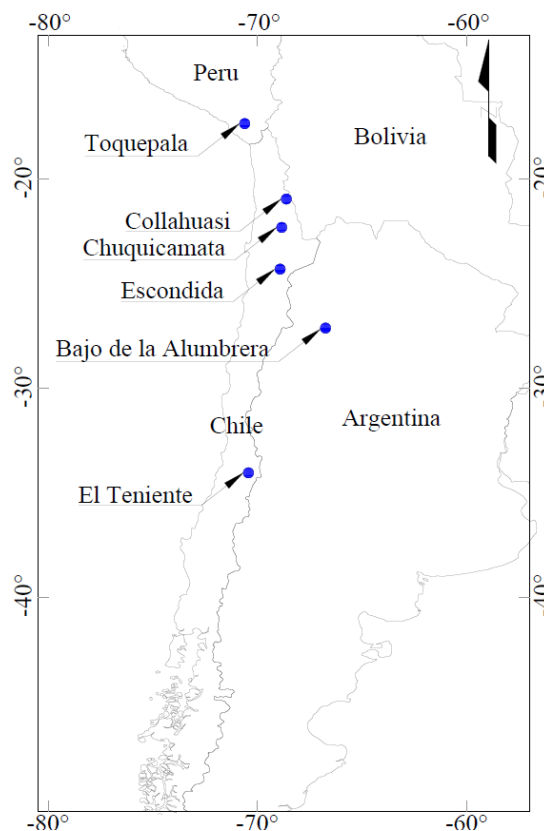


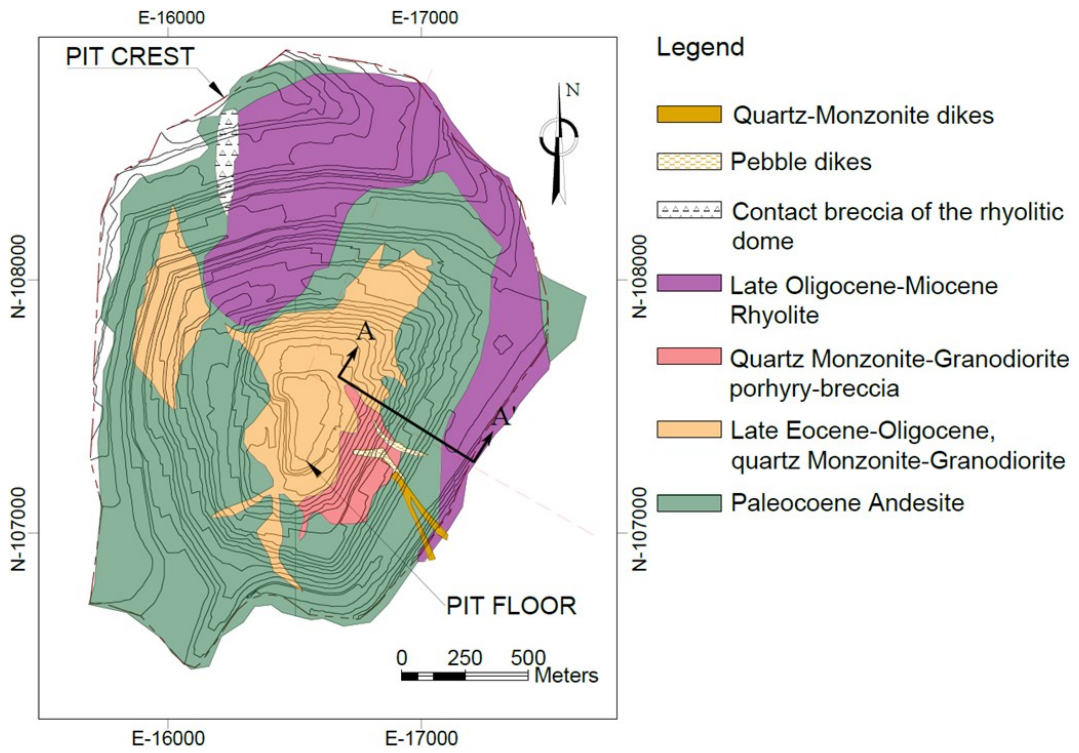
Figure 3-1: Region where the base case study inspiring the model in this work is located

The porphyry copper deposit is hosted in Late Cretaceous-Paleocene andesite. The basement consists of the following units: Paleozoic rocks composed of a succession of trachytic andesite and

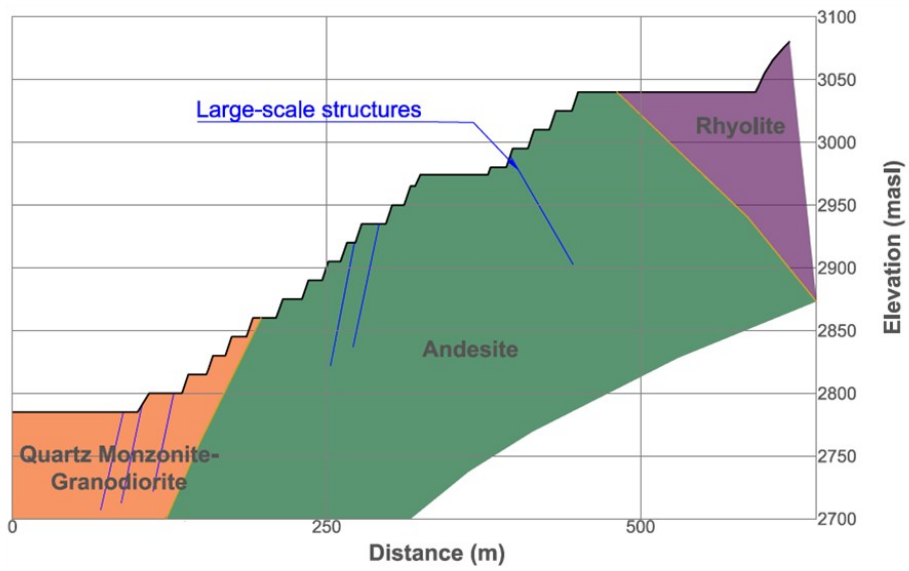
sedimentary lenses which are intruded by tonalitic, granodioritic, and granitic rocks. Late Paleozoic rocks composed of rhyolitic rocks. This sequence is overlain by Mesozoic sedimentary rocks composed of shale, limestone, and calcareous limestone, followed by Late Cretaceous–Paleocene volcanic rock, andesite.

The Paleozoic-Mesozoic-Paleocene sequence is cut by Eocene-Oligocene intrusive complexes, ranging from diorite to quartz monzonite and granodiorite. Mineralization is related to these intrusions. Three phases of emplacement are identified, the earliest two phases comprise porphyritic rocks differentiated according to the mineralogy and hydrothermal alteration, and the third one is a porphyry-breccia. A geological map on the exposed pit plan view is shown in Figure 3-2

Hydrothermal alteration types that are associated with the mineralization at the site include pervasive propylitic, silicification, and potassic alteration; vein-controlled alteration, and advanced argillic alteration controlled by principal faults. Two important fault systems are recognized: the north-northwest-striking mineralized faults (0.5 m thick) dipping toward the east and west, respectively in the west and east walls; and northeast-striking faults (0.3 m thick) dipping 60 to 70° south. The former is characterized by fractured rock and gouge that together with secondary structures form rhombic geometries, while the latter is characterized by a highly fractured zone with red clay gouge acting as the main pathways of water flow. Slope behaviour is controlled by a combination of the structure and a rock mass of medium to low strength.



a)



b)

Figure 3-2: a) Geological map of the base case used to inform this study (after Padilla et al. 2001) and b) a typical cross section (A-A') looking north

3.3 Uncertainty in rock strength

Uncertainty is an important aspect in geotechnical engineering due to the inherent variability and complex heterogeneity of geological settings. The sources of uncertainty are many and include the unforeseen geological conditions, adoption of adequate geotechnical models, the variability of design parameters, measurement errors (e.g. field and laboratory tests), amongst others (McMahon 1985; Phoon and Retief, 2016; Macciotta, 2023).

Sources of uncertainty can be categorized as natural (inherent) variability or aleatory uncertainty, and epistemic uncertainty (Ferson and Ginzburg, 1996; Baecher and Christian, 2003; Der Kiureghian and Ditlevsen, 2009; Hudson and Feng, 2015; Abdulai and Sharifzadeh, 2019; Macciotta, 2023). The former is associated with natural processes both spatial and temporal that led to the formation and/or modification of geological units. The latter is related to the lack of knowledge, and it can be reducible through further field or laboratory investigations. The distinction between both uncertainties depends on the degree of knowledge that is related to the investigations in terms of quality and quantity of information. Natural variability can only be characterised when sufficient quantity of precise information is reached (Bedi and Harrison, 2013).

Many studies have been conducted to characterize the natural variability of the rock strength, some quantifying the natural variability in terms of COV which has been associated with different rock types and its increase with the degree of anisotropy and heterogeneity (Hadjigeorgiou and Harrison 2011). For instance, Bewick et al. (2015) concluded that natural variability of Uniaxial Compressive Strength (UCS) is higher in heterogeneous rocks than homogeneous rocks due to variation in failure modes that they exhibit during laboratory tests. This natural variability is reflected in the COV_{UCS} , where homogeneous rock datasets show COV_{UCS} values less than 0.15 whereas heterogeneous rock datasets show COV_{UCS} values ranging from an average of 0.38 to 0.84. Similarly, Rafiei Renani et al. (2019) investigated the strength variability in high heterogeneous porphyry deposits, reporting COV_{UCS} values ranging from 0.7 to 0.9. The natural variability of the Hoek-Brown parameter, m_i , has not been

characterized as extensively as the UCS. Phoon and Retief (2016) reported that values of COV_{m_i} for different types of rocks ranged between 0.14 and 0.95. Table 3-1 presents a summary of some studies on rock strength variability (not comprehensive) to illustrate the uncertainty in intact rock properties, particularly UCS and m_i , in terms of COV.

Table 3-1: Coefficient of Variation of intact rock parameters from a subset of previous studies

Rock type	Name	COV	Source
Uniaxial Compressive Strength (UCS)			
Igneous	Altered secondary sulfide	0.90	
	Altered granodiorite	0.82	
	Altered porphyry chlorite	0.70	
	Amygdaloidal basalt	0.25	Rafiei Renani et al. (2019)
	Milbank granite	0.18	
	Aspo diorite	0.17	
	Lac du Bonnet granite	0.10	
	Quartz monzonite	0.38	Bewick et al. (2015)
	Porphyritic dolerite	0.25	Keyter et al. (2008)
Sedimentary	Moura mine coal	0.35	
	Shiraz limestone	0.30	Rafiei Renani et al. (2019)
	Matinenda sandstone	0.29	
	Limestone	0.38	Bewick et al. (2015)
	Quintner limestone	0.33	
	Sandy mudstone	0.31	
	Mudstone	0.24	Keyter et al. (2008)
	Shale	0.09	
Hoek-Brown parameter (m_i)			
Igneous	Granite	0.38	
	Dolerite	0.15	
	Granodiorite	0.31	Phoon and Retief (2016)
Sedimentary	Sandstone	0.54	
	Mudstone	0.76	

	Shale	0.92
	Limestone	0.47
	Dolostone	0.38
	Marble	0.40
Metamorphic	Quartzite	0.25
	Amphibolite	0.17

The natural variability in rock strength parameters can be quantified using stochastic models. Stochastic models encompass frequentist or classical probability, subjectivist probability as Bayesian statistics, among others (Bedi and Harrison, 2013). A probabilistic approach assigns a PDF to parameters evaluated quantitatively. In this regard, statistical measures such as the mean, standard deviation, and COV are commonly used to define a PDF. Lognormal and Normal distributions are among the most commonly adopted in rock slope engineering to define the PDF of the random parameters (random parameters is the common term for those parameters considered as stochastic in probabilistic slope stability analyses). Lognormal distributions can provide an adequate fit when assessing intact rock properties, although in the absence of information, a Normal distribution is suggested (Hoek, 1998; Phoon and Retief, 2016). Nevertheless, other parameters such as Rock Mass Rating (RMR) or Geological Strength Index (GSI) that are evaluated semi-quantitatively through numerical ratings can embrace different PDF. For instance, Hoek (1998) adopted a Normal distribution to represent the ranges of GSI when analysing a rock slope in the absence of information, although other distributions might also be adequate (e.g. Uniform distribution, Triangular distribution).

On the other hand, the Bayesian approach is a subjective method, and it is related to the degree of belief of the engineer when assigning probabilities. The method consists of assigning a prior PDF based on experience, representing the uncertainty of initial parameters. This initial assumption is updated to a posterior PDF with subsequent inferences and updates from observations. In this paper, a probabilistic approach is adopted to evaluate uncertainty in rock mass properties, selecting an appropriate shape of the PDF according to the availability of information. Bedi and Harrison (2013) recognized that the

choice of PDF is of most importance over the selected minimum, maximum or mean values. The geological context and slope geometry of an open pit mining operation is used as the basis for the study, and assumptions on parameter uncertainty are developed on the basis of available information and the uncertainty reported for similar materials in previous studies.

3.4 Methodology

Slope stability analyses are performed with 2D Limit Equilibrium (LE) method using SLIDE2 (software by Rocscience Inc. 2023) and adopting the Morgenstern-Price method of slices. The Morgenstern-Price method was chosen as it is appropriate, comprehensive, and widely accepted for evaluating stability in open pit slopes with diverse rock mass units. In the authors' experience, it is also a commonly used method in industry practice. Additionally, the Morgenstern-Price method was validated internally with RS2 (software by Rocscience Inc. 2023) in the original case. It is important to notice that numerical techniques will better capture the failure mechanisms in large rock slopes; however, LE method is still the approach mostly used for pit slope design. LE method was adopted to test the RBDAC under the most common design approach. The workflow adopted is outlined in Figure 3-3. The workflow initiates with the definition of Hoek-Brown failure parameters and their variability (for selected parameters), then transforming the failure criteria to equivalent Mohr-Coulomb parameters and their variability, then performing stochastic LE method for evaluation against the RBDAC in Macciotta et al. (2020, 2021, 2022).

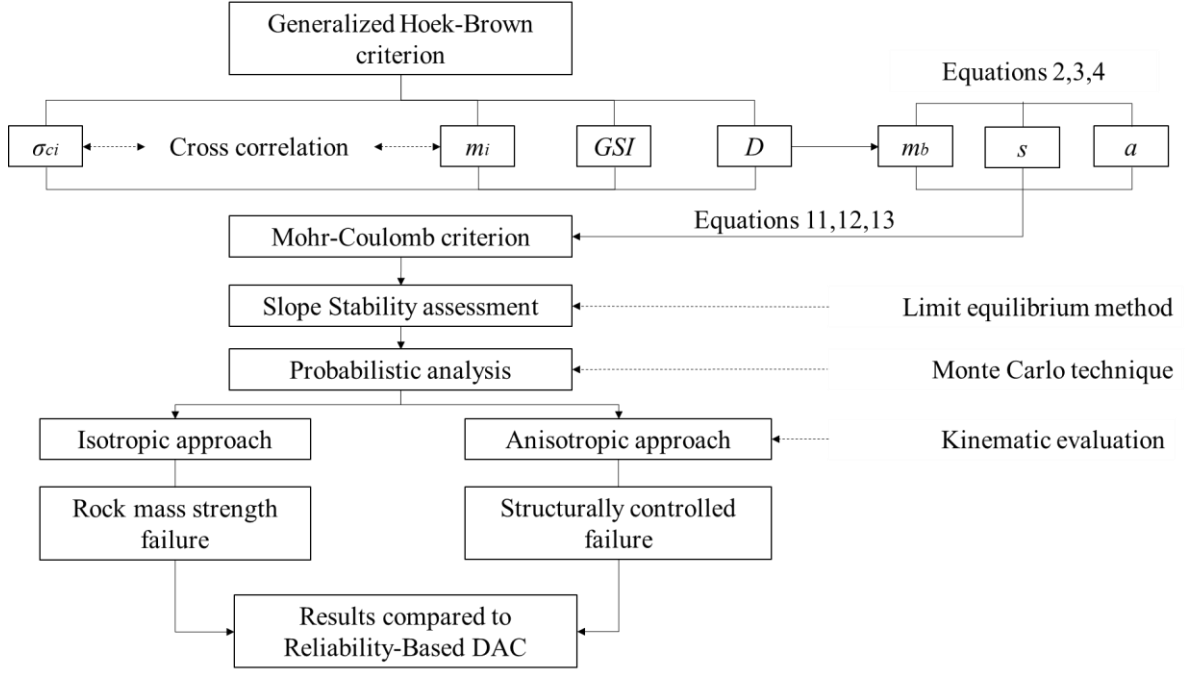


Figure 3-3: Workflow adopted for the probabilistic analyses to test the reliability-based DAC

Uncertainty in rock mass strength properties was quantified using stochastic models. PDF for σ_{ci} , m_i and GSI , which were used to randomize rock mass failure envelopes and applied to the generalized Hoek-Brown criterion (Hoek et al., 2002). The Hoek-Brown criterion is expressed as:

$$\sigma_1 = \sigma_3 + \sigma_{ci} \left(m_b \frac{\sigma_3}{\sigma_{ci}} + s \right)^a \quad (1)$$

where σ_{ci} is the intact rock unconfined strength (can be estimated as the UCS) and m_b , s , and a are material constants given by:

$$m_b = m_i \exp\left(\frac{GSI - 100}{28 - 14D}\right) \quad (2)$$

$$s = \exp\left(\frac{GSI - 100}{9 - 3D}\right) \quad (3)$$

$$a = \frac{1}{2} + \frac{1}{6} \left[\exp\left(\frac{-GSI}{15}\right) - \exp\left(\frac{-20}{3}\right) \right] \quad (4)$$

In this paper the Disturbance factor (D) was set as zero. Dependence between variables was considered in the probabilistic analyses, given its importance in producing more realistic results when using generalized Hoek-Brown criteria (Foley et al., 2023). As such, dependence between variables (rock strength parameters considered stochastic) was modelled through the Pearson correlation coefficient. The methodology adopted in this paper to represent dependent variables is described by Phoon and Chin (2015). Two sets of independent standard Normal random variables (Z_i, Z_j) were modelled. Then, the Pearson correlation coefficient was introduced to model two dependent parameters (X_i, X_j) through the following expressions:

$$X_i = Z_i \quad (5)$$

$$X_j = \delta_{ij}Z_i + \sqrt{1 - \delta_{ij}^2}Z_j \quad (6)$$

where δ_{ij} is the Pearson correlation coefficient between the variables. The Pearson correlation coefficient for UCS and m_i was obtained from information of five porphyry copper deposits according to Flores and Karzulovic (2000), Swan and Sepulveda (2000), Hormazabal et al. (2009), Carvalho et al. (2010), and Cancino et al. (2021); for the operations shown in Figure 3-1.

These two dependent parameters can be shifted to Lognormal distributions using the following expressions:

$$Y_i = \exp (\lambda_i + \xi_i X_i) \quad (7)$$

$$\lambda_i = \ln \left(\frac{\mu}{\sqrt{1 + COV^2}} \right) \quad (8)$$

$$\zeta_i = \sqrt{\ln (1 + COV^2)} \quad (9)$$

where λ_i and ζ_i are the mean and standard deviation of $\ln(Y)$ expressed by the COV and mean (μ) of Y_i . The PDF for the rock mass parameters were modeled using MATLAB software, which rendered the randomized realizations of Hoek-Brown strength envelopes.

Subsequently, each non-linear Hoek-Brown failure envelope was transformed to the equivalent linear Mohr-Coulomb criteria (cohesion and friction angle). The Mohr-Coulomb criteria has small deviation with Hoek-Brown criteria when the minimum principal stresses are low to moderate, offering sufficient accuracy in many practical applications (Wittke, 2014). This was done following common practice for pit slope probabilistic stability analyses and due to current limitations in many commonly used industry software packages which do not support the use of dependent parameters when adopting the Hoek-Brown criterion. The conversion to equivalent cohesion and friction angle depends on the confining stress. In this regard, the confining stress was estimated according to the relationship proposed by Rafiei Renani and Martin (2020). The relationship is given by the following equation:

$$\frac{\sigma_{3,max}}{\gamma H} = \frac{0.175}{\tan(\beta)} \quad (10)$$

where H is the slope height, γ is the unit weight, and β is the slope angle. Hence, the equivalent Mohr-Coulomb parameters were found using equations proposed by Hoek et al. (2002).

$$c = \frac{\sigma_{ci}[(1 + 2a)s + (1 - a)m_b\sigma_{3n}](s + m_b\sigma_{3n})^{a-1}}{(1 + a)(2 + a)\sqrt{1 + [6am_b(s + m_b\sigma_{3n})^{a-1}]/[(1 + a)(2 + a)]}} \quad (11)$$

$$\varphi = \sin^{-1} \left[\frac{6am_b(s + m_b\sigma_{3n})^{a-1}}{2(1 + a)(2 + a) + 6am_b(s + m_b\sigma_{3n})^{a-1}} \right] \quad (12)$$

where

$$\sigma_{3n} = \frac{\sigma_{3,max}}{\sigma_{ci}} \quad (13)$$

3.4.1 Uncertainty associated with structure

Kinematic evaluations and statistical analyses on discontinuity information projected onto the stereonet were completed to calculate the variability in the orientation of geological structures. This was done on large-scale structures as they were considered of kinematic importance at the inter-ramp and overall scales, with small-scale discontinuities assumed to be captured within the modelled rock mass strength (through selection of GSI values). The aim of this assessment was to gain some insight into the influence of epistemic uncertainty associated with structural orientation on the distribution of the stochastic calculations of FoS, although it is recognized not all epistemic uncertainty would be captured in this manner (e.g. persistence, the effect of geometric variations from planar assumptions, effect of stiffness not captured by LE). The results of the statistical evaluation of discontinuity orientations and kinematic analyses defined the range of geological structures that can impact the performance and the design of the pit slope. The variability of geological structures was assessed using stereographic projection techniques with the software DIPS v. 8.0 (software by Rocscience Inc. 2022). The shear strength of the geological structures throughout the stability analysis has been kept with its deterministic values. This was done to keep the parametric study within a reasonable number of variables and aid interpretation of results, with the impact of discontinuity strength uncertainty and inter-relationship with rock mass fabric in resulting FoS a matter of future study. Hence, the variability of the orientation of structures was incorporated implicitly and explicitly in the stability analyses. Implicit and explicit incorporation depended on the scenario being analyzed, as described later.

In this paper, three scenarios were analyzed. The first scenario aims to represent limited available information (limited effort in engineering common to early evaluations pre-operations). At these levels, deterministic 2D LE methods are typical, however this work performed probabilistic analyses to explore the resulting FoS distributions. It is important to note that the RBDAC matrix in Macciotta et al. (2020) can be used with deterministic analyses to calculate FoS. The aleatoric uncertainty associated with rock mass strength is characterized by the COV of the intact rock properties and by rock mass

characterization using the GSI reported in literature. These variables are modelled assigning PDF that correspond to these assumptions. The epistemic uncertainty is essentially associated to the variability of the lithological units and geological structures as well as the location of the Phreatic level. In this regard, part of the epistemic uncertainty is accounted for using regional information of lithological units and large-scale structures, although it is recognized not all epistemic uncertainty is quantifiable. The location of the phreatic water level is accounted in the model using the groundwater conditions chart proposed by Hoek and Bray (1981), which indicated that the surface water is at a distance of four times the slope height behind the toe of the slope. Two series of slope stability analyses were carried out, the first considering the natural variability in rock mass strength and the second considering in addition the influence of structures through generalized anisotropic strength. The latter will allow to take into account the epistemic uncertainty into the slope stability model. A simple generic slope configuration in terms of slope height and slope angle was utilized as it represents early phase of evaluations. This scenario is the initial design to move towards improving both structural and lithological integration into design studies.

The second scenario represents a phase-pit slope design with increased levels of engineering (moderate as per Macciotta et al. 2020), however not as advanced as for mature phase-pit operations. The aleatoric uncertainty is accounted through integration of site-specific data expressed by the COV of the rock mass strength. The COV adopted corresponded to values obtained specifically from data collected for the site (Rapiman and Sepulveda, 2006). The information from structural geology comprised primarily pit wall structural mapping of intermediate and large-scale structures. The slope configuration analysed, represents an actual slope implementation (Padilla et al., 2001) based on integration of increased knowledge of rock mass, lithologic and structural models. The epistemic uncertainty in this scenario is related to the geo-location of large-scale structures and the location of the phreatic level, both were accounted for integrating structural pit mapping and a conceptual hydrogeological model.

The third scenario represents a mature phase-pit slope. This scenario assumes a failure mode that consists of a deep-seated instability at a slope height of 560 m (deeper pit). The failure surface was developed within weak rock mass and is controlled by the orientation and persistence of large-scale structures. This scenario adopts rock mass strength parameters derived from the results of an existing failure back analysis in the original case study (Valdivia and Lorig, 2000), which calibrated the model and parameters for a FoS of 1. The reduction of the aleatoric uncertainty is reflected in the reliability level of the strength components based on this back analysis. This aimed to quantify the variation in the reliability of the analysis. Values of COV for strength parameters were assumed, as there is no information available from past failures. The epistemic uncertainty is accounted for when integrating large-scale structures implicitly and explicitly. Figure 3-4 summarizes the type of information that is used in the three scenarios assessed.

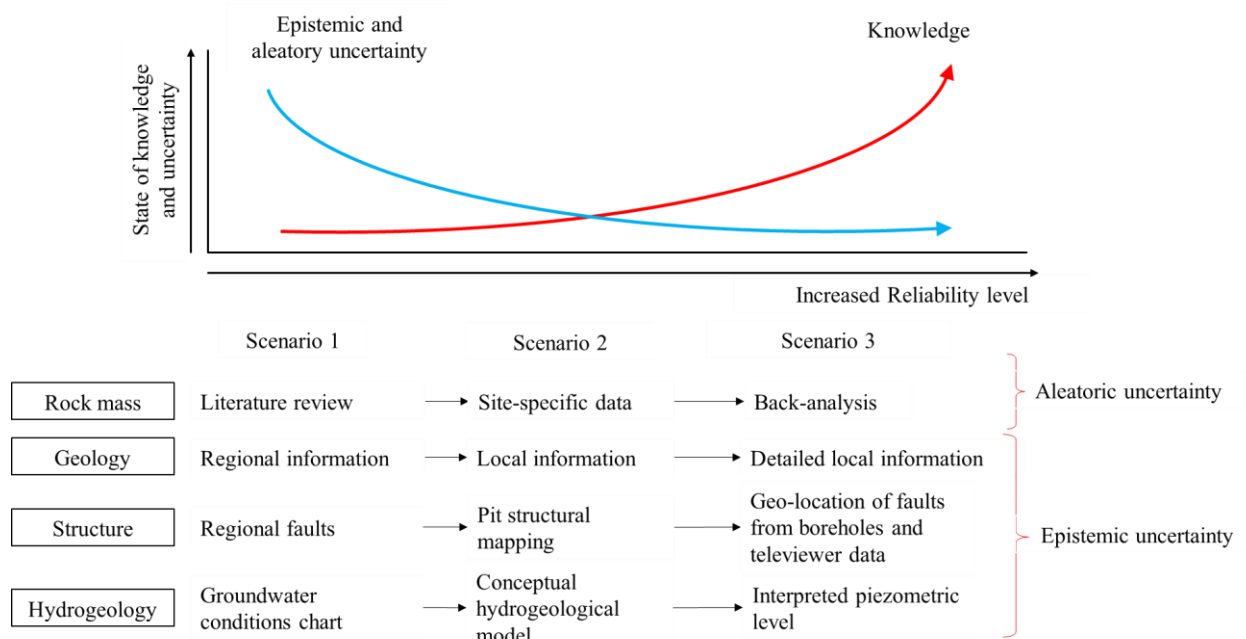


Figure 3-4: Information used for the three scenarios to account for aleatoric and epistemic uncertainty

Once all rock mass strength parameters were defined for the materials in conjunction with the variability of the structural features, a probabilistic analysis was performed using Monte Carlo simulations to calculate a distribution of resulting FoS, mean FoS, PoF and COV_{FoS} . The shape of best

fit distribution to the resulting FoS were tested using the Kolmogorov-Smirnov test and Quantile-Quantile plots (Q-Q plots). The former is a statistical method used to assess the fit between observed data and any continuous distribution. It compares the empirical distribution function of the observed data with the cumulative distribution function of the hypothesized distribution, thus providing a quantitative measure (p-value). The p-value below the significance level suggest a rejection of the null hypothesis suggesting a significant deviation from the hypothesized distribution. The latter is a graphical tool that compares the quantiles of the observed data with the quantiles of the hypothesized distribution. If a dataset perfectly follows a specified distribution, the data points should lie in 1:1 line. FoS, PoF and COV_{FoS} results were then compared to the 2020 RBDAC and discussed. Finally, the design of a pushback in the same geologic context is performed using the 2020 RBDAC to select the target FoS and PoF.

3.5 Results and discussion

3.5.1 First Scenario: limited information at pre-mining phase.

In this scenario, the rock mass strength properties were defined assuming the behaviour would correspond to the predominant lithology, granodiorite. The COV of UCS and m_i used were 0.90 and 0.31, respectively. Likewise, the mean, μ , of UCS and m_i used were 70 MPa and 26 MPa (Hustrulid et al., 2000; Read and Stacey, 2009; Phoon and Retief, 2016), respectively. It was assumed that the rock mass is blocky and fair quality (based on the descriptions from the references), and the range of GSI is defined between [35,55]. The PDFs assigned to the UCS and m_i are Lognormal distributions, and a Uniform distribution is assigned to GSI.

Dependence between the UCS and m_i was modelled according to the results from the five porphyry copper deposits in the region (Figure 3-5). The Pearson correlation coefficient obtained is approximately -0.5. The negative correlation is consistent with findings of Shen and Karakus (2014)

and Vásárhelyi et al. (2016). Importantly, the proposed relationship will provide more representative results when performing the probabilistic analysis.

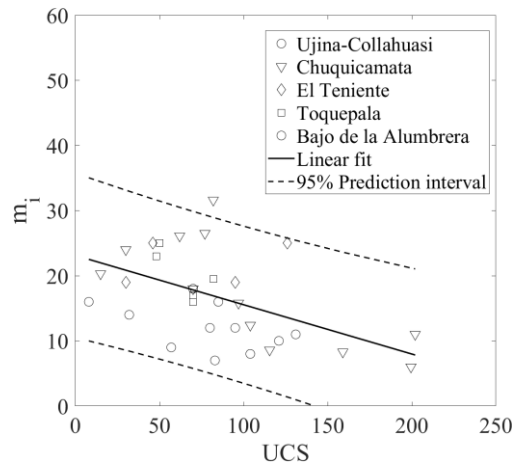


Figure 3-5: Relationship between UCS and m_i for the five porphyry copper deposits in the region

The PDF and dependence between UCS and m_i are shown in Figure 3-6 assuming Lognormal distributions and following the methodology described in the previous section.

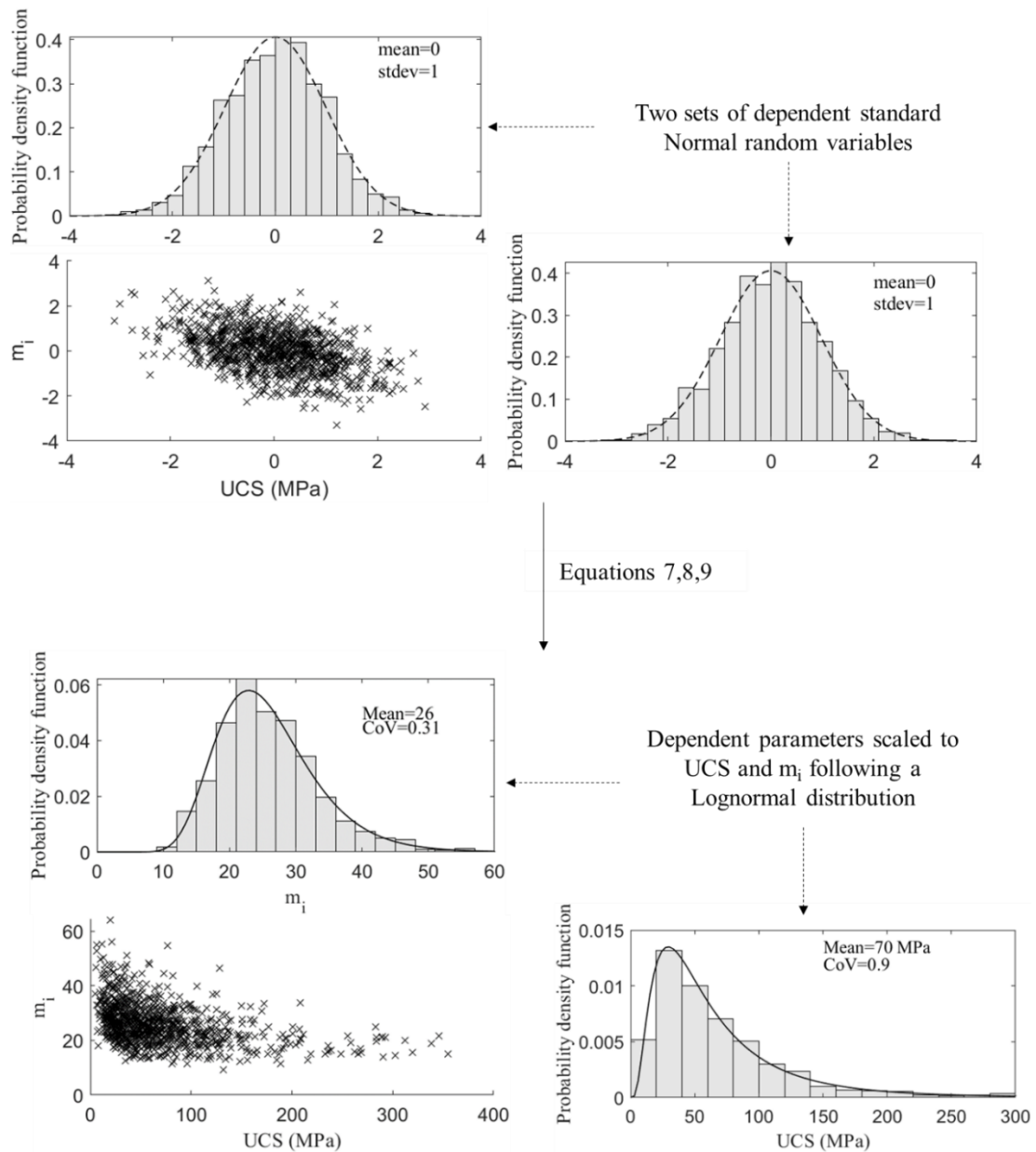


Figure 3-6: Process for the development of PDFs of dependent parameters (UCS and m_i). The flow illustrates how 2 sets of correlated Normal distributions are built and then scaled to the parameter distributions

These parameters were used to define the Hoek-Brown envelopes and subsequently each envelope was transformed to equivalent Mohr-Coulomb cohesion and friction angle. The confining stress was calculated using Eq. (10) for a height of 250 m and Overall Slope Angle (OSA) of 43° according to the slope geometry. Figure 3-7a illustrates various shapes of PDFs that might fit the observed data for equivalent cohesion. However, it can be observed that Lognormal and Gamma distributions provided better approximation to fit the data compared with other distributions. These

PDFs were further subjected to goodness of fit tests. The Kolmogorov-Smirnov test at the 5% significance level was performed to enhance the selection of a fitted distribution to cohesion results. Results for the Lognormal distribution (test statistics 0.08 and a p-value 5.0E-06) and for the Gamma distribution (test statistics 0.11 and a p-value 2.1E-11) reject the null hypothesis indicating discrepancy between the observed cohesion results and the theoretical distribution. However, as the p-value for the Lognormal distribution is greater than the p-value for Gamma, a Lognormal distribution was selected to fit the observed data with a mean of 0.69 MPa and COV of 0.33. Figure 3-7b presents different shapes of PDFs that might fit the observed data for equivalent friction angle. The goodness of fit test results from the Kolmogorov-Smirnov test for the Normal distribution (test statistics 0.02 and a p-value 0.58) and for the Lognormal distribution (test statistics 0.04 and a p-value 0.08) fail to reject the null hypothesis. As the p-value for the Normal distribution is greater than the p-value for Lognormal distribution, the observed data is suggested to be better represented with a Normal distribution with a mean of 56° and COV of 0.09. Figure 3-7c and 7d show the Q-Q plots used to evaluate the goodness of fit for the resulting cohesion and friction values. Table 3-2 summarizes the Hoek-brown strength parameters and the equivalent linear Mohr-Coulomb parameters.

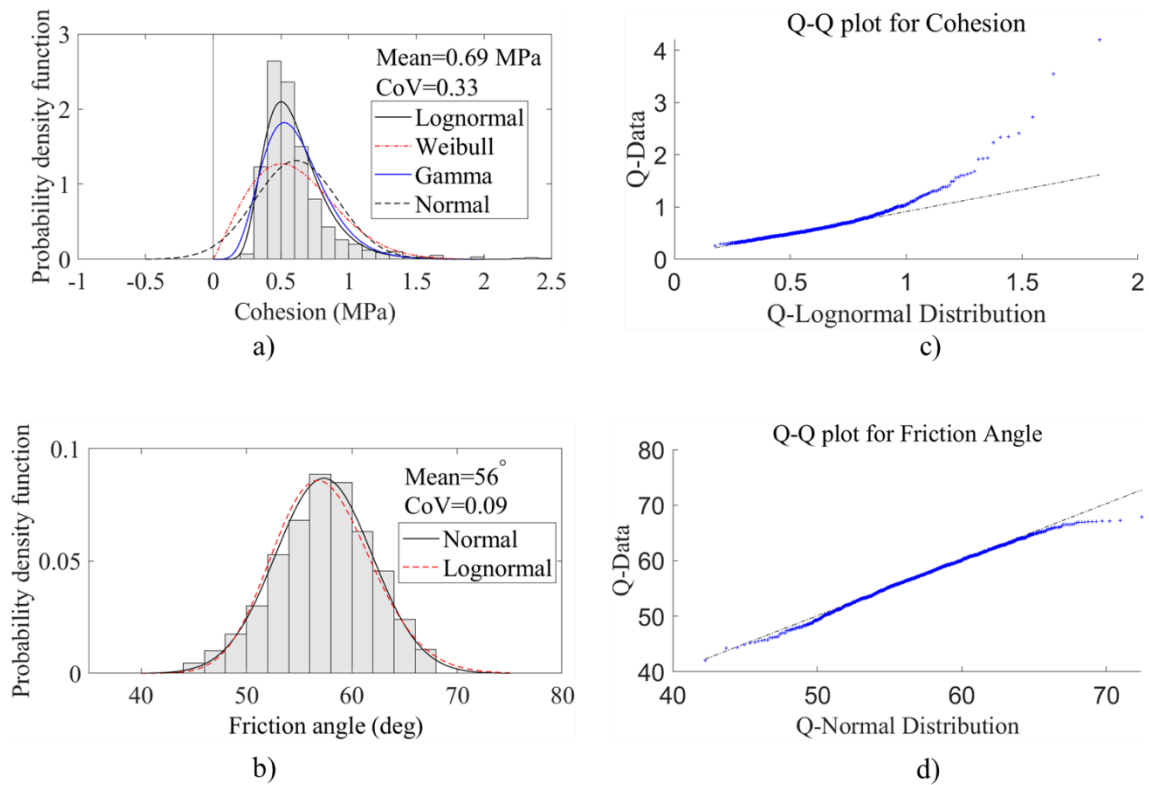


Figure 3-7: Calculated equivalent Mohr-Coulomb parameters and goodness of fit assumed in scenario 1: a) PDFs for cohesion, b) PDFs for friction angle, c) the Q-Q plot for Cohesion, d) the Q-Q plot for Friction angle

Table 3-2: Summary of Hoek-Brown parameters and Mohr-Coulomb parameters for the rock mass assumed in scenario 1

Rock unit	Hoek-Brown parameters					Mohr-Coulomb parameters			
	UCS (MPa)		m_i		GSI	Cohesion (MPa)		Friction angle (deg)	
	mean	COV	mean	COV		mean	COV	mean	COV
Granodiorite	70	0.90	26	0.31	[35,55]	0.69	0.33	56	0.09

The calculated equivalent Mohr-Coulomb parameters are used as input variables to perform probabilistic analysis. The geometry, lithology, and critical failure surface are shown in Figure 3-8. The corresponding slip surface shears entirely on rock mass exhibiting a non-circular failure surface. The results of the probabilistic analysis indicate a mean value of FoS relatively high for this configuration

(2.62), which can be categorized as excessive. The resultant value of PoF is very small. From this result, the design of the OSA would have been deemed too conservative suggesting slope modification, most likely with a slope governed by bench geometry and ramp requirements. However, this generic slope configuration should only be considered as preliminary geometry due to the source of information was not site-specific, and the objective of the analysis was to inspect the resulting distribution of FoS based on the assumptions of limited engineering effort under the assumptions of no structural control.

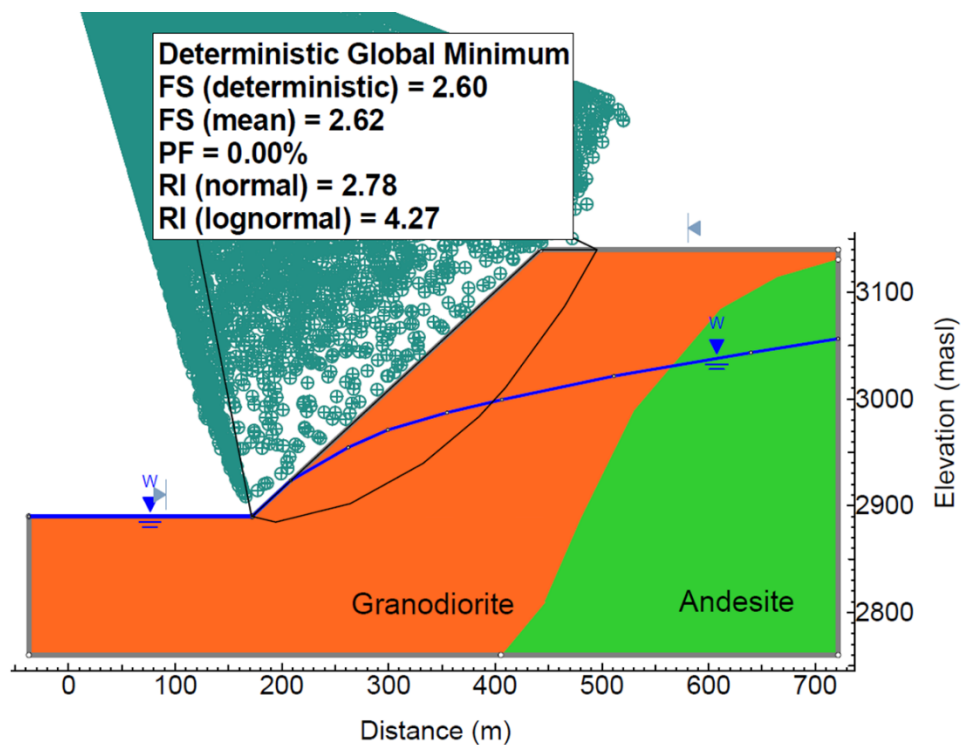


Figure 3-8: Limit equilibrium analysis result for rock mass strength failure, scenario 1

The results from the Monte Carlo simulation are shown in Figure 3-9a following a Lognormal distribution. Figure 3-9b shows the Q-Q plot to test the goodness of fit. In addition, to enhance the confidence of the fitted distribution, the Kolmogorov-Smirnov test results for Lognormal distribution (test statistics 0.03 and a p-value 0.52) fail to reject the null hypothesis, thus suggesting evidence that the observed data can be adequately fitted by a Lognormal distribution. Although the FoS for this configuration was relatively high, the calculated COV_{FoS} is consistent with the high COV values assumed for limited engineering effort and moderate design reliability in Macciotta et al. (2020).

Furthermore, for this case the resulting FoS fitted a Lognormal distribution as had been assumed in their work.

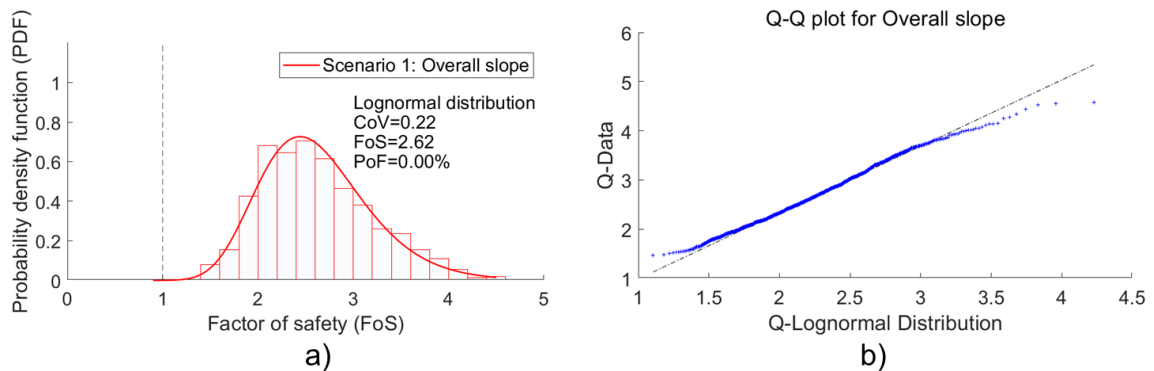


Figure 3-9: a) Calculated distribution of FoS for scenario 1 considering failure through the rock mass. b) The Q-Q plot of the Lognormal distribution fit

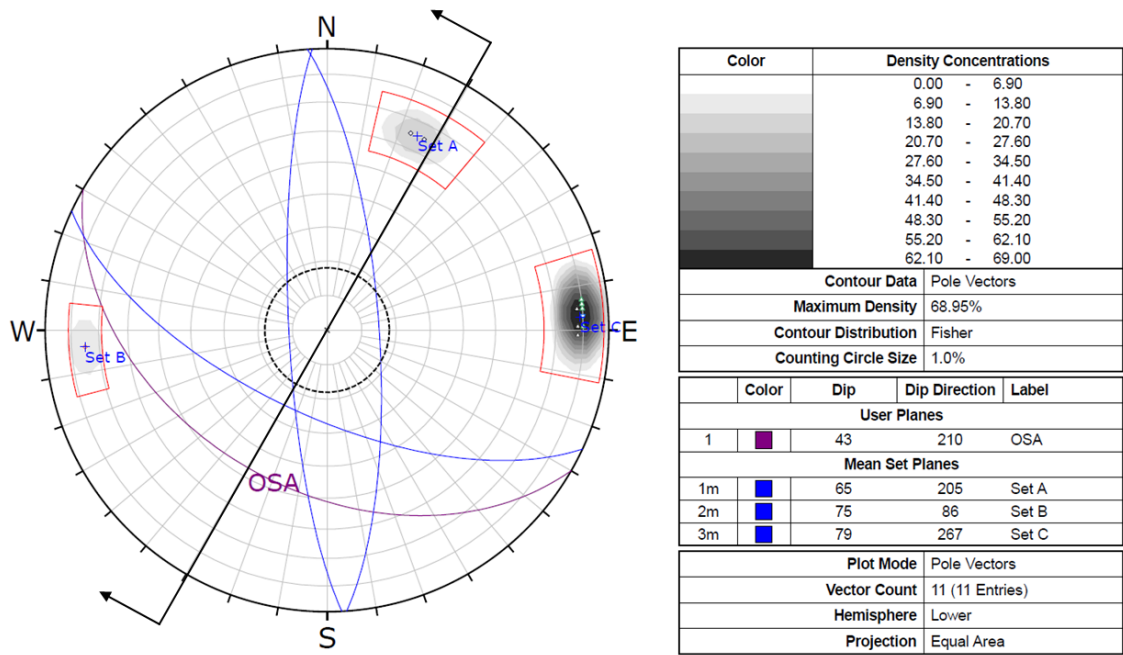
3.5.1.1 Structural Controlled Mechanisms

The second analysis in this scenario involves the evaluation of structurally controlled failure based on the regional structural data, as shown in Figure 3-10a. This figure shows the contoured stereographic projection of the large-scale structures and the orientation of the slope. This representation of structures based on a regional scale contains information about possible structural association with a local scale presented in subsequent scenarios. Three main structural sets are identified. Set A strikes east-southeast and dips moderately to the south-southwest. This set strikes nearly perpendicular to the slope and is favourably oriented with respect to the stability of the slope. Set B and Set C strike north-south and dip steeply to the east and west, respectively. Both sets strike obliquely into the slope. Set A and Set C could potentially form moderately plunging planar or wedge failures. Figure 3-10b shows the kinematic window considered for incorporating such structures into the stability analysis. Review of Figure 3-10b indicates that Set A is a slope-parallel structure considered as a non-daylighting structure, but its interaction with rock mass fabric can contribute to develop a structurally controlled failure. The integration of this structural feature into the slope stability analysis is through the Generalized Anisotropic Strength. It considers a preferred failure direction based on discrete angular ranges of the large-scale structure orientations as the shear strength is expected to be

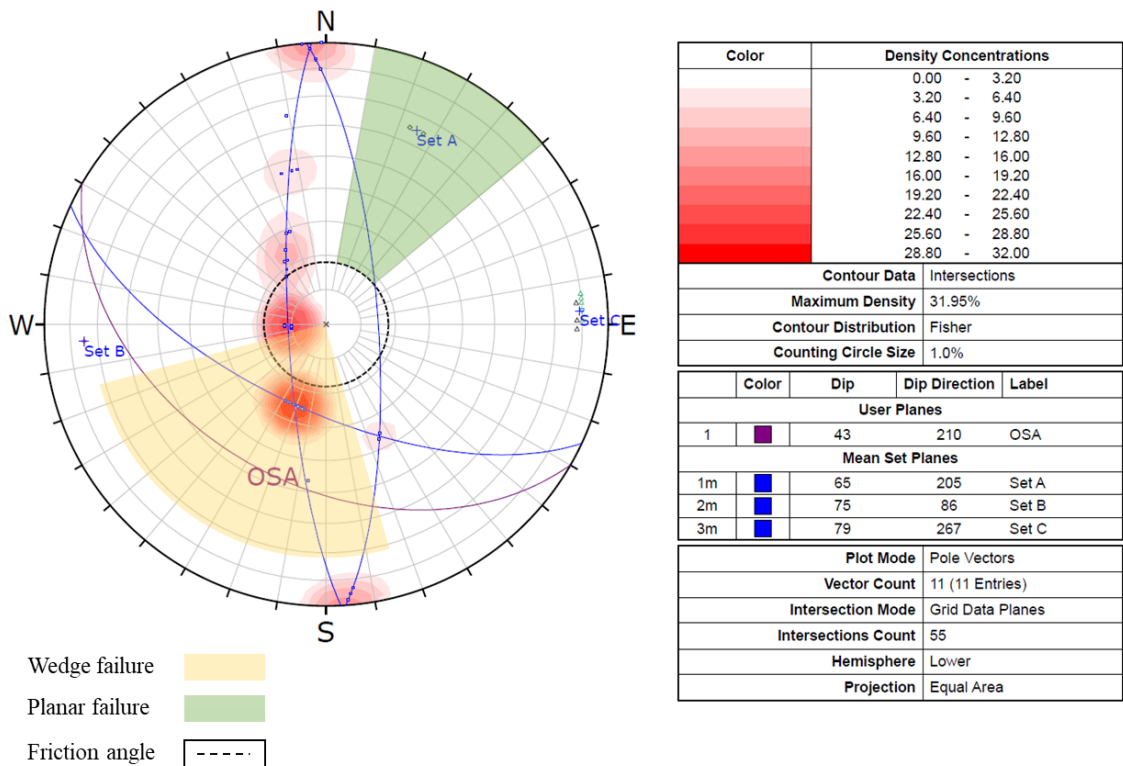
weaker in their direction. The shear strength of the large-scale structures was considered as cohesionless with a friction angle of 18° (Flores and Karzulovic, 2000; Valdivia and Lorig, 2000), assuming clay gouge that has undergone shear deformation. From Figure 3-10a, it can be seen that the plotted discontinuity normal or poles over the hemispherical projection is not widely scattered, and the clusters identified by the sampling window are defined by a group of subparallel discontinuities. As such, the statistical evaluation following the mean and standard deviation of the angles (dip direction, dip) reflect low variability. Table 3-3 summarises the orientation ranges and their 99% confidence limits. The orientation range of Set A was incorporated into the slope stability as a discrete value (not stochastic).

Table 3-3: Orientation of principal large-scale structures, scenario 1

Fault planes		
System	Dip ($^\circ$)	Dip direction ($^\circ$)
Set A	65 ± 4	205 ± 2
Set B	75	86
Set C	79 ± 3	267 ± 4
Wedge-type structure		
System	Plunge ($^\circ$)	Trend ($^\circ$)
Set A and Set C	65 ± 2	200 ± 22



a)



b)

Figure 3-10: Scenario 1: a) Main structural orientation of large-scale structures. b) Structural orientation of Planar/Wedge-type structures. OSA is the overall slope angle and orientation

The shape and location of the failure surface for the overall scale is shown in Figure 3-11. The resulting failure mechanism is relatively deep and exhibits characteristics of a rotational shear. It

primarily involves a pre-aligned non-daylighting structure and rock mass. This can be considered a plausible failure mechanism given conditions of the rock mass units and structural features of Set A.

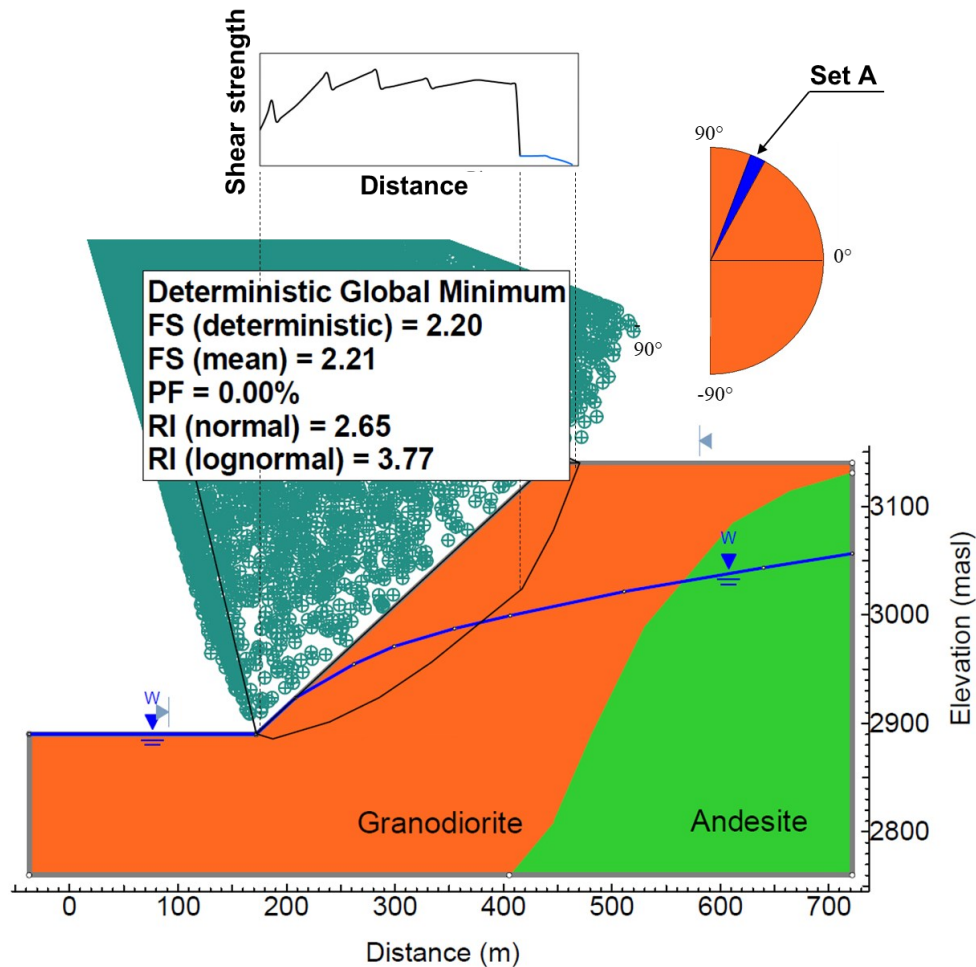


Figure 3-11: Limit equilibrium analysis result for structurally controlled failure, scenario 1

The mean FoS when considering structure is approximately 16% lower than the model for isotropic strength. The variation of PoF between both analyses is negligible; both are very small. The results of the Monte Carlo simulation are shown in Figure 3-12a. Additionally, the Kolmogorov-Smirnov test for the fitted Lognormal distribution resulted in test statistics of 0.02 and a p-value 0.68, therefore failed to reject the null hypothesis suggesting evidence that the observed data follow a Lognormal distribution. Figure 3-12b shows the Q-Q plot of the fitted distribution. The COV_{FoS} is 0.21, 5% lower than the previous analysis. This value corresponds to Moderate design reliability according to Macciotta, 2020.

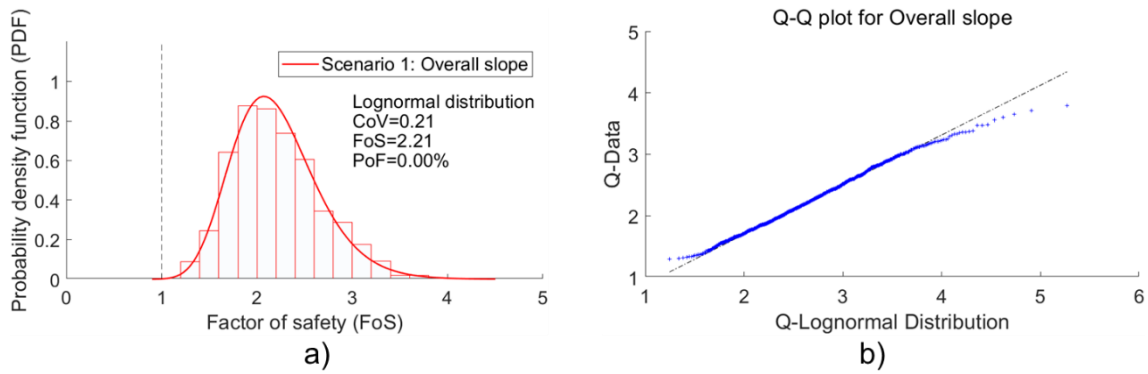


Figure 3-12: a) Calculated distribution of FoS for scenario 1 considering structurally controlled failure. b) The Q-Q plot of the distribution fitted

3.5.2 Second scenario: increased design reliability

The COV for the UCS and m_i were obtained from the site-specific information. The COV_{UCS} ranges between 0.26 and 0.40. This paper adopts a COV_{UCS} of 0.40 for both lithological units. These COV_{UCS} are assumed to follow a Lognormal distribution. The site-specific GSI has a COV of 0.16 and 0.10 for granodiorite and andesite, respectively. In this scenario, these values are considered to follow Normal distribution.

The PDF of m_i was built assuming COV ranges between 0.20 and 0.25, according to the literature on typical m_i variability discussed earlier. In this scenario, a PDF with a COV of 0.20 and Lognormally distributed was adopted. Table 4 shows the mean and COV adopted for defining the Hoek-Brown envelopes. Dependence between UCS and m_i was applied to obtain the Hoek-Brown envelopes. The confining stress was calculated using Eq. (10) for a height of 255 m and OSA of 36° according to the overall slope geometry. The resulting PDF of the equivalent Mohr-Coulomb parameters and the Q-Q plots for the fitted distributions for the granodiorite unit are shown in Figure 3-13. For the granodiorite rock unit, Kolmogorov-Smirnov test results for cohesion following a Lognormal distribution (test statistics 0.03 and a p-value 0.28) and for friction angle following a Normal distribution (test statistics 0.03 and a p-value 0.26) fail to reject the null hypothesis, thus suggesting evidence that both parameters follow these specific distributions.

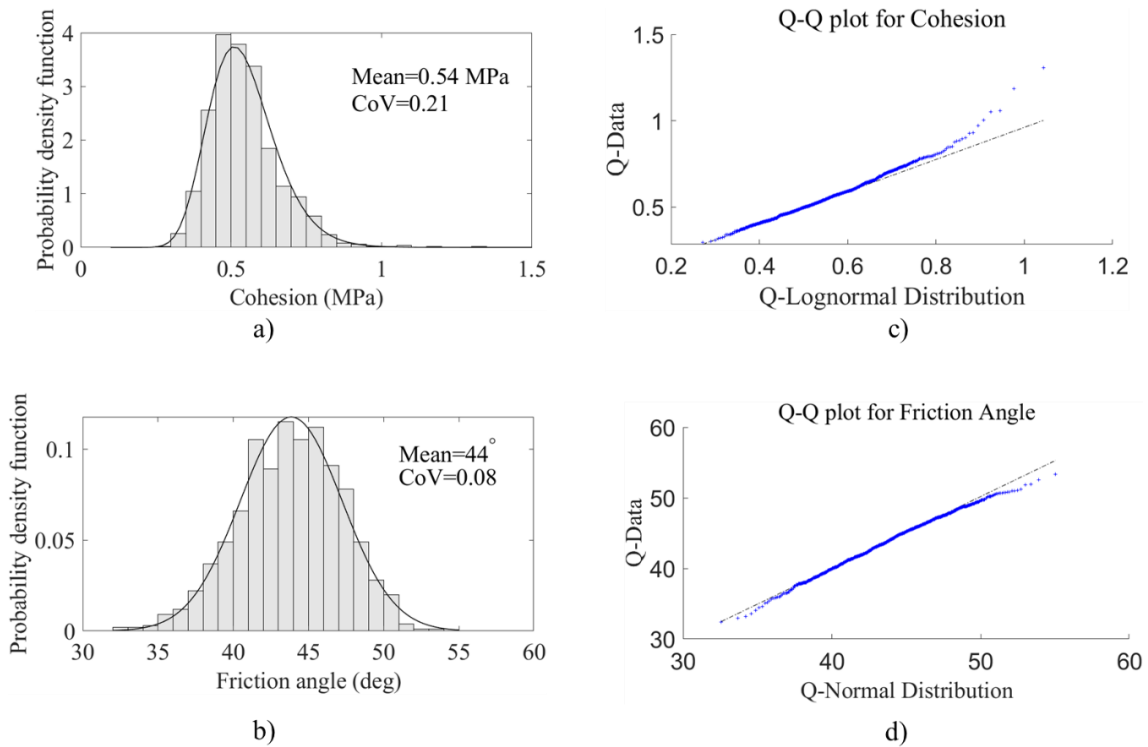


Figure 3-13: PDFs of equivalent Mohr-Coulomb parameters for granodiorite unit assumed in scenario 2: a) Cohesion and b) Friction angle. The Q-Q plots for: c) cohesion and d) friction angle

The distributions of equivalent Mohr-Coulomb parameters and the Q-Q plots for the andesite unit are shown in Figure 3-14. Kolmogorov-Smirnov test results for cohesion following a Lognormal distribution (test statistics 0.03 and a p-value 0.21) and for friction angle following a Normal distribution (test statistics 0.02 and a p-value 0.88) suggest that both cohesion and friction angle follows these specific distributions.

For both rock units, the PDF of the equivalent cohesion is best fitted with a Lognormal distribution whereas equivalent friction angle is best fitted with a Normal distribution. It is important to notice, that the equivalent Mohr-Coulomb parameters presented in Figure 3-13 and Figure 3-14 remain constant under the degree of confinement stress calculated in this scenario. Therefore, any slope height lower than the overall slope height adopts the same Mohr-Coulomb parameters and their respective distributions. This is common in industry practices. Table 3-4 summarizes the Hoek-brown strength parameters and the equivalent linear Mohr-Coulomb parameters.

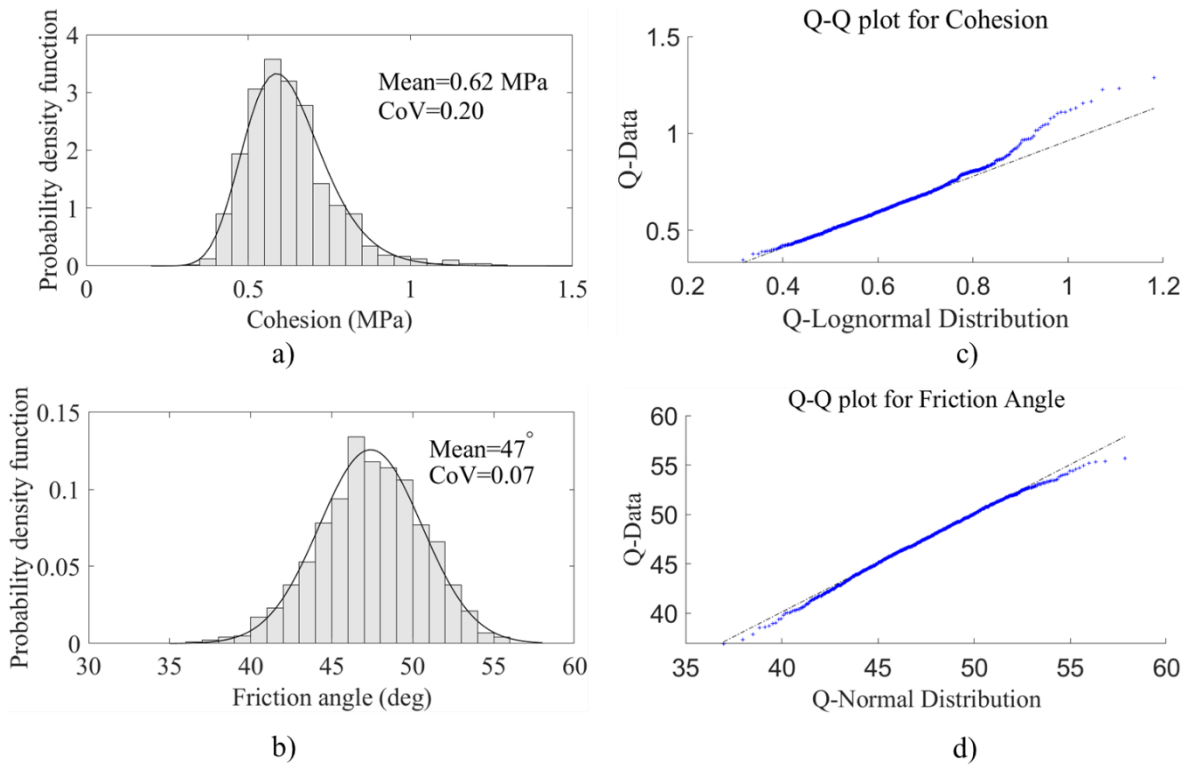


Figure 3-14: PDFs of equivalent Mohr-Coulomb parameters for andesite unit assumed in scenario 2: a) cohesion and b) friction angle. The Q-Q plots: c) cohesion and d) friction angle

Table 3-4: Summary of Hoek-Brown parameters and Mohr-Coulomb parameters assumed in scenario 2

Rock unit	Hoek-Brown parameters						Mohr-Coulomb parameters			
	UCS (MPa)		m_i		GSI		Cohesion (MPa)		Friction angle (deg)	
	mean	COV	mean	COV	mean	COV	mean	COV	mean	COV
Granodiorite	37	0.40	12	0.20	43	0.16	0.54	0.21	44	0.08
Andesite	42	0.40	15	0.20	45	0.10	0.62	0.20	47	0.07

The stability assessments were performed considering the natural variability of the granodiorite and andesite rock units. The geometrical configuration of the section evaluated comprised an OSA of 36° with a slope height of 255 m. Figure 3-15 shows the slope stability results for the given slope configuration. The failure surfaces for the lower and upper Inter-ramp slope, and Overall slope, are non-circular and shear entirely through the rock mass which represents a mix of intact rock and smaller-

scale discontinuities not explicitly mapped at this level of design reliability. Resulting FoS indicate a stable configuration, with relatively high FoS, particularly at the upper Inter-ramp slope. The results obtained from the Monte Carlo simulation are shown in Figure 3-16a-c. The best fit PDF are also shown in this figure. Kolmogorov-Smirnov test results of the Overall slope (test statistics 0.03 and a p-value 0.57), lower Inter-ramp slope (test statistics 0.03 and a p-value 0.56), and upper Inter-ramp slope (test statistics 0.02 and a p-value 0.85) suggest strong approximation to the Lognormal distribution. The Q-Q plots for the distribution fits shown in Figure 3-16d-f also suggest that a Lognormal distribution fit well the resulting distribution of FoS. The calculated COV_{FoS} is 0.12 for the Overall slope and lower Inter-ramp slope, whereas the COV_{FoS} is 0.16 for the upper Inter-ramp slope.

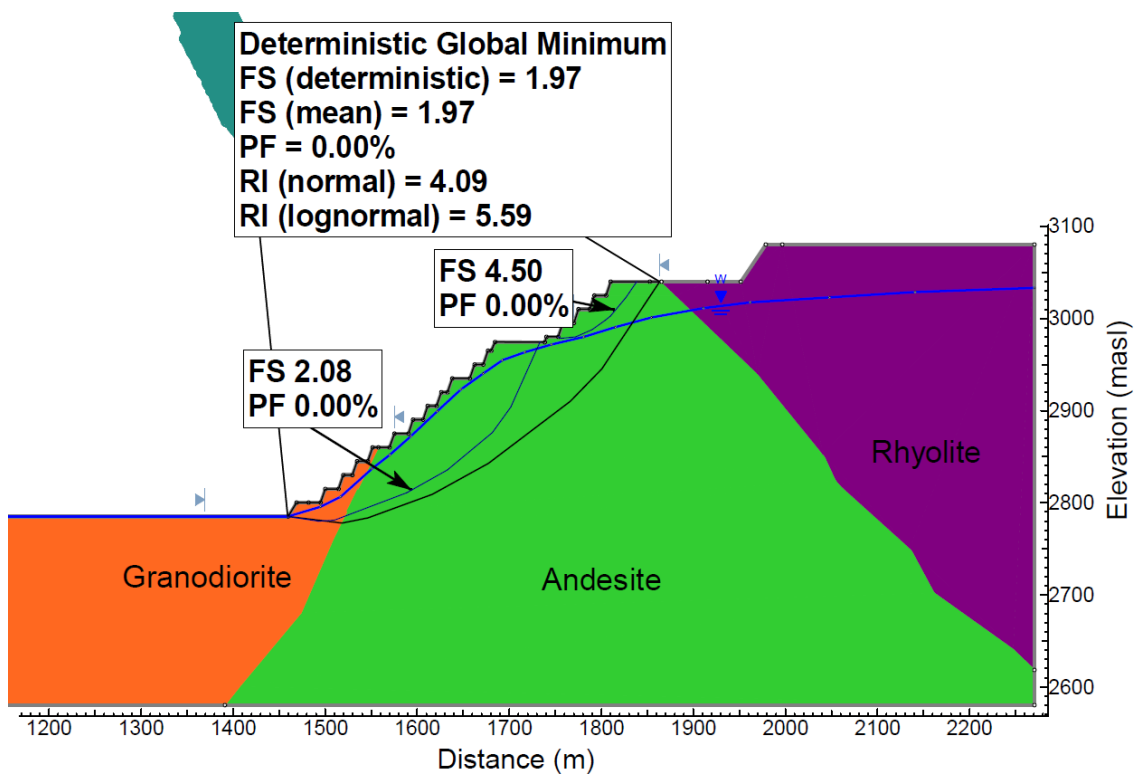


Figure 3-15: Limit equilibrium analysis result for rock mass strength failure, scenario 2

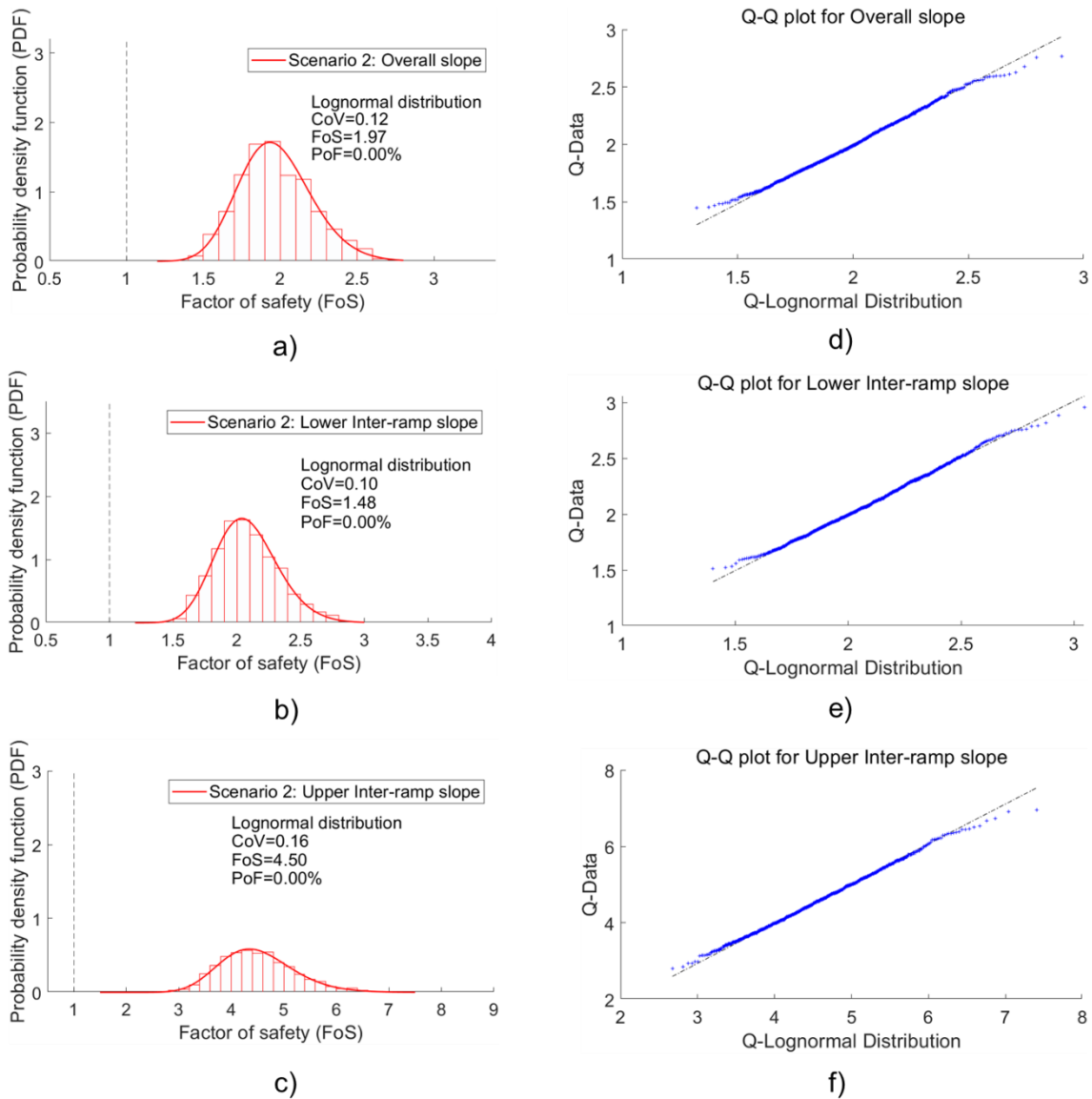


Figure 3-16: Calculated distribution of FoS for scenario 2 considering rock mass strength failure for: a) Overall slope, b) Lower Inter-ramp slope, and c) Upper Inter-ramp slope. The Q-Q plot of the distribution fitted for each Monte Carlo simulation: d) Overall slope, e) Lower Inter-ramp slope, and f) Upper Inter-ramp slope

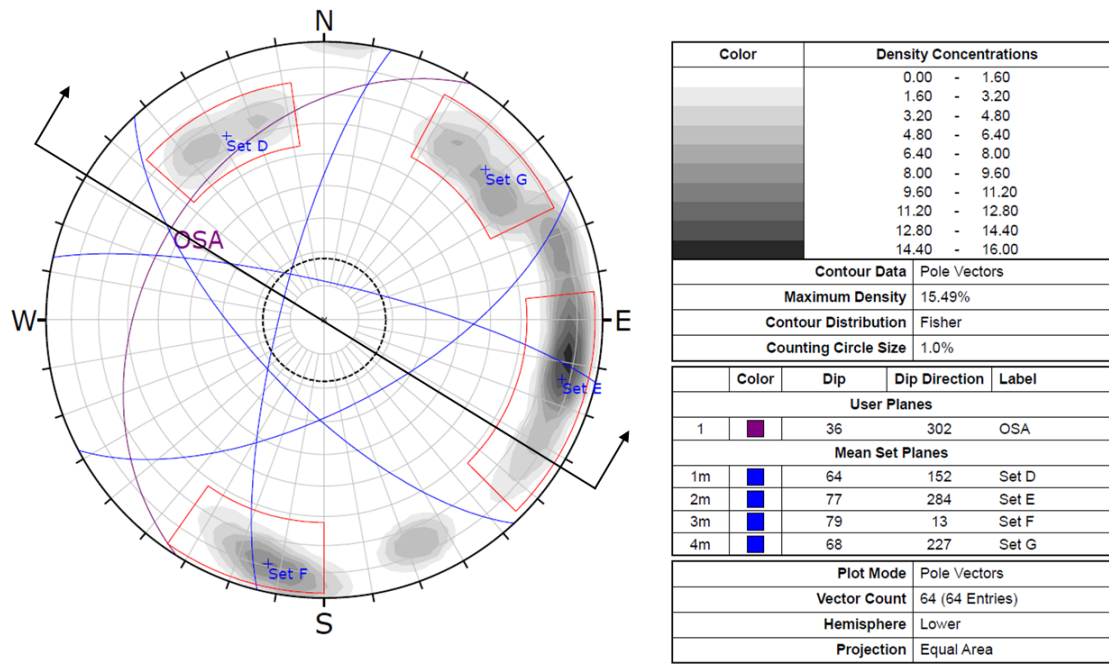
3.5.2.1 Structural Controlled Mechanisms

Integration of large-scale structures considered site-specific data from structural mapping, as presented in Figure 3-17a. Four main structural sets are identified. Set D strikes east-northeast and dips moderately to the southeast. Set E strikes south dipping steeply to the west, this set strikes perpendicular into the slope. Set F strikes west and dips steeply to the north. Set G strikes south-southeast and dips moderately to steeply to the southwest. Set F and set G could form moderately

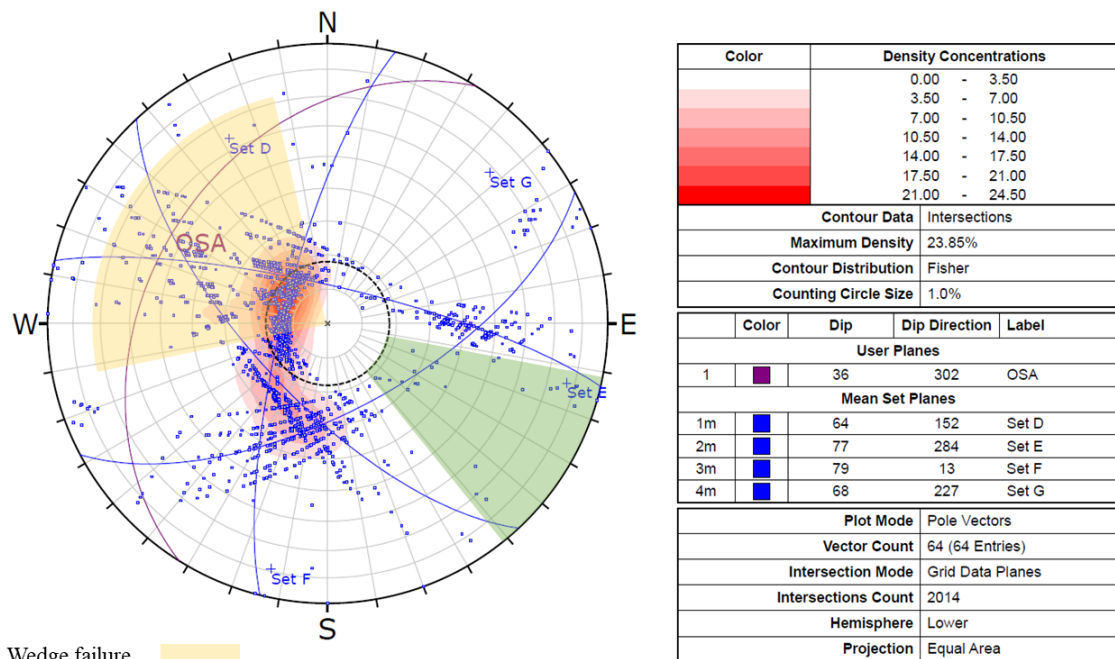
plunging wedge failures whereas Set E and Set F could form steeply plunging wedge failures. The kinematic window considered for incorporating such structures into stability analysis is shown in Figure 3-17b. Set E is a non-daylighting planar structure and the wedges of Set E combining with Sets F and G are non-daylighting structures as well, although they could contribute to develop multi-bench instability particularly considering breakage of rock bridges. Table 3-5 summarizes the orientation ranges and their 99% confidence limits. Discrete orientation ranges of Set E and the wedge-type structure formed of Set E and Set G were incorporated into slope stability analyses through generalized anisotropic strength as they were considered of primarily importance in the slope stability given the geometric interpretation discussed.

Table 3-5: Orientation of principal large-scale structures, scenario 2.

Fault planes		
System	Dip (°)	Dip direction (°)
Set D	64±9	152±12
Set E	77±6	279±12
Set F	78±6	13±9
Set G	67±7	226±12
Wedge-type structure		
System	Plunge (°)	Trend (°)
Set E and Set F	74±1	295±20
Set E and Set G	49±2	283±25



a)



Wedge failure
 Planar failure
 Friction angle

b)

Figure 3-17: Scenario 2: a) Main structural orientation of large-scale structures and b) Structural orientation of Planar/Wedge-type structures

The result of the stability analysis is shown in Figure 3-18. The FoS indicates stable conditions for lower and upper Inter-ramp slope, and Overall slope when considering feasible kinematic failures and modelled as generalized anisotropic strengths. The mean global FoS is greater than 1.4 and all the

slip surfaces shear through the rock mass and along the modelled anisotropy that corresponds to the wedge-type structure. The results show a clear reduction in mean FoS from 1.97 to 1.52 in comparison with results from Figure 3-15. The PoF is very small in both analyses.

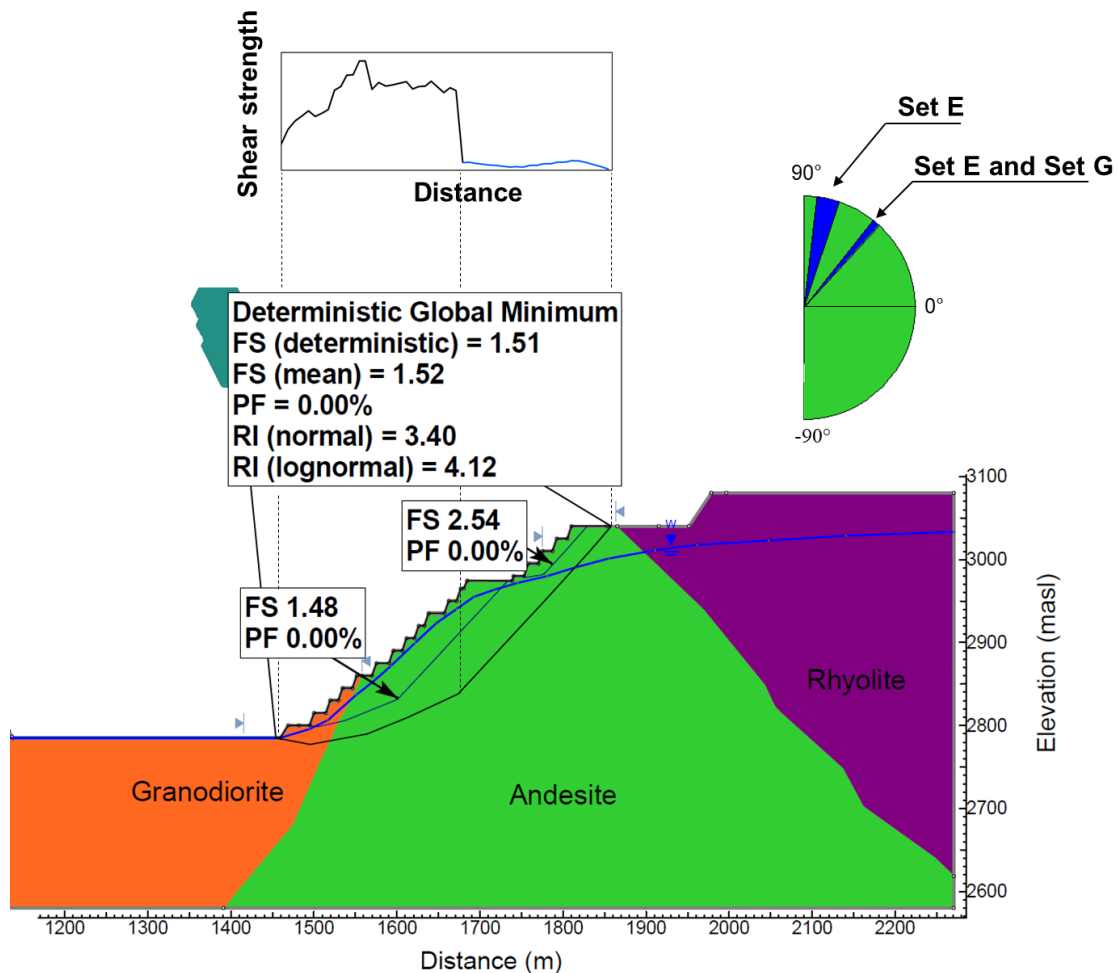


Figure 3-18: Limit equilibrium analysis results for structurally controlled failure, scenario 2

The resulting FoS PDF, fitted distribution and corresponding Q-Q plot; are shown in Figure 3-19. Kolmogorov-Smirnov test results for Overall slope (test statistics 0.02 and a p-value 0.69), lower Inter-ramp slope (test statistics 0.03 and a p-value 0.53), and upper Inter-ramp slope (test statistics 0.03 and a p-value 0.51) suggest that the Lognormal distribution provide an adequate fit. The COV_{FoS} ranges between 0.10 and 0.13 depending on the scale and location of the failure surface. There is a drop in the COV_{FoS} in comparison with the analysis in Figure 3-16, 17% for the Overall slope and lower Inter-ramp

slope, and 19% for the upper Inter-ramp slope. The drop is caused by the explicit inclusion of large-scale structures which start to dominate the failure surfaces.

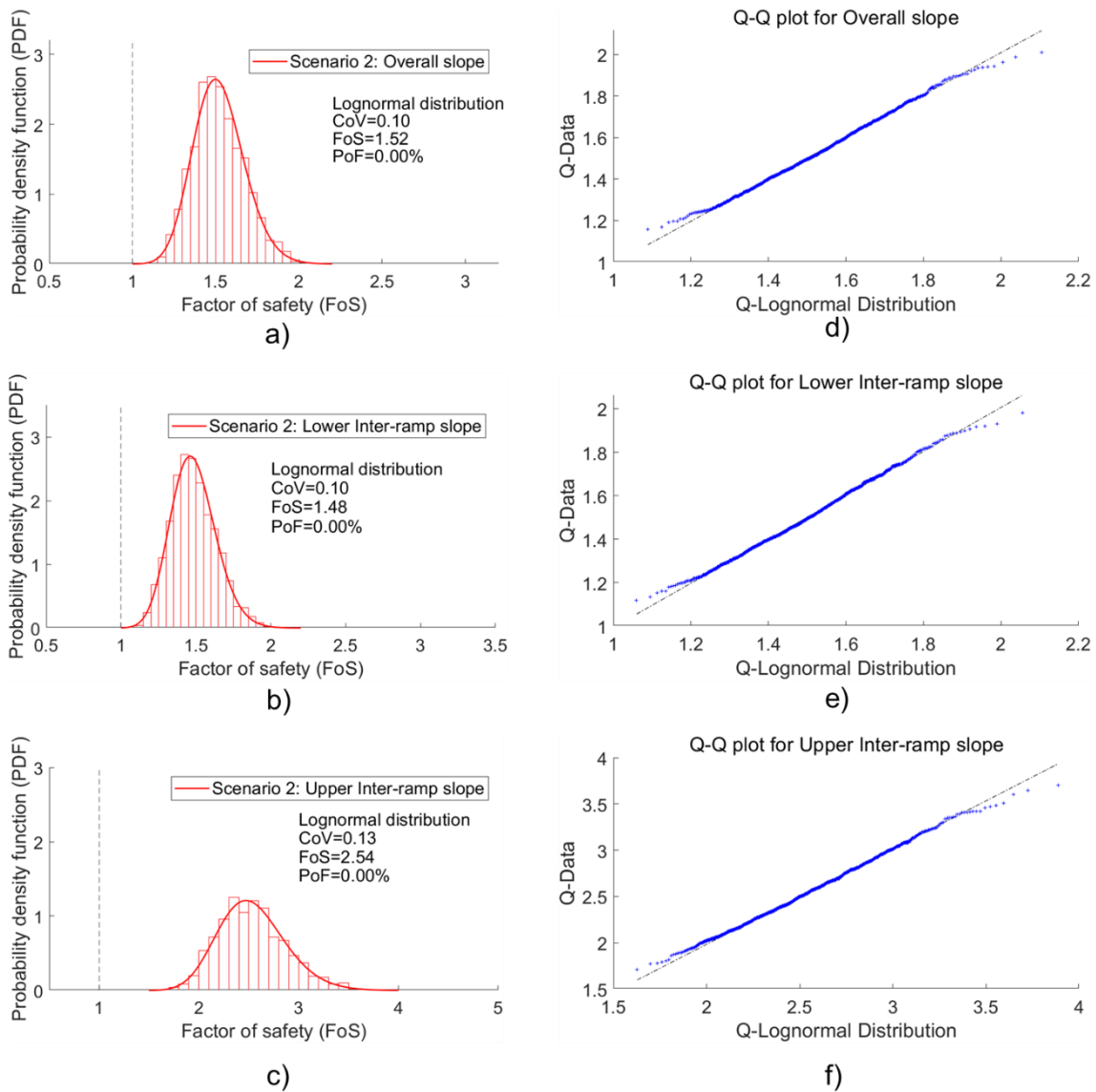


Figure 3-19: a) Calculated distribution of FoS distribution for scenario 2 considering structurally controlled failure for a) Overall slope, b) lower Inter-ramp slope, c) upper Inter-ramp slope. The Q-Q plot of the distribution fitted for each PDF d) Overall slope, e) lower Inter-ramp slope, f) upper Inter-ramp slope

3.5.3 Third scenario: Very high design reliability at mature phase of operations

The calibrated parameters for the third scenario are summarized in Table 3-6, the lithological units are subdivided in more domains according to the type of alteration. Geomechanical parameters are expressed in terms of equivalent cohesion and friction angle. The PDF assigned to these parameters

were based in the information of COV obtained for the original base case study. The COV is less than 0.15 and less than 0.10 for equivalent cohesion and friction angle, respectively. Unfortunately, no exact COV values were reported.

Table 3-6: Calibrated rock mass strength properties assumed in scenario 3, from Valdivia and Lorig (2000)

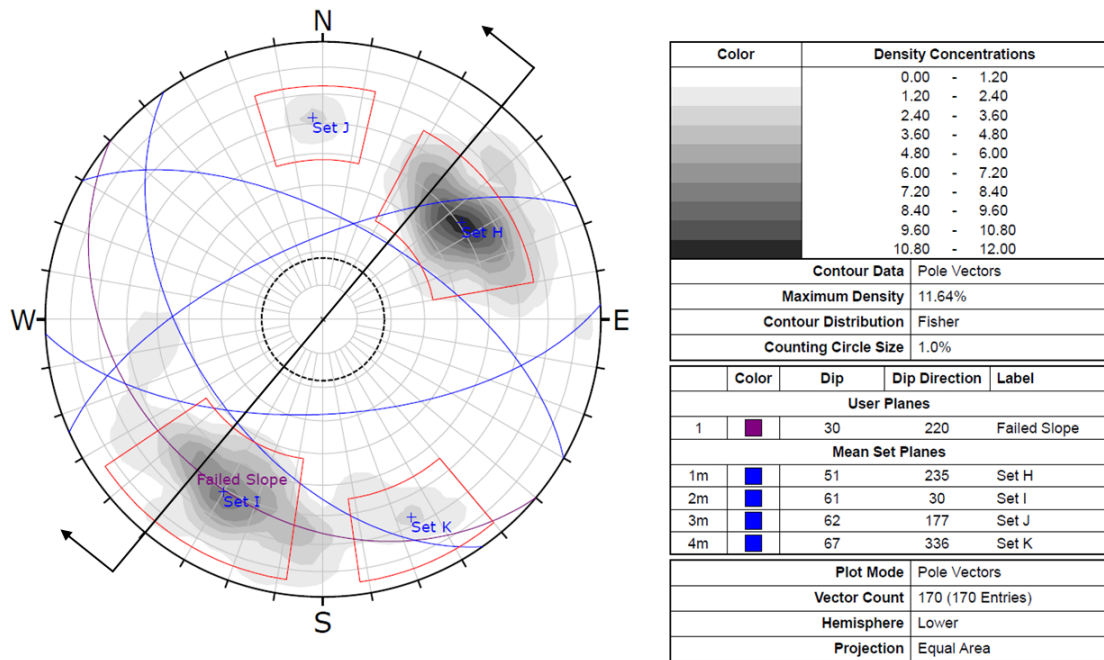
Rock unit	Mohr-Coulomb parameters			
	Cohesion (kPa)		Friction angle (deg)	
	mean	CoV	mean	CoV
Altered granodiorite	40	<0.15	25	<0.10
Moderate granodiorite	150	<0.15	28	<0.10
Silificated granodiorite	780	<0.15	36	<0.10
Andesite	150	<0.15	31	<0.10

The structural model adopted in this scenario is less uncertain due to the quality of information utilized, including fault outcrop mapping, core evaluation, and acoustic televiewer surveys. This leads to a higher reliability of structure characteristics.

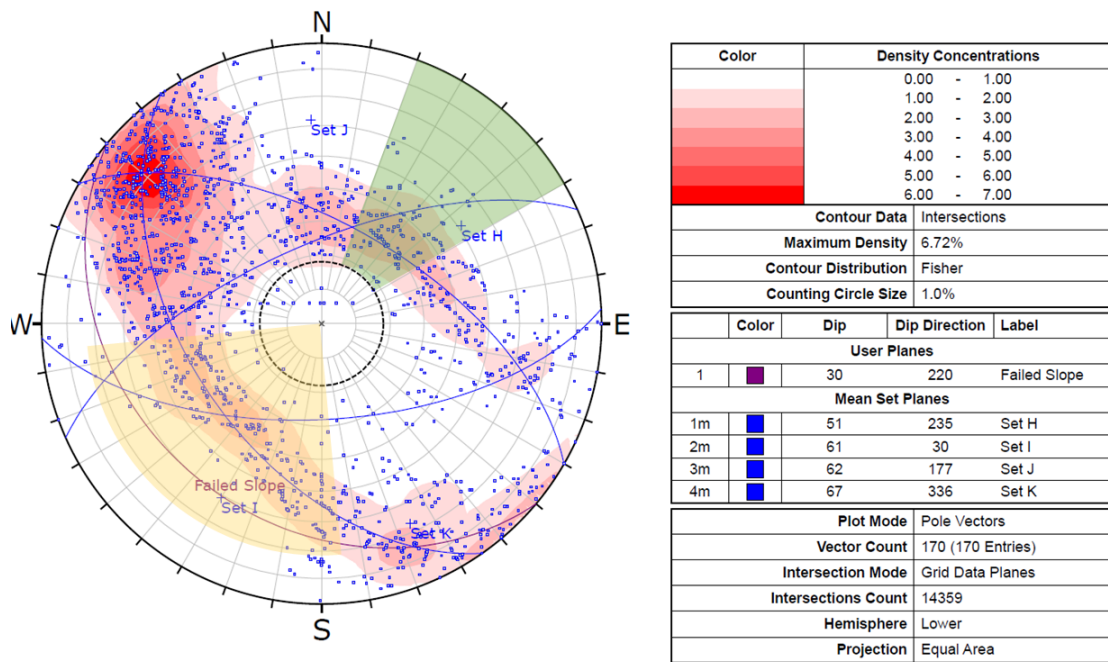
The results of the statistical analysis of the structures mapped and the kinematic analyses relative to the orientation of the pit slope are shown in Figure 3-20. Set H strikes south-southeast and dips moderately to the southwest. This set strikes almost perpendicular to the slope and is favourably oriented in terms of kinematic stability. Set I strikes west-northwest and dips moderately to the northeast. Set J strikes east and dips moderately to the south. Set K strikes west-southwest and dips moderately to the northwest. Set H and Set J have the potential to form moderately plunging wedge failures. Set H is the most critical structure that influence the slope stability. Table 3-7 summarises the orientation ranges and their 99% confidence limits.

Table 3-7: Orientation of principal large-scale structures, scenario 3

Fault planes		
System	Dip (°)	Dip direction (°)
Set H	51±4	230±15
Set I	66±5	35±18
Set J	61±5	179±6
Set K	70±8	338±12
Wedge-type structure		
System	Plunge (°)	Trend (°)
Set H and Set J	47±1	219±10



a)



Wedge failure
 Planar failure
 Friction angle

b)

Figure 3-20: Scenario 3: a) Main structural orientation of large-scale structures and b) structural orientation of Planar/Wedge-type structures

Set H was incorporated in the limit equilibrium analysis implicitly through generalized anisotropic strength. It is noteworthy that generalized anisotropic strength does not consider the

continuity of the structures, this can impact the extent and shape of the critical failure surface. The results of the critical failure surface and the strong influence of the large-scale structures in the instability developed are shown in Figure 3-21. The mean FoS is 0.98 with a PoF of 63.30%. The results of the Monte Carlo simulation for this scenario and their best fit PDF (Normal distribution in this scenario) are shown in Figure 3-22a. Kolmogorov-Smirnov test results (test statistics 0.03 and a p-value 0.50) suggest the adequacy of the Normal distribution to fit the results. The Q-Q plot to evaluate the goodness of fit is shown in Figure 3-22b. This plot also suggests the distribution fit is adequate.

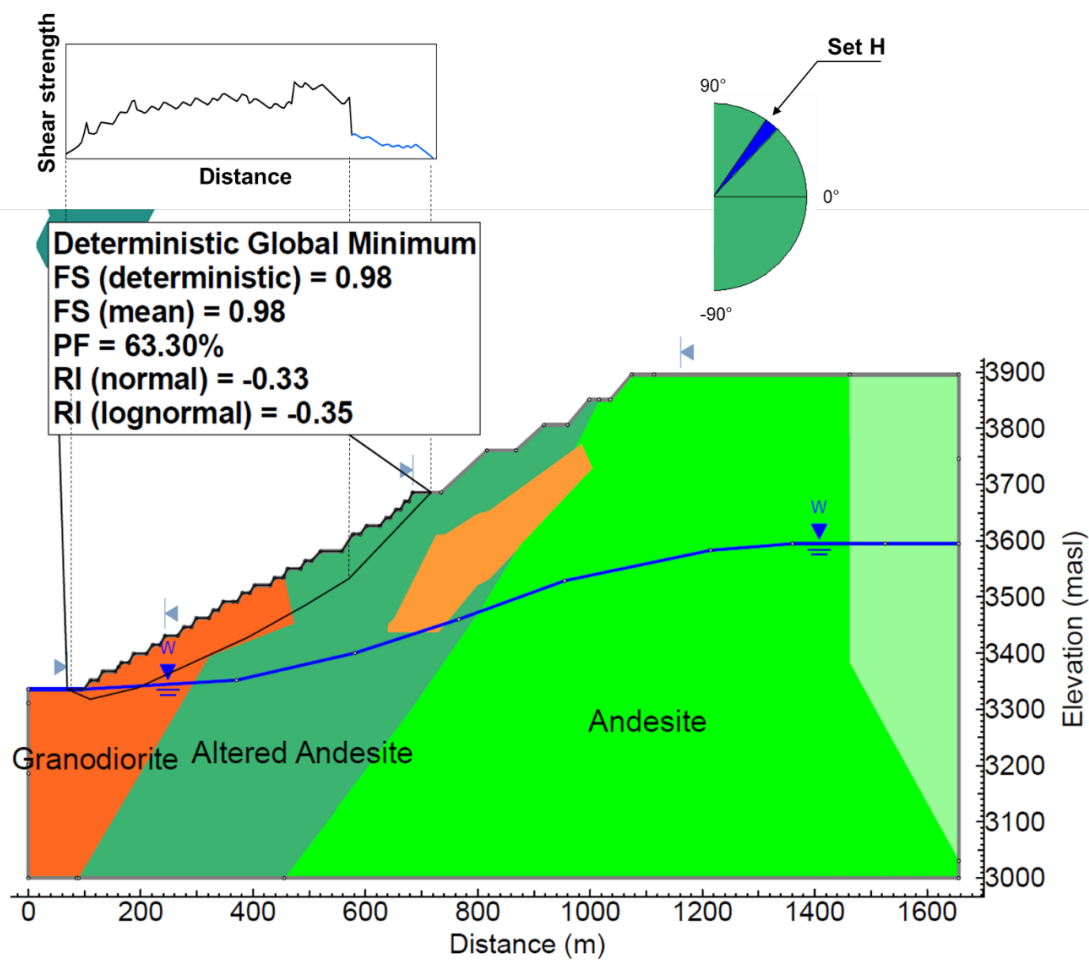


Figure 3-21: Limit equilibrium results of back analysis considering large-scale structures implicitly, scenario 3

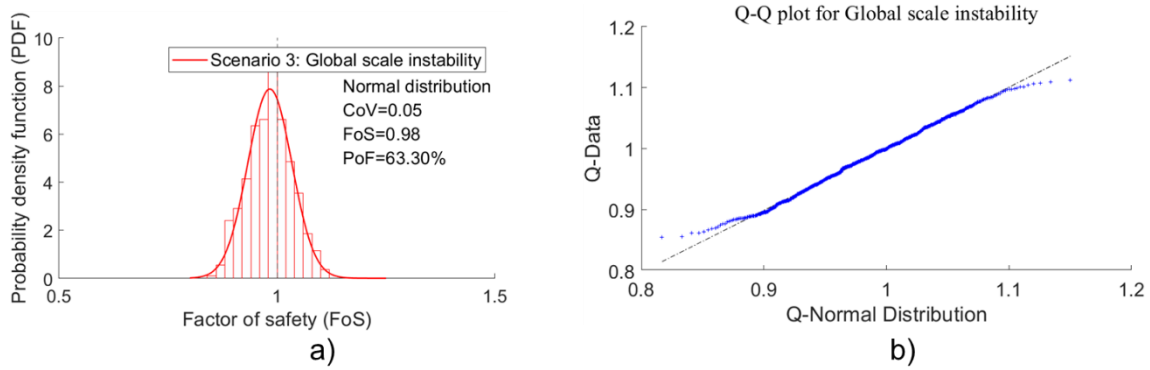


Figure 3-22: a) Calculated distribution of FoS for scenario 3 considering large-scale structures implicitly. b) The Q-Q plot of the distribution fitted

Another approach for the stability calculation considered the large-scale structures in an explicit manner, with the aim to compare the results in terms of FoS, PoF and COV_{FoS} with the implicit approach. The results of this model are shown in Figure 3-23. The mean FoS is calculated at 1.01, PoF of 43.2% and a COV_{FoS} of 0.05. These values are similar to the implicit approach in terms of mean FoS. The distribution of FoS from the Monte Carlo simulation is shown in Figure 3-24 together with the best fit PDF and the Q-Q plot used to evaluate the goodness of fit. Kolmogorov-Smirnov test results (test statistics 0.03 and a p-value 0.53) suggest the results can adequately be fitted with a Normal distribution.

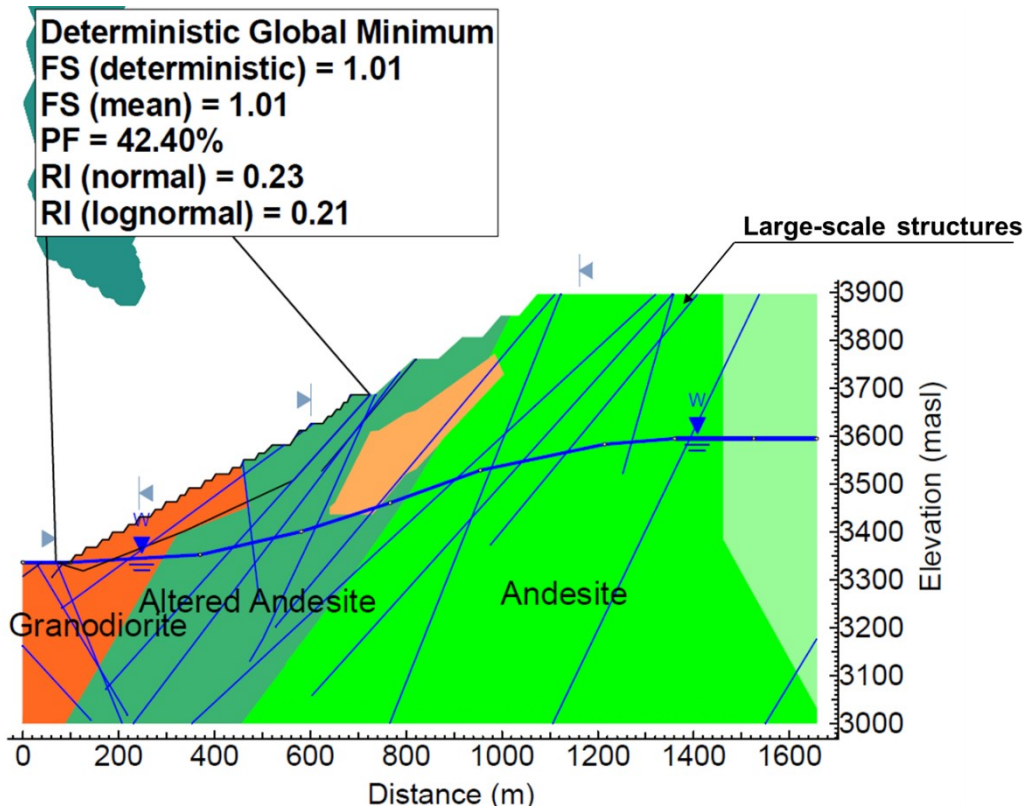


Figure 3-23: Limit equilibrium results of back analysis considering large-scale structures explicitly, scenario 3

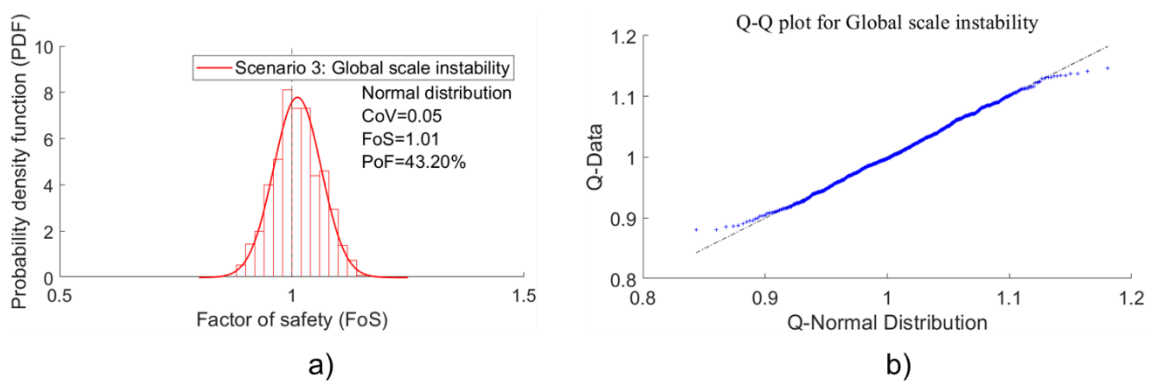


Figure 3-24: a) Calculated distribution of FoS for scenario 3 considering large-scale structures explicitly. b) The Q-Q plot of the distribution fitted

The resulting mean FoS and high PoF are expected given the definition of structure in this scenario reflects the most advanced knowledge in this sector of the pit, and the fact that a previous multi-bench failure had occurred under these geologic conditions and pit geometry; with input parameters corresponding to a previous back analysis. Although it is acknowledged that numerical

approaches are capable of better capturing failure mechanisms in rock slope failure that involve rock mass and discontinuities; the higher reliability in the model allowed for a representative analysis.

3.6 Reliability-Based DAC

As expected, these results suggest the integration of large-scale structures plays a significant role in the result of probabilistic slope stability analyses, and increased knowledge on structure, lithologic detail and parameters lead to the reduction of COV_{FoS} as it provides defined critical failure paths. The drop in COV_{FoS} also suggests an impact of the improved understanding of material parameters through back analyses and therefore further reduction in epistemic uncertainty. Nevertheless, uncertainty associated with the shear strength of large-scale structures was not part of the scope in this analysis and can play a significant role in the COV_{FoS} . The results from the three scenarios are presented in Figure 3-25. This figure illustrates the evolution of uncertainty in results as design and operations evolve. It is important to notice, however, that there are some differences in input parameters and the process of analysis among the different scenarios, which reflect some common practices. In this regard, the results in Figure 3-25 do not only represent uncertainty associated with parameters but also with processes and the knowledge available at the time of the assessments.

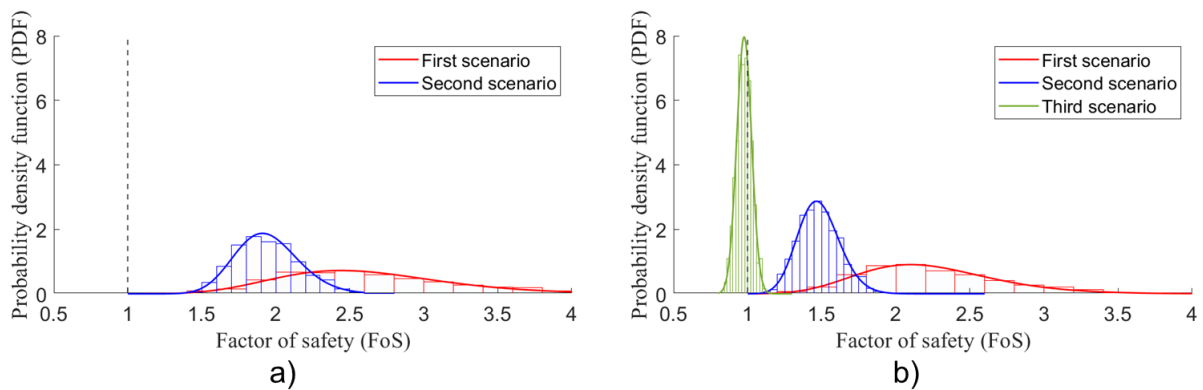


Figure 3-25: a) PDFs for overall scale of rock mass strength failure. b) PDFs for Overall slope of structurally controlled failure

The stability analysis results obtained from the three scenarios in Figure 3-25 have been summarized in Table 3-8, and plotted on the 2020 RBDAC in Figure 3-26. Values of FoS enclosed by parenthesis within the matrix indicate a mean value obtained from a Normal distribution, the other values indicate values obtained from Lognormal distributions. The results of COV_{FoS} and pairs of FoS-PoF for Scenarios 1 and 2 would correspond to the suggested ranges defined in the 2020 RBDAC matrix for very high economic consequence, although, some results are considered conservative (some results in scenarios 1 and 2). Scenario 3 is a special case that shows an unsuccessful performance of an implemented slope design. Results show that slope design did not meet either the 2009 DAC or 2020 RBDAC.

Table 3-8: Summary of FoS-PoF pairs and COV_{FoS} obtained from three scenarios evaluated

	Slope Design	Slope Height (m)	Slope Angle (deg)	Analysis	Factor of Safety (FoS)	Probability of Failure (PoF)	COV_{FoS}
Scenario 1	Overall Slope	250	43	Isotropic	2.62	0.00	0.22
				Anisotropic	2.21	0.00	0.21
Scenario 2	Overall Slope	255	36	Isotropic	1.97	0.00	0.12
				Anisotropic	1.52	0.00	0.10
	Upper Inter-ramp slope	66	41	Isotropic	4.50	0.00	0.16
				Anisotropic	2.54	0.00	0.13
	Lower Inter-ramp slope	189	41	Isotropic	2.08	0.00	0.12
				Anisotropic	1.48	0.00	0.10
Scenario 3	Overall Slope	560	30	Anisotropic	0.98	67.40	0.05
					1.01	43.20	0.05

Based on the results from Scenario 3, the higher reliability gained can be leveraged to develop a pushback without considering conservative geometry but an alternative that attempts to balance risk and reward. This can be achieved targeting the 2020 RBDAC.

The results of the parametric analysis plotted in the RBDAC matrix show the flexibility to understand a proposed geometry in light of knowledge and potential consequences, therefore facilitating risk-informed design processes. However, limits of the modelled uncertainty in the analyses need to be clearly understood when assessing slope designs using the 2020 RBDAC.

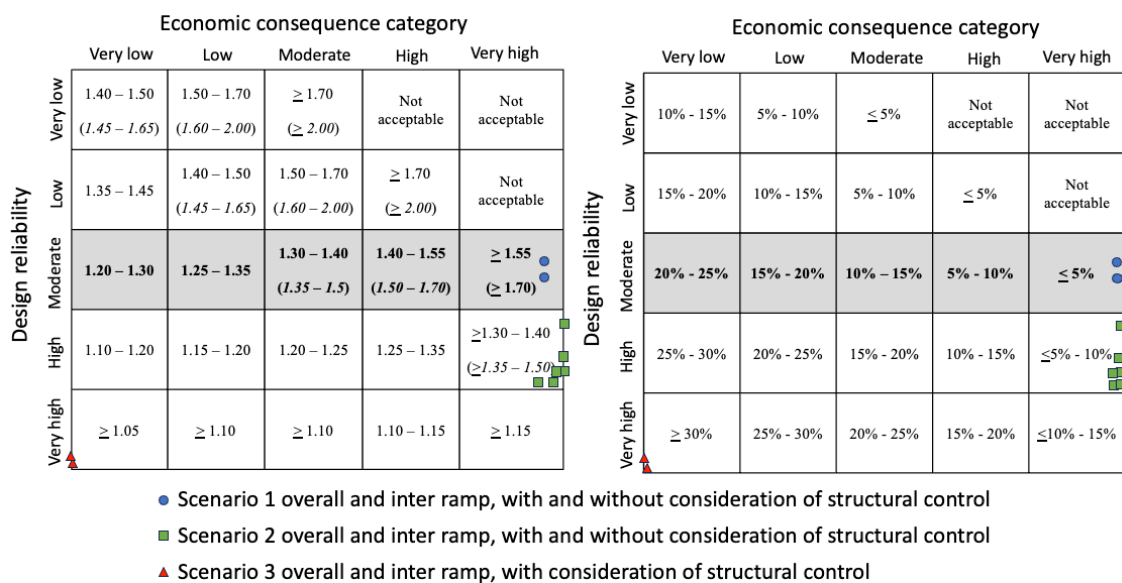


Figure 3-26: Plot of $COV_{FoS-FoS/PoF}$ results in the 2020 RBDAC (modified from Macciotta et al. 2020)

3.7 Use of the RBDAC for Design

Another important aspect is to evaluate the magnitude of potential gains when adopting the 2020 RBDAC that allows less conservative designs for high levels of design reliability. As it is clear from Figure 3-23, the pit slope design in Scenario 3 would not have met the 2020 RBDAC. The results of Scenario 3, which would correspond to high engineering effort, provided an excellent base for understanding of the governing large-scale structures in terms of continuity and rock bridges influence effects. As the pit is deepened, these structural features become more important due to their inter-relationship with the geometry of future slope design. For the next pushback design, the high reliability

of the model would allow to accomplish an optimum design reducing the excavation volumes while meeting accepted levels of risk. The 2020 RBDAC and the available information from the third scenario were used to develop a preliminary slope design for an assumed future pushback (this assumes a common pit scenario where the geotechnical team is tasked with the design of a future pushback after the knowledge gained from the third scenario, further geotechnical investigation, performance monitoring and back analysis of historic pit failures). Mitigative adjustments on the slope configuration can be considered for both inter-ramp and overall slope angles in order to satisfy the 2020 RBDAC. The design is interpreted to be associated with a high to very high economic consequence, therefore targeting a minimum FoS of 1.2 and a maximum PoF of 10% according to the 2020 RBDAC. The slope stability analysis for the suggested slope configuration that will be considered for the next pushback is shown in Figure 3-27.

Rock mass strength parameters and natural variability, as well as the knowledge about the geometry of major structures are the same as the third scenario. Buttressing, slope flattening, and offloading the pit crest are remedial efforts that can be implemented in case the proposed geometry does not meet the target FoS or PoF. Buttressing the slope might result unfeasible due to geometrical constrains in the pit thus affecting the operations at the bottom of the pit. In this regard, flattening the slope with an unloading was considered for the proposed design coupled with a depressurization plan. This can typically be accommodated in the mine plan.

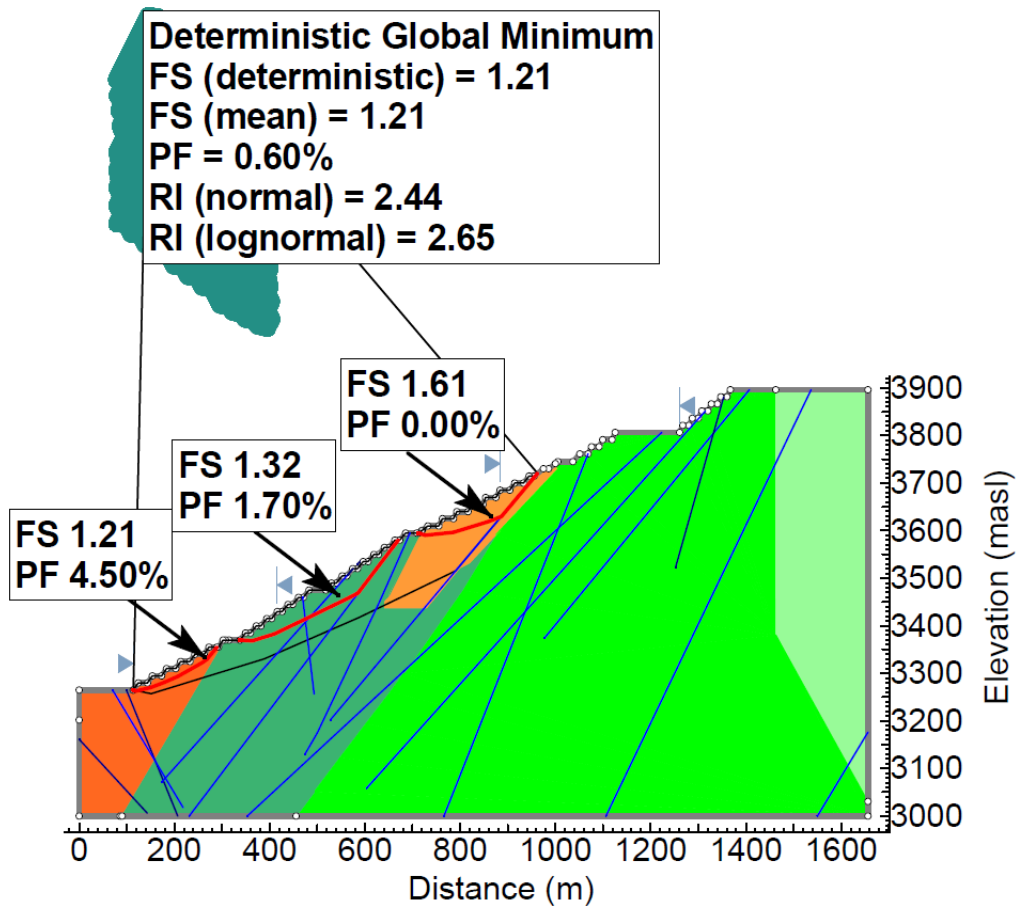


Figure 3-27: Limit equilibrium analysis results for the next pushback targeting the 2020 RBDAC

The analysis results shown in Figure 3-27 indicate that a slightly more conservative Inter-ramp slope angle design should be considered for the granodiorite. The Inter-ramp slope angle for the granodiorite is 26° whereas for the andesite is higher (up to 34°). The OSA was reduced by 1° to meet the target 2020 RBDAC, which would be considered feasible.

Calculated values of FoS, PoF, and COV_{FoS} are presented in Table 3-9. The FoS/PoF results meet the 2020 RBDAC and the COV_{FoS} are within the range defined in the 2020 RBDAC matrices, with small deviation in one case. In general, the geometrical reliability of the pushback can be considered optimized, risk informed and practicable.

Table 3-9: Summary of the limit equilibrium analysis for the design proposed for the next pushback

Slope Design	Angle (deg)	Height (m)	FoS	PoF (%)	COV _{FoS}
Inter-ramp slope	26	150	1.61	0.0	0.09
	34	225	1.32	1.7	0.11
	26	210	1.21	4.5	0.10
Overall slope	29	540	1.22	0.6	0.07

Conversely, designing with the current DAC that suggest a minimum FoS of 1.3 would increase the stripping costs. To this end, a slope configuration was developed to meet the DAC in the 2009 guidelines. Figure 3-28 shows the limit equilibrium analysis for a slope design configuration. Analysis results indicates that the OSA should be decreased by 1° in comparison to the design targeting the 2020 RBDAC.

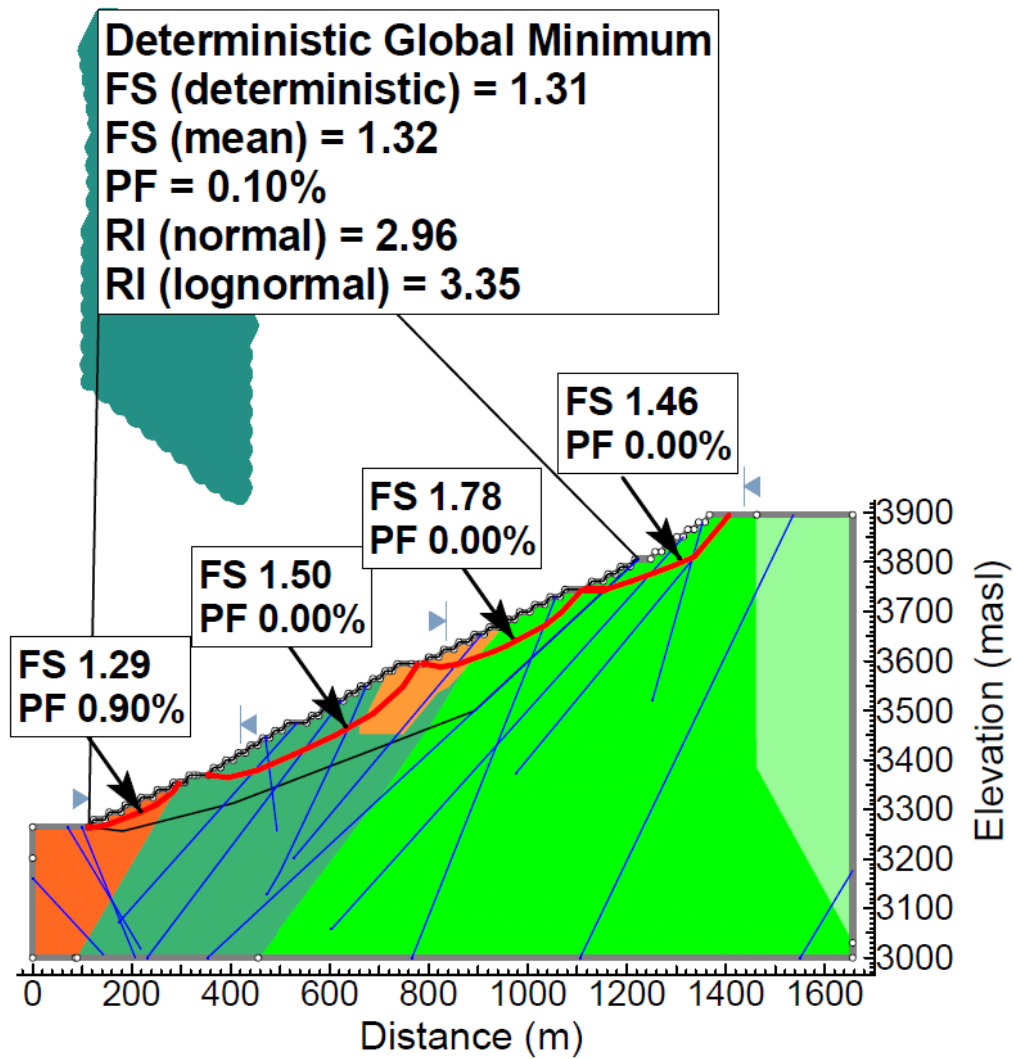


Figure 3-28: Limit equilibrium analysis results for the next pushback targeting the 2009 DAC

Figure 3-29 shows the next slope design configuration meeting the 2009 DAC and the 2020 RBDAC. The slope design with the 2009 DAC will result in mining additional 30.61 Mt considering a total pit sector length of 500 m affected by this design. This represents a significant optimization and shows the process for risk-informed reliability-based open pit design.

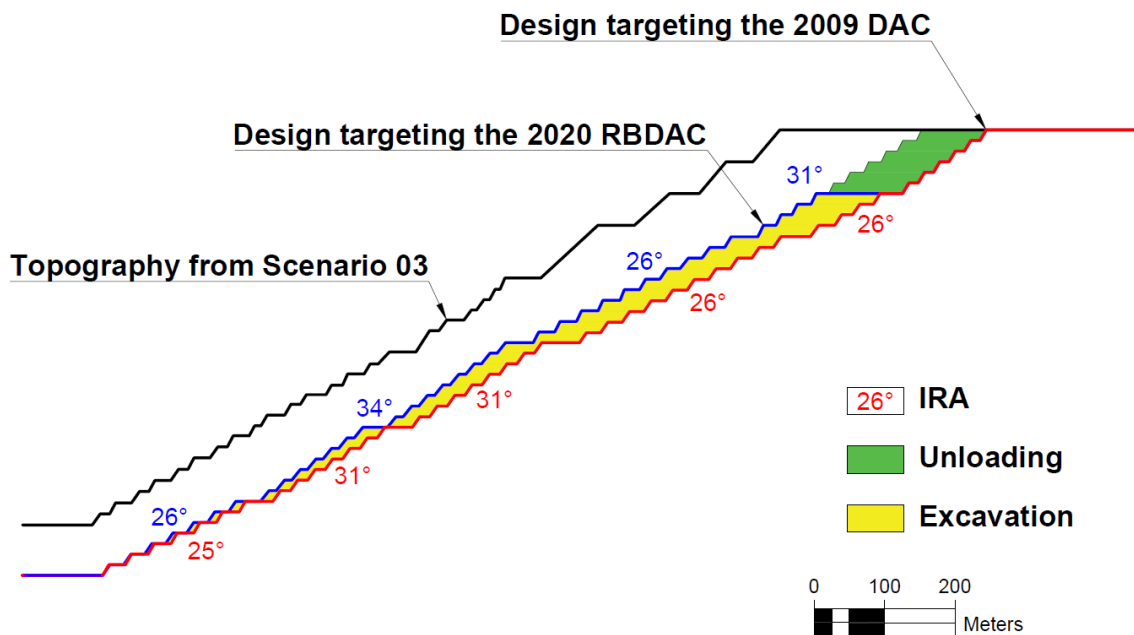


Figure 3-29: Slope design configurations for the next pushback targeting both the 2020 RBDAC and the 2009 DAC

3.8 Conclusions

This paper has demonstrated an approach applying a Reliability-Based Design Acceptance Criteria (RBDAC) to open pit slope design taking into consideration levels of reliability and consequence. Adopting a RBDAC that considers reliability of design inputs and outputs provides an opportunity to optimize slope design.

The results of the first scenario that considers a generic simple geometrical configuration show pairs of FoS, Probability of Failure (PoF), and COV of the FoS distribution (COV_{FoS}) indicating moderate reliability for a very high consequence category. The results of the second scenario that considers an implemented slope configuration with increased knowledge of the slope behaviour show pairs of FoS-PoF and COV_{FoS} that indicates a high reliability for a very high consequence category. The integration implicitly of large-scale structures through generalized anisotropic strength in the first and second scenario led to a reduction of about 5% and 17% in the COV_{FoS} , respectively. The results of the

third scenario are consistent with experience in the operation where slope failures were reported under similar geological and geometrical conditions. Material parameters and structure data were informed by back analyses of the mature slope configuration. The results show pairs of FoS-PoF and COV_{FoS} that indicate a very high reliability. All results were able to be evaluated on the basis of the RBDAC matrix in terms of design reliability and which consequence level would the FoS/PoF pairs would have been targeting (although no information was available in this regard to make a direct comparison).

Finally, a pushback was designed considering the same level of engineering effort as the third scenario. Two geometrical configurations were analysed for the pushback, targeting the DAC proposed in the 2009 guidelines and the RBDAC matrix in Macciotta et al. (2020). A comparison between these two design configurations reveals a difference of 1° in the Overall Slope Angle. Targeting the 2009 DAC would require an additional mining volume of 30.61 Mt than targeting the 2020 RBDAC matrix, assuming a pit sector length of 500 m.

The results of this study show the practicability and flexibility of a 2020 RBDAC matrix, and the adequacy, under the conditions of the case study utilized as basis for the study, of assuming Normal and Lognormal distributions to define the 2020 RBDAC matrix. The results also show the potential optimization gains of taking advantage of increased knowledge of slope performance translated to increased design reliability. It is noted that each operation should evaluate their own threshold criteria for defining economic risks and the organization's tolerance and appetite to those risks; as well as their approach towards evaluating design reliability as a function of engineering effort and the geomechanical complexities in their operations.

Acknowledgments

The authors acknowledge the financial support of the Large Open Pit Project (LOP <https://www.lopproject.com>) as well as the valuable reviews and comments that allowed the development of this paper.

4.0 Effect of uncertainty in fracture normal stiffness on pit slope stability calculations

A version of this chapter is being submitted for publication at Engineering Geology.

4.1 Introduction

There is considerable interest in managing uncertainties to enhance reliability in the open pit slope design process. Uncertainty can potentially impact the business outcomes. It can be classified as natural variability and epistemic uncertainty (Baecher and Christian, 2003), and although it cannot be eliminated, it can be reduced. Importantly, understanding and reporting data uncertainty are needed to define current and target levels of reliability (Read and Stacey, 2009). Understanding geotechnical uncertainty can lead to evaluate slope design options in terms of risk and associated economic and safety outcomes (Creighton et al., 2022). Open pit operators are increasing design reliability through more sophisticated numerical modelling and evaluating slope performance with robust reconciliation and monitoring programs (Macciotta et al., 2020). Consequently, uncertainties are being more formally addressed.

In this manner, numerical modelling, specifically deformation analysis, is increasingly becoming a routine practice in geotechnical applications, allowing the evaluation of the stress-strain behaviour of materials (Kafash et al., 2022). This type of analysis can evaluate the complex interaction between discontinuity/fractures and rock mass responses to excavation, which leads to stress redistributions capable of triggering progressive failure of excavated slopes. Coupling performance monitoring with deformation analysis can predict slope behaviour and support slope design analysis (Sharon and Eberhardt, 2020). The fundamental criterion in this approach is to match the model behaviour with the actual observed behaviour, enhancing confidence in calibration and providing a field-scale assessment of properties (Sharon and Eberhardt, 2020). This process can contribute to a further reduction of epistemic uncertainty by enhancing our understanding of controlling factors established during initial stages, such as strength or behavior of the materials involved, and constraint them for future slope

designs. However, the stiffness of fractures, difficult to characterize due to its extreme variability, has been identified as potentially influencing slope performance (Macciotta and Martin, 2016; Martin et al.,2022)

For example, in their recent work, Martin et al. (2022) analyzed the role of the joint stiffness and in-situ stress on slope deformation patterns. The authors used a finite element model to simulate an unloading and loading process of a shale slope. The results show that the slope deformation pattern in the unloading process is primarily controlled by the joint normal stiffness. The joint normal stiffness was reduced in several orders of magnitude from the initial value, obtained in laboratory and in-situ tests, in order to history match the measured displacement and the predicted displacement. In the loading process, the slope deformation pattern is controlled by a combination of low joint normal stiffness and gravitational in-situ stresses, with a low horizontal stress component. The authors concluded that the joint shear stiffness does not influence the slope deformation pattern for the characteristics in their case study.

Other studies have focused on the role of normal stiffness in back analysis. Back-analysis has been extensively used to determine mobilised shear strength and the deformation patterns of failed slopes and to provide sensitivity cases for different scenarios. For example, Lana (2014) conducted a numerical modelling of failure mechanism in an open pit slope mine in Brazil. Through a parametric analysis for in situ stresses and fracture stiffness, the author suggested that the failure mechanism is better represented by lower values of stiffness and a high in situ stress ratio. Furthermore, Macciotta and Martin (2016) investigated the impact of fracture stiffness in the back analysis of rock tensile strength using a discontinuum model. They analyzed different slope configurations with different fracture networks, adjusting fracture normal stiffness and shear stiffness to find the required rock tensile strength to achieve an incipient slope failure. The results revealed that the required tensile strength increases with decreasing shear stiffness while keeping the normal stiffness constant. Similarly, it was found that the required rock tensile strength increases with decreasing normal stiffness while keeping

the shear stiffness constant. The authors concluded that the inherent variability of fracture stiffness and rock tensile strength play a key role in slope stability analysis and should be taken into account in slope designs.

These studies suggest that normal stiffness is a controlling factor in slope performance and stability which contributes significantly to geotechnical uncertainty in pit slope stability. However, its effects on the unloading process of open pit slopes are not well understood and have received little attention. Studying its effects in low stress environments is necessary to enhance our understanding of the role of this parameter in slope stability. This can help to reduce epistemic uncertainty and increase the reliability level in the implementation of open pit slopes.

This chapter presents a sensitivity analysis to examine the effect of fracture normal stiffness on calculated FoS or SRF for a given pit slope configuration and fracture geometries. Based on this sensitivity analysis, the displacement deformation is also evaluated. The pit slopes configurations were analyzed using both a continuum model and discontinuum model, while varying the fracture normal stiffness while keeping constant the fracture shear stiffness. The aim of the work is to understand the uncertainty associated with fracture normal stiffness and its role in design reliability.

4.2 Fracture Normal Stiffness

The rock mass behind a rock slope is unique, whose behaviour depends on rock mass stress-strain responses and can be dominated by the presence and characteristics of discontinuities. These discontinuities exhibit high degrees of geometric, spatial and strength variability due to the various orogenic processes of rock formation and mineralization leading to complex geological settings.

In rock mechanics, the term ‘discontinuity’ is defined as any plane of weakness, mechanical break, or fracture with negligible tensile strength, and is often universally applied to describe most of the geological features present in a rock mass (Herget, 1977; Goodman, 1991; Hoek and Bray, 1981; Priest 1993, Hudson and Harrison, 2000). Herget (1977) adopted the term discontinuity to describe

these features in the investigation of open pit mining and analyzing structural information to support open pit slope design. These features were classified in a hierarchy fashion into major and minor discontinuities to define structural domains. Read and Stacey (2009) adopted the term structural defects to describe the geological features based on scale and fabric. However, in structural geology literature (Ramsay et al., 1983; Passchier and Trouw, 2005; Fossen, 2016), the term ‘fracture’ is used to refer to structures formed by brittle failure that shows particular alignments in the crust. A more detailed terminology is used in structural geology to describe geological and geomorphological modes of formation and to explain geological history. Therefore, both terms and their definitions are used to describe geological features such as faults, joints, beddings, veins, schistosity, cleavage, and among others. However, the terminology depends on specific field-oriented literature.

A particular focus is given to faults and joints, which are formed by brittle deformation and are important in slope stability analysis. Joints are defined as fractures in a rock which there has been little or non-movement (Lisle, 2020; Passchier and Trouw, 2005; Fossen 2016). They are classified as systematic and non-systematic depending on their arrangement in the rock mass, often correlated in terms of orientation with large-scale structures like folds and faults. On the other hand, a fault is described as a fracture discontinuity (Ramsay et al., 1983) or a plane of shear failure in rock where significant differential displacement has occurred (Priest, 1993). Faults exhibit evidence such as lithological offset and presence of fault gouge (powdered rock) or the presence of a large zone of broken rock. These faults or fault zones are also known as brittle shear zones as a result of deformation in high-strain zones (Passchier and Trouw, 2005; Fossen, 2016). Shear zones have a significant shear component and vary in size, orientation, length, thickness, displacement, and deformation mechanism. Passchier and Trouw (2005), Fossen (2016) subdivided shear zones into brittle zones and ductile zones. A special terminology is used for rocks deformed in shear zones. Brittle fault rock includes fault breccia, cataclasite and fault gouge (Priest, 1993; Passchier and Trouw, 2005). Figure 4-1 shows the distribution of types of rock faults and a schematic cross-section through shear zones at different depths

of the crust (Passchier and Trouw, 2005). More detailed explanations can be found in Structural Geology literature. The types of rock faults and the dominance of brittle fracturing or ductile deformation can be found in open pits with strong structural control. This chapter will use the terminology of fractures and the concept of faults as important features in controlling failure mechanisms in open pit slopes.

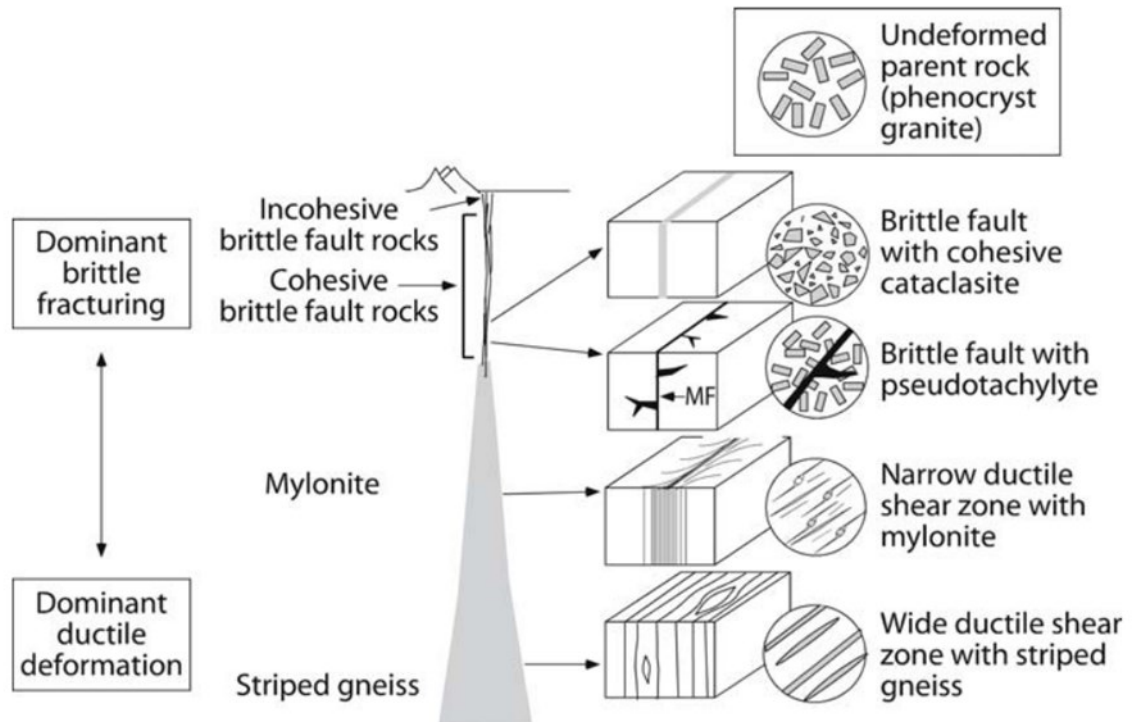


Figure 4-1: Distribution of types of rock faults and schematic cross-section through shear zones at different depths of crust (Passchier and Trouw, 2005 with permission)

The genesis of geological features is widely variable and reflects the deformation of the crust throughout geologic history. Understanding them is paramount for their description and to obtain mechanical parameters for deformation analysis to support open pit slope design. Generally, the input variables of these types of analyses are: (1) geometrical properties and (2) mechanical properties. Geometrical properties comprise spacing, orientation, persistence, roughness, aperture, discontinuity sets, and block size, whereas mechanical properties comprise strength and stiffness (Priest, 1993; Hudson and Harrison, 2000; Brady and Brown, 2006).

To determine these mechanical properties, the most common and widely used approach in rock mechanics is the controlled laboratory test known as the direct shear test. MacDonald et al. (2023) delved into the current state of practice in the direct shear test of unfilled rock fractures. In their work, they explained the boundary conditions most often used in practice to represent the rock mass behaviour under two principal conditions: gravity-driven conditions near surface excavations and ground stress conditions near underground excavations.

The direct shear test provides shear strength and fracture stiffness parameters. Typically, the shear strength of smooth discontinuities has been determined using the linear Mohr Columb failure criterion, whereas the shear strength, accounting for the roughness of the fracture and the strength of the rock adjacent to the fracture, has been determined by the non-linear Barton-Bandis failure criterion. In terms of deformation behaviour, fracture stiffness is determined by the stress-displacement characteristics and is treated as normal stiffness (normal to the local fracture plane) and shear stiffness. Fracture stiffness depends on factors such as rock wall properties, filling material, the matching between rock walls, and loading cycles. Fracture normal stiffness is described by the normal stress-displacement characteristic that exhibits distinct behaviour under specific conditions and varying complexity. Consequently, different fracture closure laws have been proposed in an effort to describe the behaviour and to determine the fracture normal stiffness.

Hungr and Coates (1978) proposed a linear fracture closure law, attributed to the precompression of the fractures by pressures greater than those applied in the laboratory test as shown in Figure 4-2a. Conversely, based on cycling experimental tests (loading and unloading cycles) conducted on both matched and mismatched fracture surfaces, a highly non-linear behaviour (e.g., Bandis et al., 1983; Goodman, 1991) was observed. Subsequently, several function models have been proposed to describe the non-linear behaviour and, in turn, to determine the fracture normal stiffness. For instance, Goodman (1991) proposed an empirical hyperbolic model which requires two parameters that are determined experimentally. Moreover, Bandis et al. (1983) proposed a semi-logarithmic model, suggesting that it

gives the best approximation to the non-linear behaviour of the experimental tests of mismatched fractures. The suitability of the semi-logarithmic model was supported by Zangerl et al. (2008). The difference between these two models is that the empirical hyperbolic model has two free parameters whereas the semi-logarithmic model has a single free parameter known as the stiffness characteristic (Evans et al., 1992), offering greater practicability in engineering projects (Zangerl et al., 2008).

Pachulak (2018) conducted several direct shear tests on granitic and gneisses rocks using both linear and semi-logarithmic models. The author concluded that using a linear model provides a softer stiffness compared to the semi-logarithmic model. In addition, based on statistical analysis, the latter provides adequate values for fracture normal stiffness. On the other hand, during unloading cycles, the normal stress-displacement curve exhibits marked hysteresis and differs from the loading curve (Bandis et al., 1983) as shown in Figure 4-2b. Repeated reloading-unloading sequences results in steeper curves. For numerical modelling of excavations, Pachulak (2018) suggested that the fracture normal stiffness of the unloading curve may produce closer results to in-situ conditions. The author also suggested that the linear closure law is suitable for calculating the fracture normal stiffness of the unloading curve.

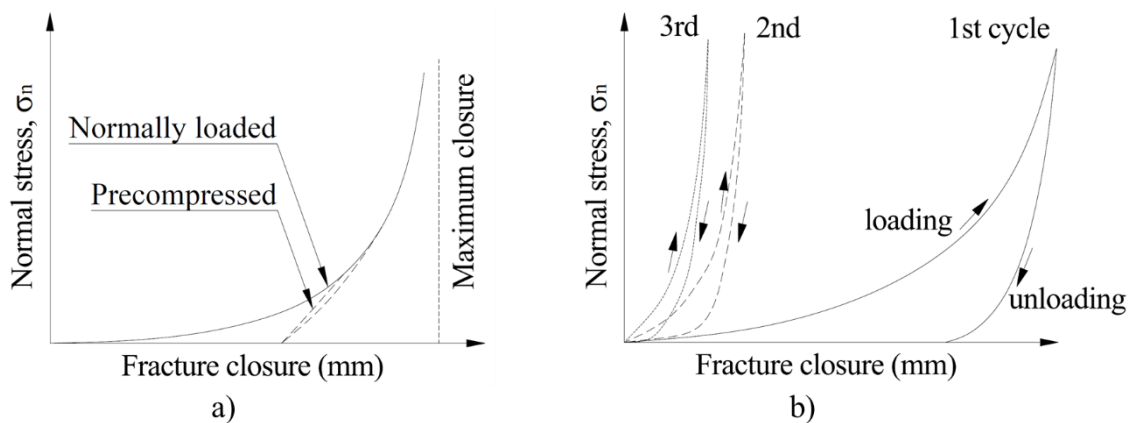


Figure 4-2: Stress-displacement characteristic of discontinuities under both a) normal loading and precompressed conditions (modified from Hungr and Coates 1983 with permission); and under b) repeated loading cycles (modified from Bandis et al. 1983 with permission)

Despite efforts to reduce sources of uncertainty related to testing procedures, the transformation of laboratory measurements into fracture normal stiffness through different models, and the accounting

for statistical errors and other factors, have resulted in a great variability of fracture normal stiffness is reported in literature.

Zangerl et al. (2008) compiled different results of fracture normal stiffness in granitic rocks obtained from both laboratory and in situ test and published in the literature. Their study revealed a wide range of fracture normal stiffness for the same type of rock. Read and Stacey (2009) reported a broad spectrum of values for fracture normal stiffness for different types of rocks. Day et al. (2017) conducted a series of direct shear tests using a servo-controlled shear apparatus to determine the normal stiffness and shear stiffness of shear surfaces and shear zones in limestone. Pachulak (2018) conducted a series of direct shear test on granitic and metamorphic rocks reporting a range of stiffness values. In light of the wide range of fracture normal stiffness values, the author suggested using the lower end of the range for near-ground surface applications (e.g., excavated slopes) and the upper end of the range for large confinement environments such as deep tunnels. Thus, the broad ranges of fracture normal stiffness values encountered in practice highlight the inherent uncertainty associated with this parameter and the selection of an adequate value is a difficult task in the slope design process. Table 4-1 shows a compilation of values of normal stiffness obtained from the references cited above.

Table 4-1: Summary of fracture normal stiffness from a subset of previous studies

Type	Wall rock	Normal Stiffness (GPa/m)	Normal stress (MPa)	Fracture description	Source
Joints	Sandstone	7-24	0.4-0.9	Bedding planes	Rode et al. (1990)
		17-25		Fresh fractures, good matching	
		8-12		Fresh fractures, poor matching	
	Limestone	0.5-1	5	Joint in weathered	Bandis (1993)
		4-5		Joint Fresh	
		4-10	0.2-0.8	Fracture	Day et al. (2017)
		5-11		Intrablock	
	Quartzite	15-30	10-20	Clean joint	Ludvig (1980)

		10-25		Joint with clay gouge	Ludvig (1980)
	Granite	74-121	25-30	Clean joint	Makurat et al, (1990)
		50-635	8.6-9.3	Clean Joint	Martin et al. (1990)
		0.01-62000	1.4-30		Zangerl et al. (2008)
		2-60	1-8	Unfilled	Pachulak (2018)
	Quarzt Monzonite	15.3	-	Clean Joint	Goodman and Dubois (1972)
	Rhyolite	16.4	-	Clean Joint	
	Hard rock	8-99	-	Clean joint	Rosso 1976
		1620	-	Clean fracture	Ruqvist (1990)
		>100	-	Good match, interlocked	Itasca (2004)
		0.01-0.1	-	Soft clay filling	
	Gypsum	3-13	-	Fresh joint	Rode et al. (1990)
Fault/ Shear zone	Basalt	0.6-1.2	0.15-0.40	Montmorillonite and weathered basalt	Infanti and Kanji (1978)
		0.15	0.35-0.6	Silty Sand	
		1.15-1.8	0.2-0.9	Clay film and sandy silt	
	Sandstone	1.7	-	Shear zone with clay gouge	Wittke (1990)
	Granite	2-266	0.5-20	Shear zone	Martin et al. (1990)
	Weak rock	5-40	-	With clay gouge	Barton (1982)
	Hard rock	0.005	-	Fault with clay gouge	Karzulovic (1988)
		0.8	-	Rough structure with a fill of rock powder	

4.3 Methodology

The methodology adopted in this chapter involves slope stability analysis using numerical modelling techniques in two cases, each with a different open pit slope configuration. The study aimed to determine the effect of the fracture normal stiffness on the slope stability analysis results. This effect can not be observed by adopting limit equilibrium analyses, even though they are extensively used in the open pit slope design process. The simulation was conducted using a continuum approach and a discontinuum approach. The continuum modelling was carried out using RS2 (software by Rocscience Inc. 2023) whereas the discontinuum approach was carried out using Slope Model (software by ITASCA 2018).

4.3.1 Open Pit Slope configurations and material parameters

4.3.1.1 Case one

The analyzed open pit slope configuration comprises three Inter-ramp Slopes Angles (ISA) of 50° with slope heights of 60 m and an Overall Slope Angle (OSA) of 45° with a total slope height of 180 m. The final slope configuration was achieved through an excavation sequence consisting of three stages, as shown in Figure 4-3. The Hoek-Brown parameters for the rock mass unit adopted in this study are given in Table 4-2. These parameters are meant to model rock mass as defined by intact rock bridges and small-scale fractures (joints).

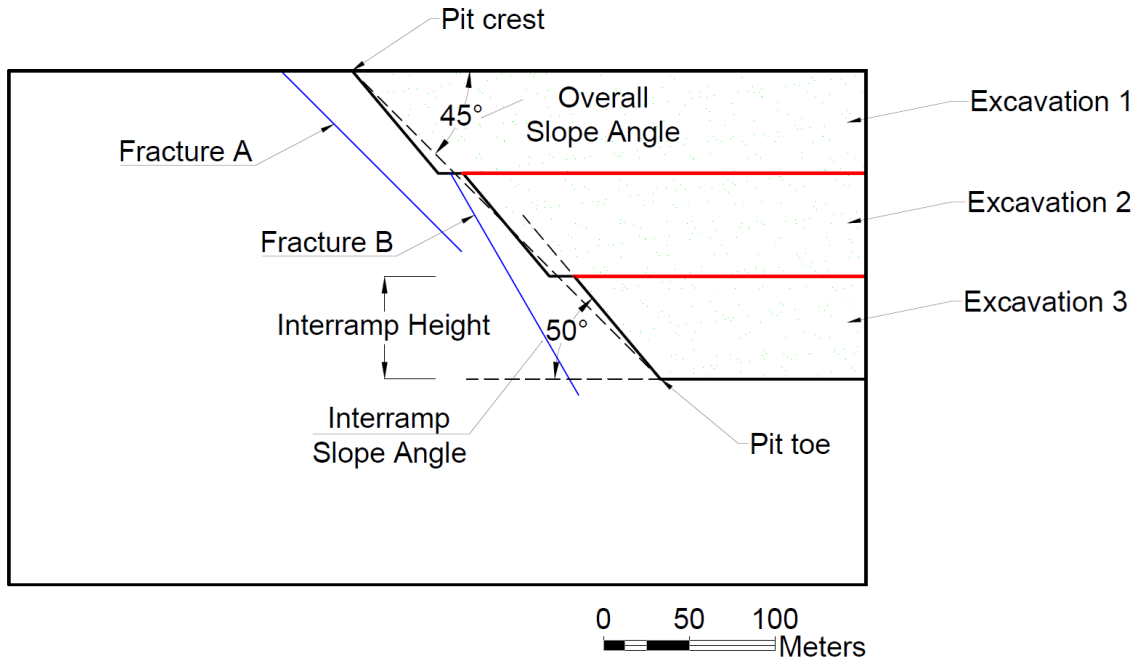


Figure 4-3: Dimensions of the open pit slope analyzed for Case 1

Table 4-2: Rock mass parameters adopted in the sensitivity analysis for Case 1

Parameter	γ (kN/m ³)	σ_{ci} (MPa)	m_i	GSI	D	E_{rm} (GPa)
Values	25	40	10	40	0	4.8

Two main structural features were considered explicitly in the numerical models. The first fracture, fracture A, has a strike that is parallel to the slope and dips towards the excavation at angle of 45°. The second fracture, fracture B, also has a strike that is parallel to the slope and dips towards the excavation at angle of 60° as illustrated in Figure 4-3. The shear strength of the two discontinuities was assumed to be cohesionless with a friction angle of 30°.

The fracture normal stiffness and shear stiffness values for fracture A and fracture B were 1000 MPa/m in the first simulation. Subsequently, the normal stiffness was systematically reduced from 1000 MPa/m to 100 MPa/m and 50 MPa/m, while the shear stiffness value was kept constant for each simulation. It is noteworthy that the value as low as 50 MPa/m and lower have been reported in literature as described in Table 4-1. The effect of fracture normal stiffness on the calculated SRF in this study was examined under several simulations at discontinuity shear to normal stiffness ratios greater

than 1. Table 4-3 shows the pairs of fracture normal-shear stiffness considered for the sensitivity analysis.

Table 4-3: Pairs of fracture normal-shear stiffness evaluated

Continuum Model		Discontinuum model	
Pairs of fracture Normal-Shear Stiffness (MPa/m) k_n - k_s	Ratio ks/kn	Pairs of fracture Normal-Shear Stiffness (MPa/m) k_n - k_s	Ratio ks/kn
1000.00-1000	1.00	1000-1000	1.00
800.00-1000	1.25	750-1000	1.33
500.00-1000	2.00	500-1000	2.00
333.33-1000	3.00	250-1000	4.00
250.00-1000	4.00	200-1000	5.00
200.00-1000	5.00	150-1000	6.67
166.68-1000	6.00	100-1000	10.00
142.86-1000	7.00	50-1000	20.00
125.00-1000	8.00	-	-
111.11-1000	9.00	-	-
100.00-1000	10.00	-	-

The horizontal-to-vertical stress ratio used in this study was 0.3, this choice was done according to the findings of Martin et al. (2022), where they suggested that predicting displacement rates within a slope deformation model requires gravitational vertical stress with low horizontal stress resulting in ratios less than 1. Also, the selection of this horizontal-to-vertical stress ratio is in line with the typical gravity-driven nature of most rock slope failures. The groundwater conditions were not included in the analysis.

4.3.1.2 Case two

In this case, a mature open pit slope configuration is analyzed which comprises an OSA of 37° with an overall height of 540 m, as shown in Figure 4-4. The final slope geometry was achieved through an excavation sequence consisting of 18 stages. It is noteworthy that this general configuration was adapted from the examples provided to the user of Slope Model. This particular configuration aims to enhance the understanding of the fracture normal stiffness on the calculated FoS, and it is not intended to compare with previous results.

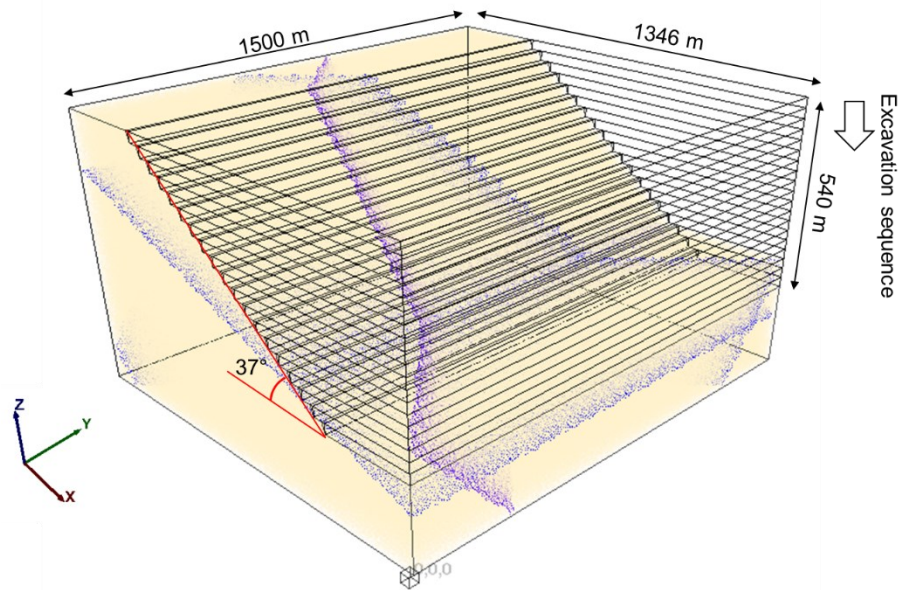


Figure 4-4: Dimensions of the open pit slope analyzed for Case 2

The strength parameters for the intact rock unit adopted in this case are given in Table 4-4. Two sets of joints were considered explicitly in the numerical models to describe the fracture geometry of the rock mass. In addition, three large-scale fractures were integrated in the numerical models. A stereographic projection of structural data for this case is shown in Figure 4-5. The shear strength of the fractures was assumed to be cohesionless with a friction angle of 30° .

Table 4-4: Intact rock parameters adopted in the sensitivity analysis for Case 2

Parameter	γ (kN/m ³)	σ_{ci} (MPa)	σ_{ti} (MPa)	E_i (GPa)
Values	27	160	8	65

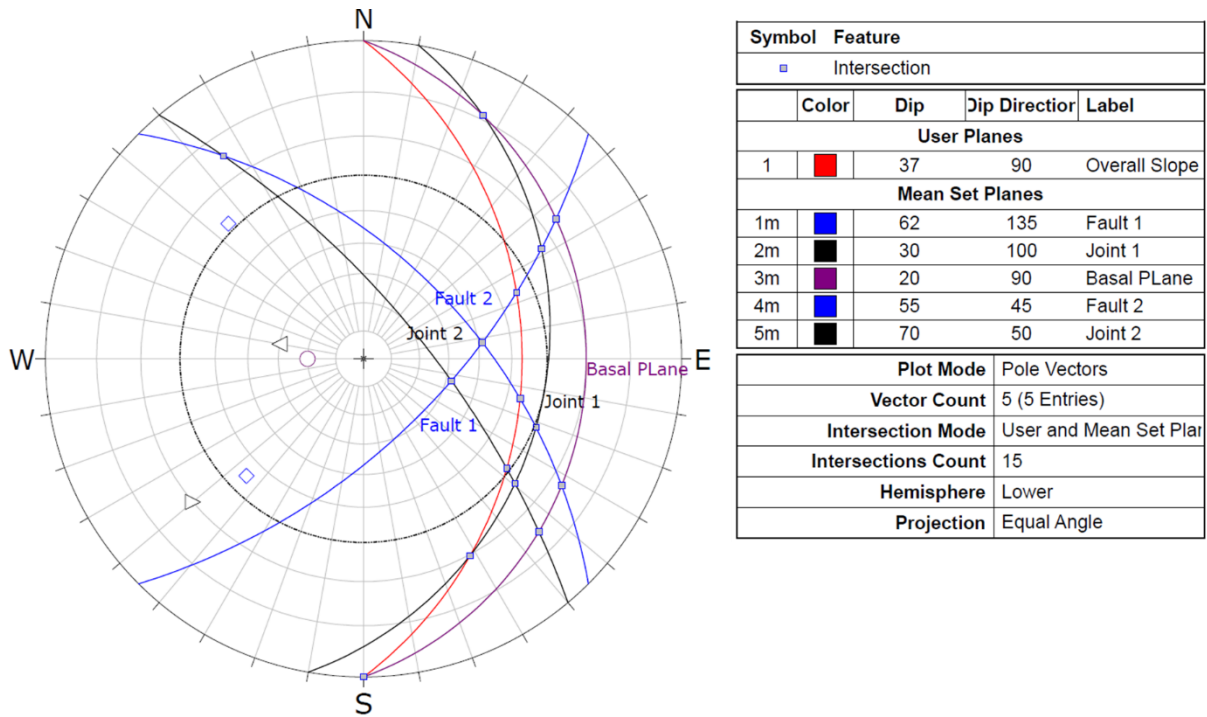


Figure 4-5: Stereographic projection of structural data considered for the Case 2

The fracture normal stiffness and shear stiffness values for the two faults and basal plane were set at 1000 MPa/m in the first simulation. Subsequently, the normal stiffness was systematically reduced from 1000 MPa/m to 500 MPa/m and then to 100 MPa/m, while keeping constant the shear stiffness value of 1000 MPa/m for each subsequent simulation. However, it is important to outline that the decrease of normal stiffness was undertaken on the faults and basal plane and not on joints. The rationale behind this systematic reduction in normal stiffness of these fractures was to analyze and to understand the impact on the behavior of the rock mass block bounded laterally between these fractures. To this end, the normal and shear stiffness of the joint sets were set as 5 GPa/m and were kept constant throughout the models.

4.3.2 Continuum model setup with RS2: Case one

The Finite Element (FE) method simulations in this chapter for the Case1 were carried out using the software RS2 that assumes the rock mass as an equivalent continuum. The material assigned to the model is based on the non-linear Hoek-Brown failure criteria with an elasto-plastic model. A discrete fracture boundary can be explicitly modeled within the continuum model. The software RS2 can properly reproduce these fracture boundaries, either through explicit definition or by specifying joint networks following defined statistical parameters (RS2-2D Rocscience User Guide). In this study, the two fractures, A and B, were modeled explicitly within the continuum rock mass.

When defining the dimensions of the model, the computation section should be large enough so that stress changes and displacements resulting from the excavation sequence do not reach the boundaries of the model (Wittke, 2014). Typically, the lateral extension of the computation section should be greater than the width of the slope, and the vertical extension greater than half the height of the slope (Wyllie and Mah, 2004; Read and Stacey, 2009). In this chapter, the computation section was laterally extended to more than the two times the height of the slope and horizontally extended to more than three times the width of the slope. This configuration of the computation section was kept the same for all the cases modelled. The displacement boundary conditions were set as: fixed x-direction (lateral movement) at the left and right boundaries of the model, fixed x and y (vertical) direction at the base of the model. The geometry of the model, displacement boundary conditions and the excavation sequence are illustrated in Figure 4-6.

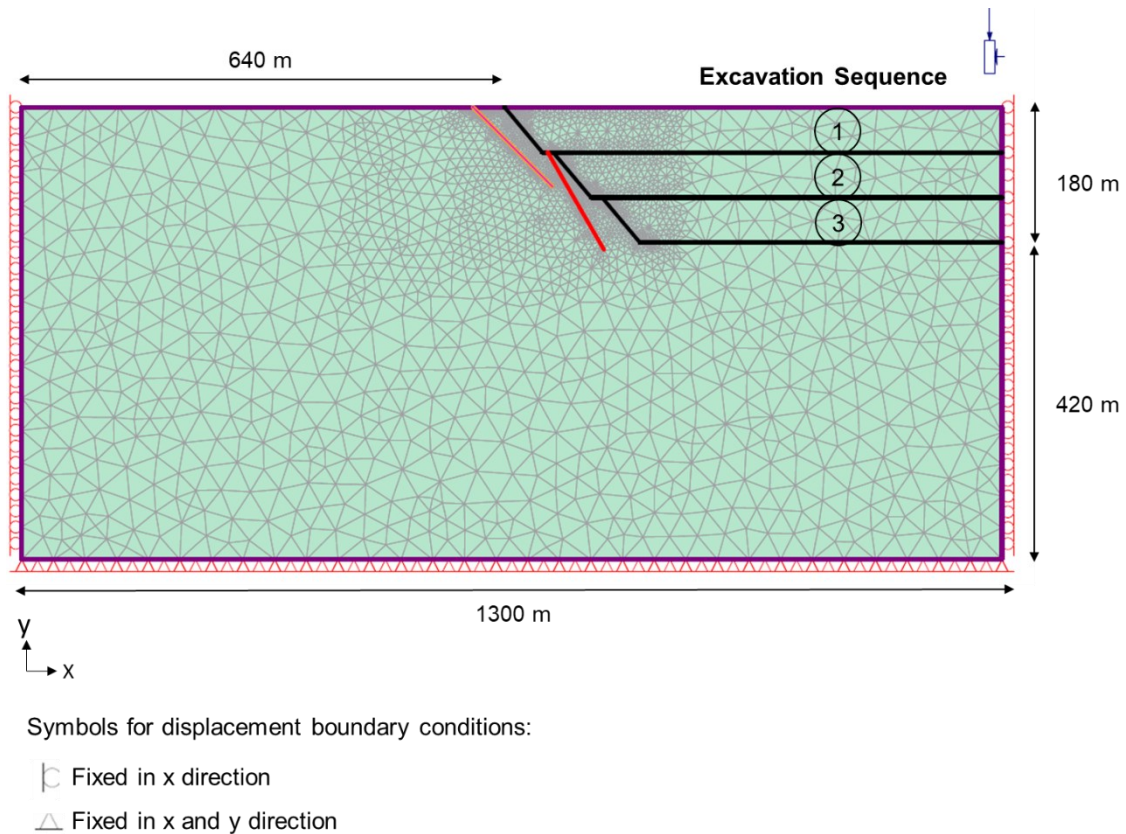


Figure 4-6: RS2 finite element model used for the sensitivity analysis

The ability of numerical modeling to simulate the responses of the model to imposed changes is essential for further validation of the numerical model. The software RS2 allows users to obtain data from anywhere within the computation section through the generation of a ‘query’ (RS2-2D Rocscience User Guide). This option can include either single points or line segments, simulating monitoring prisms or monitoring extensometers, respectively. In this section, a virtual horizontal extensometer was considered as reference to record the displacement. Additionally, three history points were considered to record the changes in horizontal stress. The location of this model extensometer and history points are shown in Figure 4-7: For clarity, the magnitude of displacement analyzed in this study are focused on the excavation sequence with any displacements generated before excavation being removed. Subsequently, the SRF was calculated on the final geometrical configuration of the slope.

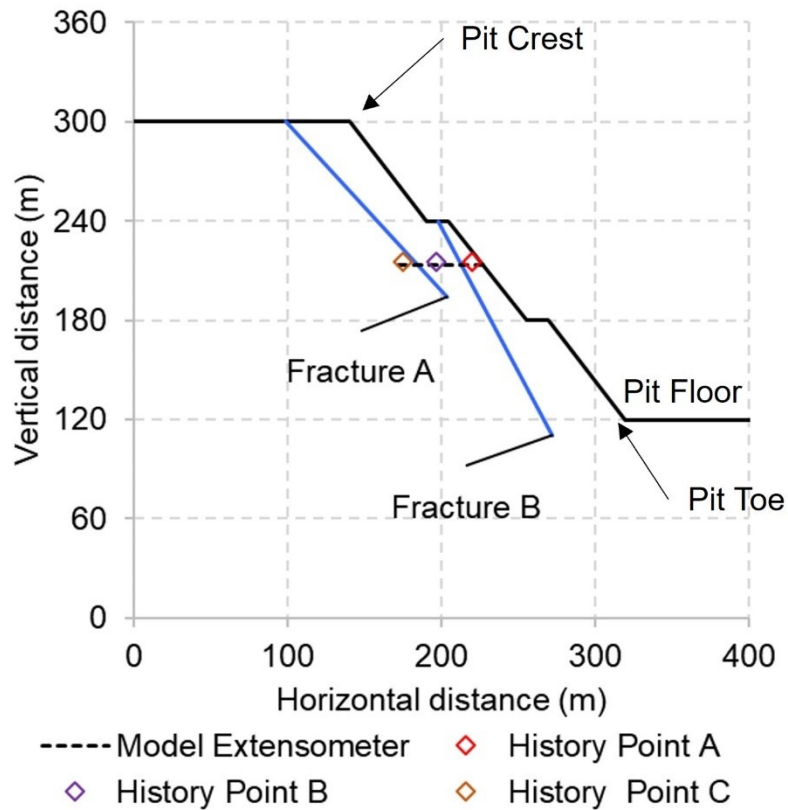


Figure 4-7: Location of history points and horizontal extensometer

4.3.3 Discontinuum model setup with Slope Model: Case one

Discontinuum models are capable to simulate complex rock mass behaviour. Among various codes available, the Slope Model lattice code uses an explicit and time-marching formulation. This code uses an assembly of zero-dimensional nodes placed randomly which are connected by springs, see Figure 4-8. This lattice approach simulates rock fracture through breakage of springs in shear and tension along with joint slip (Lorig et al., 2010; Cundall et al., 2016). This approach follows a non-linear behaviour consisting of rock fracture and joint slip/opening. Discontinuities can be modelled through a Discrete Fracture Network (DFN) or can be modelled in an explicit manner such as large-scale structures. These structural features are superimposed in the into the lattice springs, assigning them shear and stiffness properties. This approach models rock bridge failure and brittle fracturing in rock slopes, coalescence of pre-existing fractures and fracturing through intact rock.

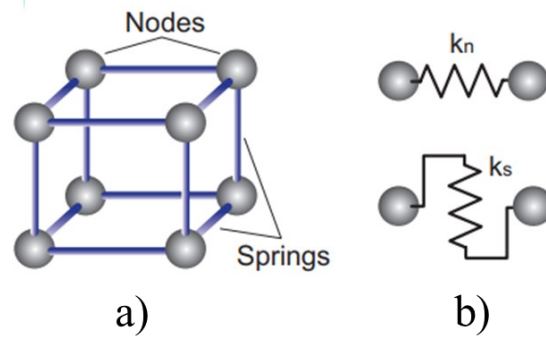


Figure 4-8: Representation of the lattice formulation as a) an assembly of nodes connected by springs and b) stiffness components of each spring. (Macciotta and Martin 2016)

The contact in the lattice approach can be represented by the Smooth Joint Model (SJM) and the flat joint model (FJM). The former allows slip and rotation of particles without offering resistance. In the latter, the spring is subdivided into sub-springs that allows resistance even when they are broken (Lorig et al., 2010; Havaej et al., 2013; Al-E'Bayat et al., 2023). In this chapter, the FJM was used as the initial models adopting SJM resulted in unrealistic displacements, unlike the FJM. The FJM adopted peak and residual friction angles, both set as 30° .

The model generation comprised a lattice resolution of 4 m in order to have reasonable computation time as finer resolutions require significantly longer times of computation. This was considered adequate due to the homogeneity in the material modelled, the scale of the model, and simplicity of the geometry of explicit structures and excavation.

The boundary conditions were similar to those described earlier. However, Slope Model is a 3-dimensional slope and a small dimension of 10 metres was defined in the out-of plane to simulate a 2-dimensional analysis. This implies the pseudo 2-dimensional model was under plain strain conditions. Figure 4-9 shows the dimensions of the model, the boundary conditions, and the history points to monitor the displacements trends. The model was initialized with in-situ stress according to gravity loading.

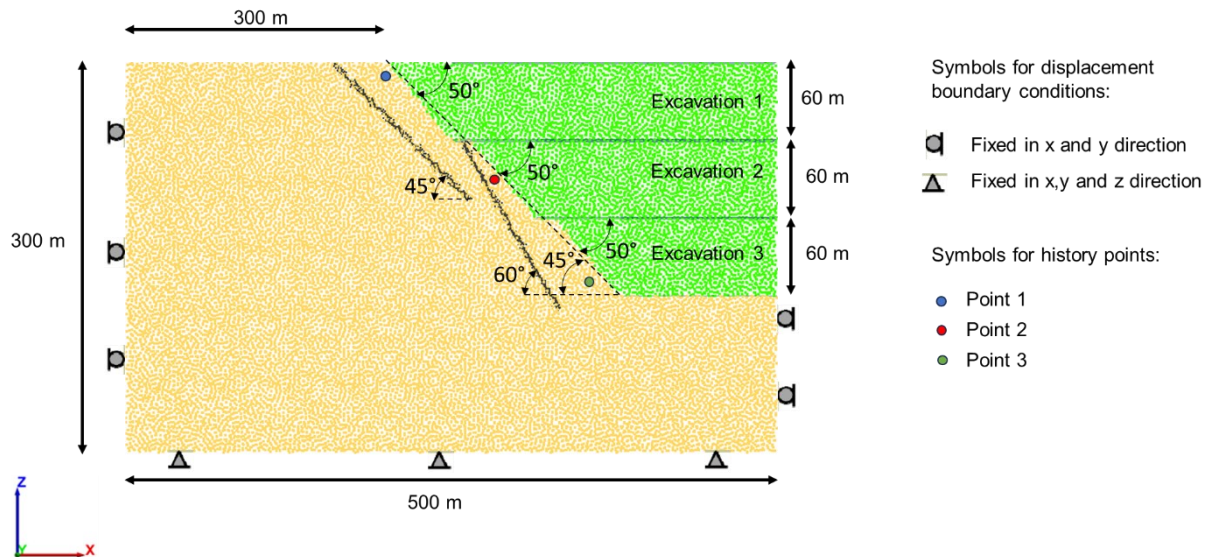


Figure 4-9: Model setup in Slope model for Case 1

The model is excavated to reach the final slope configuration through a batch simulation. The model was allowed to reach a new equilibrium state after each excavation sequence, evaluated as the state when no more deformation is measured at history points placed at the upper, middle, and lower parts of the Overall Slope. Also, additional computation time was considered to assure no progressive failure was triggered (e.g., the occurrence of a second phase of acceleration). This modeling procedure was applied for various fracture normal stiffness values. Furthermore, the microcracks generated for each simulation were tracked and analyzed to describe the failure mechanisms.

4.3.4 Discontinuum model setup with Slope Model: Case two

A 3-dimensional analysis was constructed using Slope Model. This model aims to represent a failure mechanism that involves a non-daylighting wedge. The model generation comprised a coarse lattice resolution of 20 m in order to have reasonable computation time as finer resolutions require significantly longer times of computation. The boundary conditions were similar to those described earlier. Figure 4-10 shows the dimensions of the model, and the history points to monitor the displacements trends. The in-situ stress ratio was assumed to be 0.3, where the vertical stress is dictated by the overburden pressure.

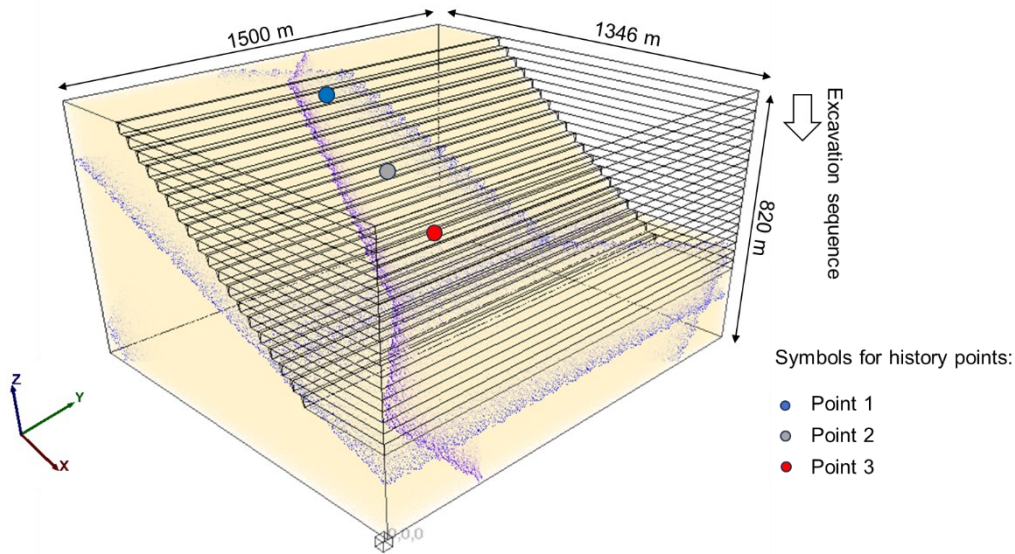


Figure 4-10: Model setup in Slope model for Case 2

The model is excavated to reach the final slope configuration through a batch simulation. For this case it was considered a total of 6 batch simulations. The first simulation within the batch represents initial conditions. The second simulation within the batch represent an excavation of 10 benches. The third simulation within the batch represents an additional 5 benches. The fourth, fifth, and sixth simulation within the batch represents the excavation of 1 bench respectively. This was done in order to get more detail when the excavation sequence approaches the final height of the slope and not at initial excavations. After each simulation within the batch, a new equilibrium state has been reached which is done by giving additional time of computation. This is tracked by observing the trends of the history points. Similarly, as the previous case, the microcracks generated for each simulation were tracked and analyzed to describe the failure mechanisms.

4.4 Results and discussion

4.4.1 Displacement and stresses

4.4.1.1 Continuum model: Case one

The displacements trends were analysed in both horizontal and vertical axes along the extensometer. The magnitudes of displacements were obtained after the final excavation sequence.

Figure 4-11 shows the horizontal displacement along the extensometer. This figure clearly depicts the increase in horizontal displacement when decreasing the fracture normal stiffness. It can be seen two markedly changes in the displacement trend, which are tightly linked to the position of the two sets of discontinuities. The horizontal displacement trend indicates greater displacement in fracture B rather than the fracture A. This can be attributed to the difference in confinement stress being lower when the fracture is closer to the slope surface. The increase of horizontal displacement as normal stiffness decreases is as expected due to the orientation of the fractures. It is noted, however, the substantial increase in displacement out of slope for the fracture closer to the excavation face. This suggests the importance of stiffness parameters and confinement if trying to history-match slope performance measurements in terms of displacements.

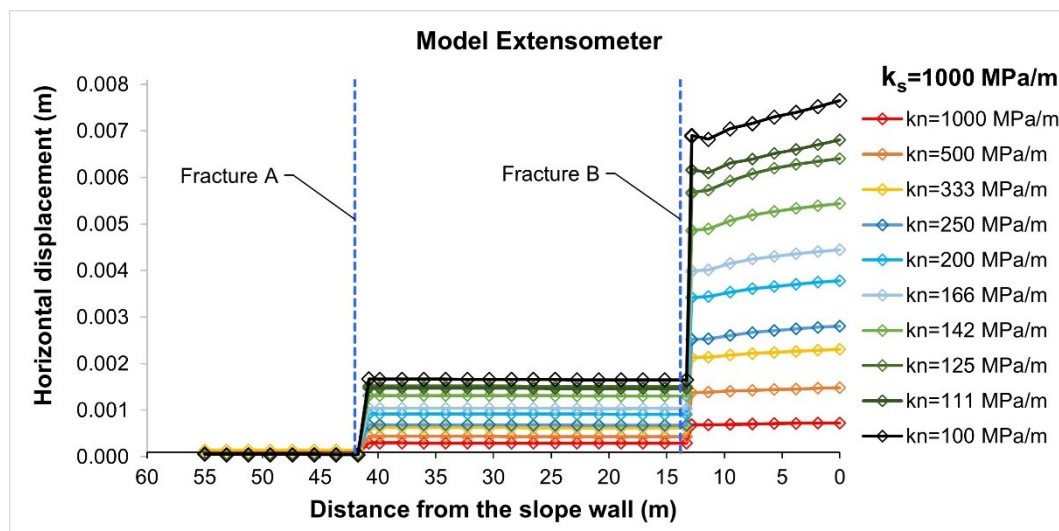


Figure 4-11: Horizontal displacements

A similar pattern was also observed in the vertical displacements, shown in Figure 4-12. The location of the two sets of fractures also exhibited a change in the vertical displacement patterns. This change can be attributed to difference of stiffness between the rock mass and the discontinuities. Given the orientation of the fractures, there is an elastic rebound (upwards) that becomes very noticeable due to the lower normal stiffness of the fractures compared to the rock mass. As we move closer to the excavation face, the rebound becomes less until we reach the fracture closer to the excavation face,

where elastic rebound is larger due to the increased loss of confinement. The magnitude of both horizontal and vertical displacement is relatively small.

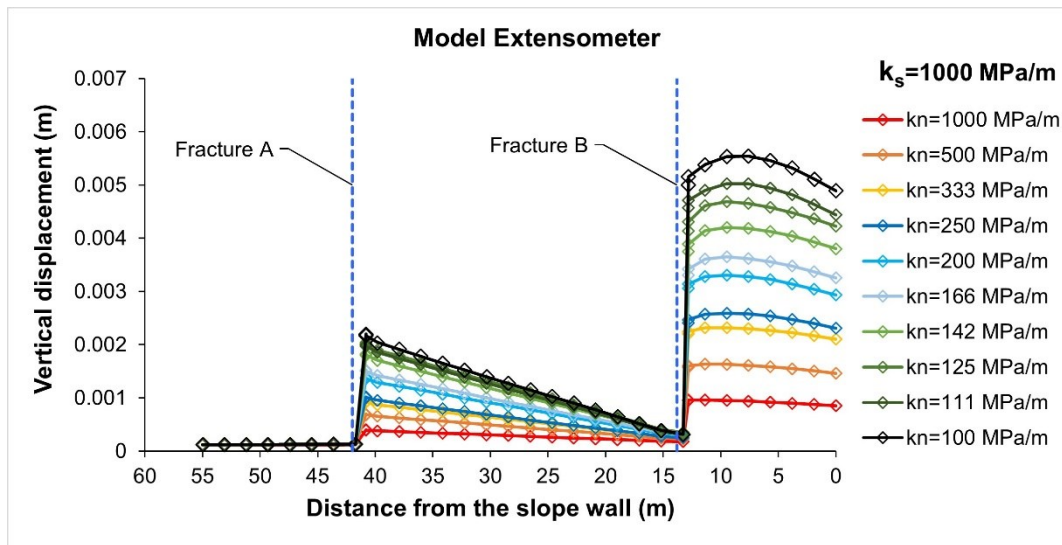
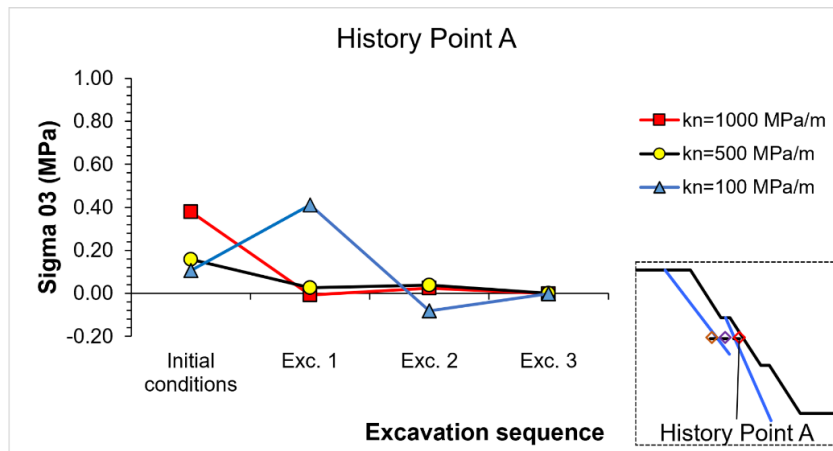


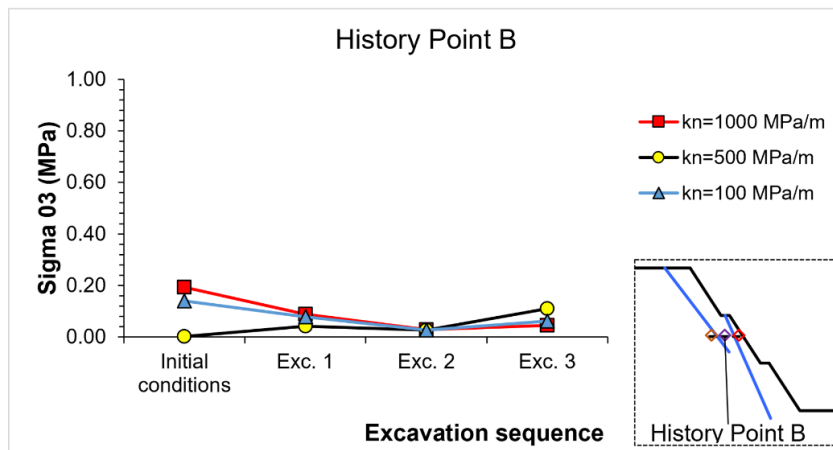
Figure 4-12: Vertical displacement

The changes in minimum principal stress (σ_3) through the course of the excavation sequence were compared for three fracture normal stiffness values: 1000 MPa/m, 500 MPa/m, and 100 MPa/m. Figure 4-13 shows the variation of σ_3 at history point A, B and C at initial conditions and the stages of the excavation sequence. From this figure it can be seen that σ_3 at initial conditions varies, this can be attributed to the fracture stiffness as it influences in the distribution of the stresses in the vicinity of the fractures. Moreover, the lower the fracture stiffness the softer the system. Figure 4-13a shows σ_3 changes at History Point A, close to the excavation face. The stress magnitudes become very low with initial excavation stages, corresponding values less than 0.1 MPa. This is to be expected due to the proximity to the face of excavation, however, clearly shows the significant reduction in confinement for rock masses adjacent to major fractures close to the excavation face and corresponding reduction in frictional resistance. Figure 4-13b shows σ_3 changes at History Point B, deeper into the slope and behind the first fracture. The reduction is also very drastic and for early in the excavation sequence, corresponding values less than 0.2 MPa. This indicates that the loss in confinement would also have a significant effect on the behaviour of the rock mass in this location. Figure 4-13c shows σ_3 changes at

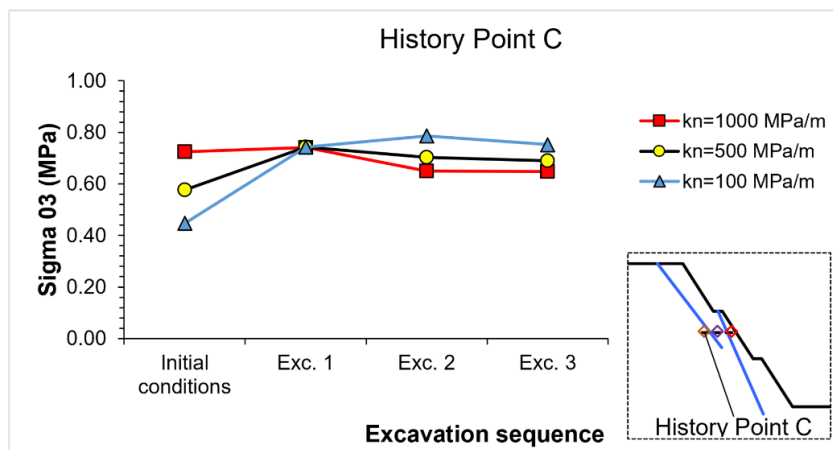
History Point C, behind the second fracture. At this location, the stress magnitude does not change significantly throughout the course of excavation sequence.



a)



b)



c)

Figure 4-13: Minimum principal stress changes through the excavation sequence for: a) History Point A, b) History Point B, and c) History Point C

4.4.1.2 Discontinuum model: Case one

Figure 4-14 shows the horizontal and vertical displacement monitored at three locations: near the crest, near the slope surface in the middle part, and near the toe of the slope. The displacements trends reflect the changes imposed by the initial conditions and excavation sequence, reaching equilibrium at the end of each sequence. These trends were monitored in the eight modelling simulations that were carried out.

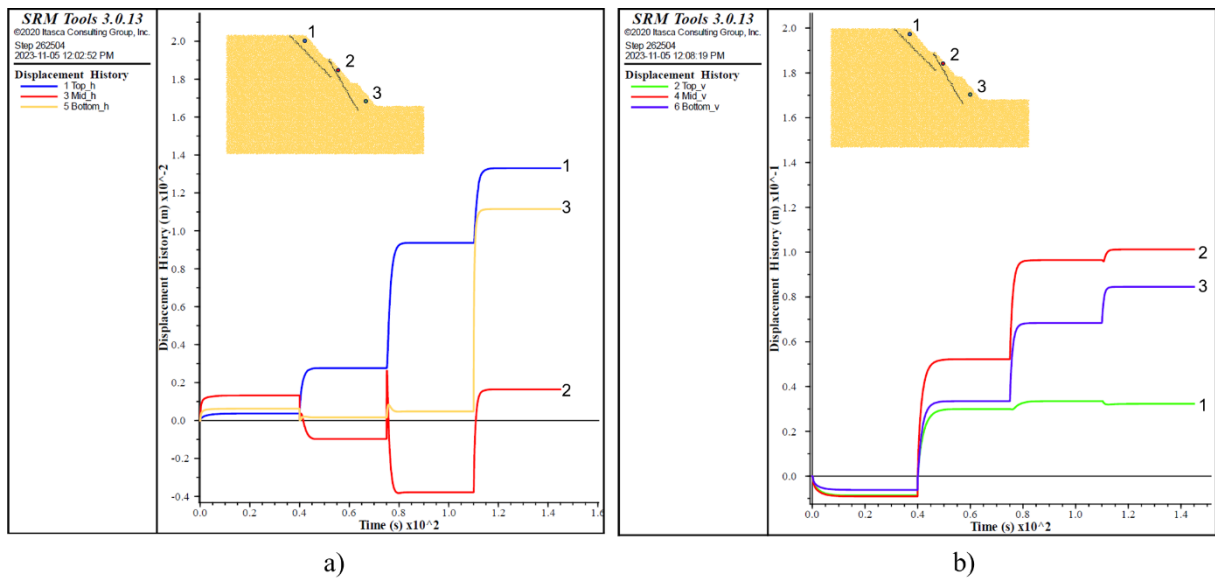


Figure 4-14: Displacement recorded by the three history points in the a) horizontal direction and b) vertical direction

Displacement contours after the final stage of the excavation sequence are compared between the different fracture normal stiffnesses adopted. The displacement contour in the horizontal direction is shown in Figure 4-15. It can be seen that the horizontal displacement increases near the crest of the slope and its magnitude becomes higher when the fracture normal stiffness decreases. At a fracture normal stiffness of 150 MPa/m, the increase in horizontal displacement increases substantially for the rock block defined by fracture B and the face of excavation. This increase in horizontal displacement is more pronounced at a fracture normal stiffness of 50 MPa/m. This increase in magnitude suggest that slope instability could be developing. The strain compatibility between the block defined by Fracture B and intact rock at the toe would lead to stress concentrations in the rock bridge at the toe.

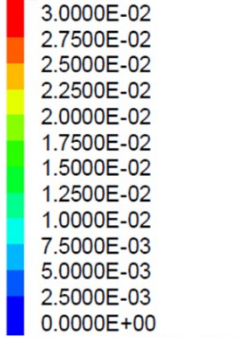
SRM Tools 3.0.13

©2020 Itasca Consulting Group, Inc.
Step 262504
2023-09-05 3:27:18 PM

Joint Trace

Joint Trace
■ Joint Set 1

Displacement Contour



Component: X Direction

Normal stiffness- k_n

Shear stiffness- k_s

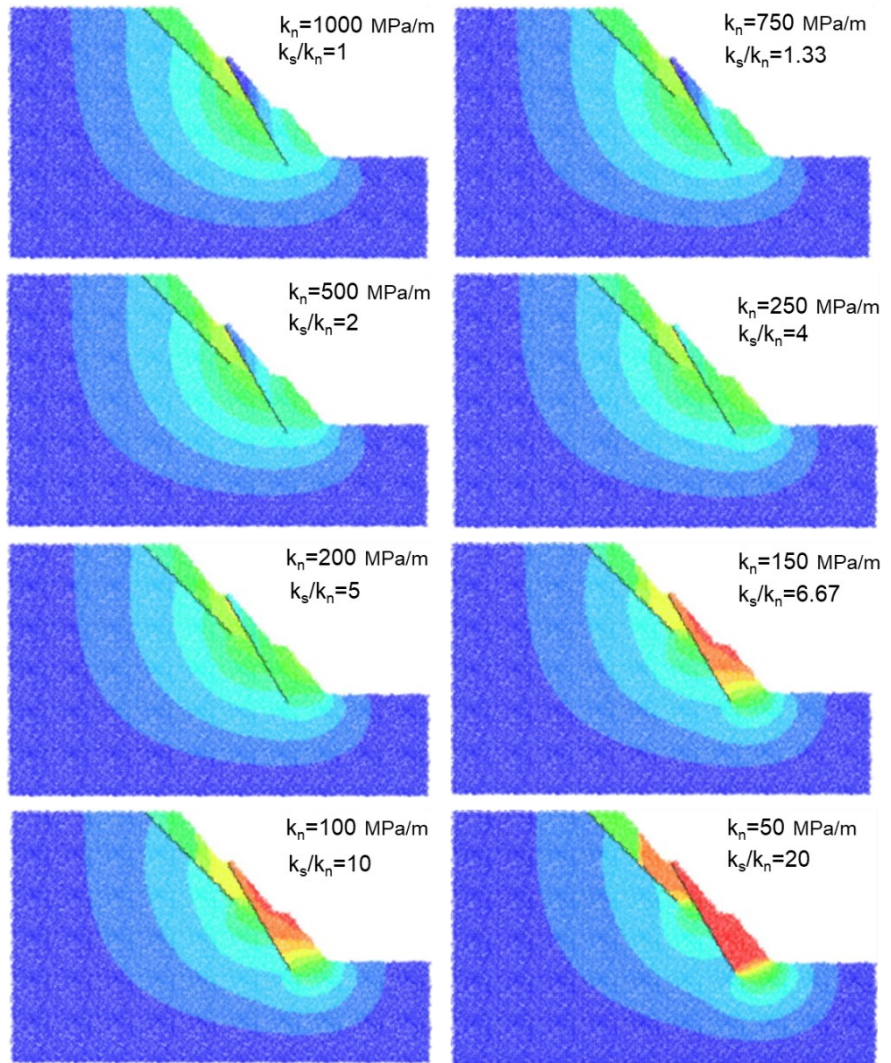


Figure 4-15: Horizontal displacement contours for different fracture normal stiffness values.

Case one

Similarly, a comparison between the vertical displacement contours obtained by a decrease of fracture normal stiffness is shown in Figure 4-16. It can be seen that the magnitude of vertical displacement is higher for the rock block defined by fracture B and the face of excavation. This in turn reflects the unstable areas that can lead to global failure. Although there is an increase in vertical displacement as the fracture normal stiffness is reduced, it is not as extreme as for the horizontal displacement.

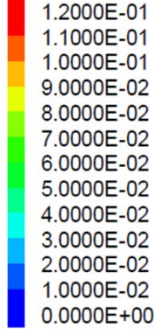
SRM Tools 3.0.13

©2020 Itasca Consulting Group, Inc.
Step 262504
2023-09-05 3:30:25 PM

Joint Trace

Joint Trace
Joint Set 1

Displacement Contour



Component: Z Direction

Normal stiffness- k_n

Shear stiffness- k_s

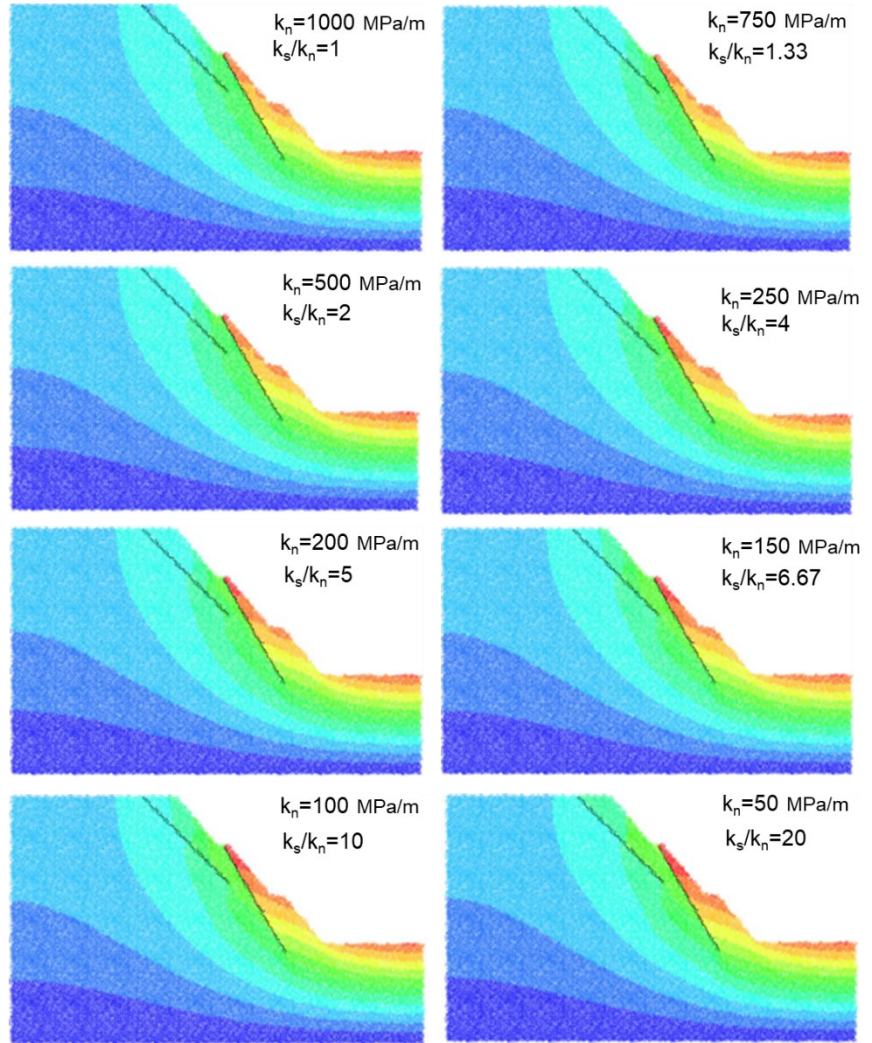


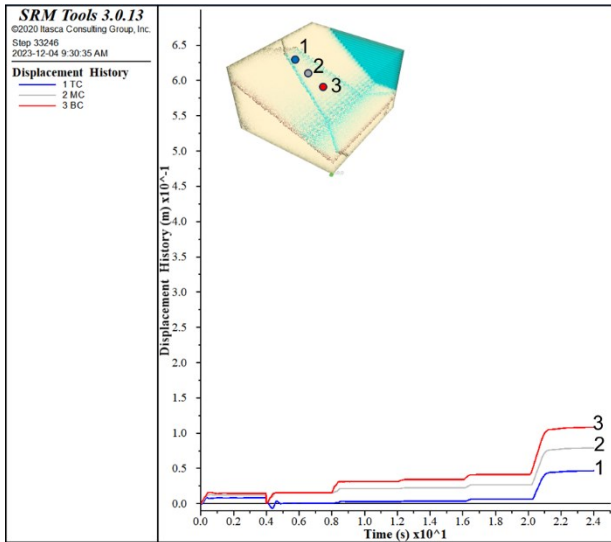
Figure 4-16: Vertical displacement contours for different fracture normal stiffness values.

Case one

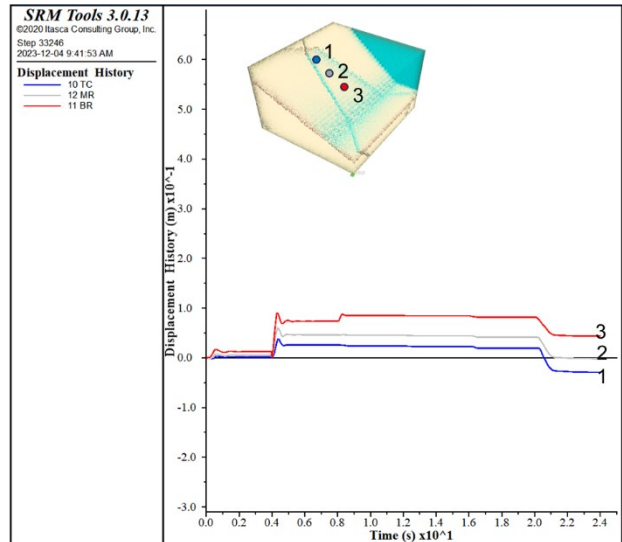
While Slope Model provides valuable information about factors that impact the slope stability, it does not offer a same level of detail in terms of principal stresses tracking as other sophisticated software (e.g., UDEC developed by ITASCA).

4.4.1.3 Discontinuum model: Case two

Figure 4-17, Figure 4-18, and Figure 4-19 show the horizontal and vertical displacement results monitored by three history points located along the slope surface. The displacement trends captured by the history points reflects the initial conditions and excavation sequence. These trends vary widely among the three values of fracture normal stiffness adopted.

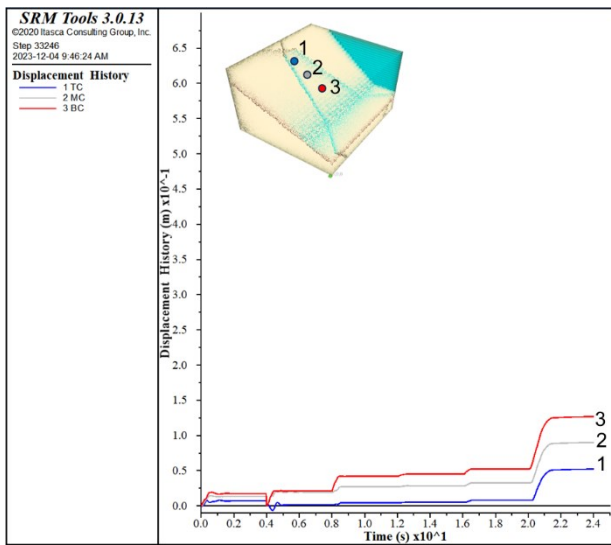


a)

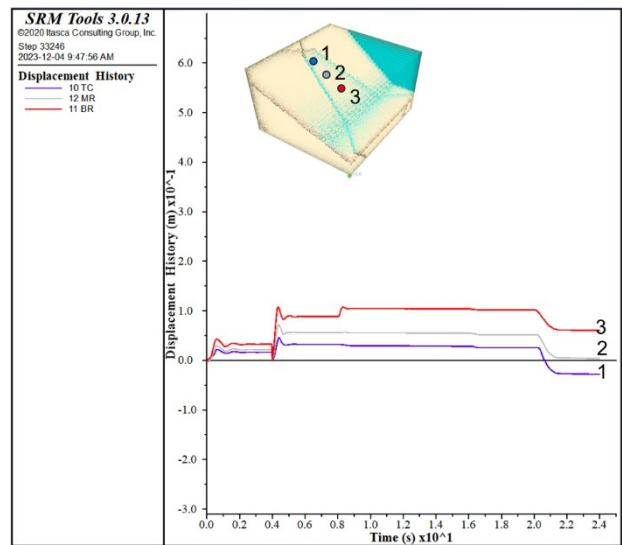


b)

Figure 4-17: Displacement recorded by the three history points in the a) horizontal direction and b) vertical direction adopting a normal stiffness of 1000 MPa/m



a)



b)

Figure 4-18: Displacement recorded by the three history points in the a) horizontal direction and b) vertical direction adopting a normal stiffness of 500 MPa/m

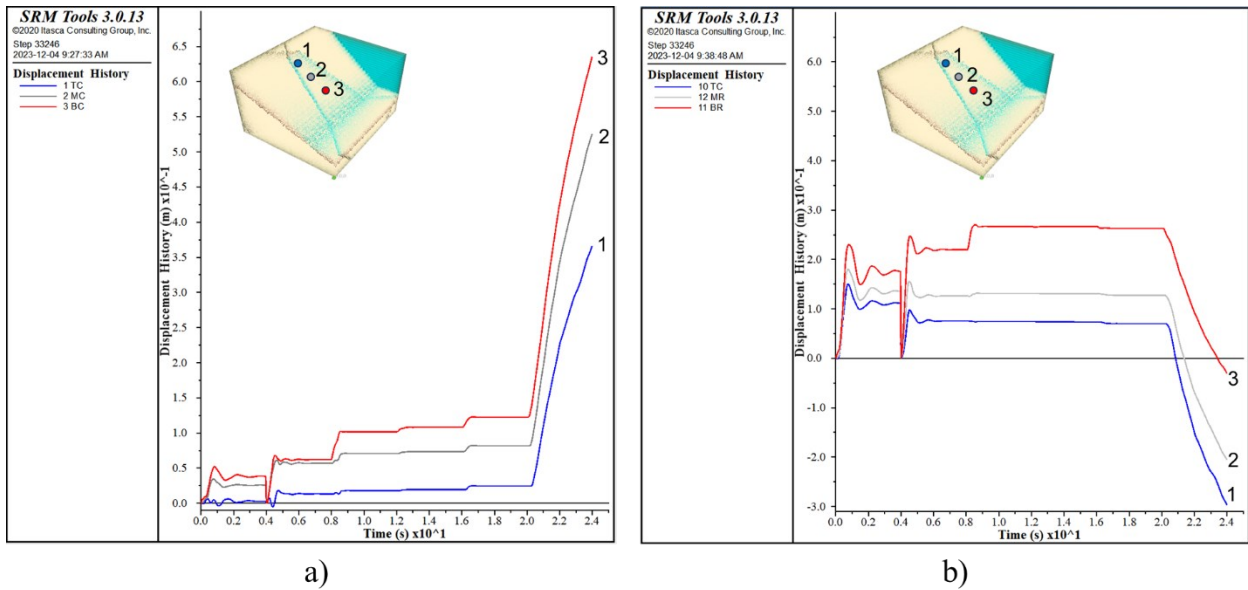


Figure 4-19: Displacement recorded by the three history points in the a) horizontal direction and b) vertical direction adopting a normal stiffness of 100 MPa/m

The horizontal displacement trend of the initial model (Figure 4-17) adopting a fracture normal stiffness of 1000 MPa/m is approximately in the order of 0.15 m. The second model (Figure 4-18) adopting a fracture normal stiffness of 500 MPa/m, the horizontal displacement trend increases only slightly in comparison to the initial model. In both cases, the horizontal displacement trends show close similarity indicating a stable system characterized by the steady state line at the final stage of the excavation sequence. Notably, in the third model (Figure 4-19) adopting a fracture normal stiffness of 100 MPa/m the horizontal displacement exhibits a continuously increasing curve at the final stage of the excavation sequence. This indicates that the slope is unstable.

An opposite pattern can be seen in vertical displacement results at the final stage of the excavation sequence. In the initial and second models, the vertical displacement trends decrease in magnitude which can be related to settlement of the rock mass adjacent to the faults. However, this settlement remains constant and does not increase exponentially but linearly. In contrast, in the third model adopting a normal stiffness of 100 MPa/m, the settlement is quite higher and exhibits an increased curve that indicates instability. This confirms that the normal stiffness plays an active role on the displacement results and prediction of potential instability.

Additionally, displacement contours after the final stage of the excavation sequence are also compared between the different fracture normal stiffnesses adopted. The displacement contour in the horizontal direction is shown in Figure 4-20. This figure compares well the increase of horizontal displacement delineating the rock mass block formed by the faults network. In the central part of this block, the magnitude of the horizontal displacement is approximately 0.2 m for 1000 MPa/m and 500 MPa/m. However, for 100 MPa/m, after the final stage of excavation, the magnitude of the horizontal displacement increased two to three times compared to the values obtained in the previous models. Although, this magnitude will continuously increase towards failure according to the trend in Figure 4-19.

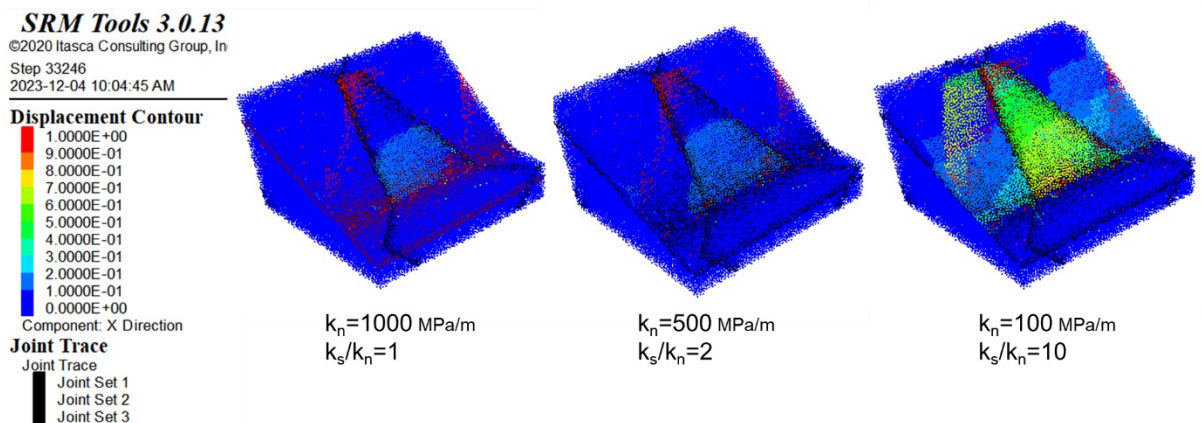


Figure 4-20: Horizontal displacement contours for different fracture normal stiffness values.

Case two

Similarly, a comparison between the vertical displacement contours obtained by a decrease of discontinuity normal stiffness is shown in Figure 4-21. The vertical displacement observed in this figure shows the settlement in the upper part of the block, which increases in area when decreasing the fracture normal stiffness.

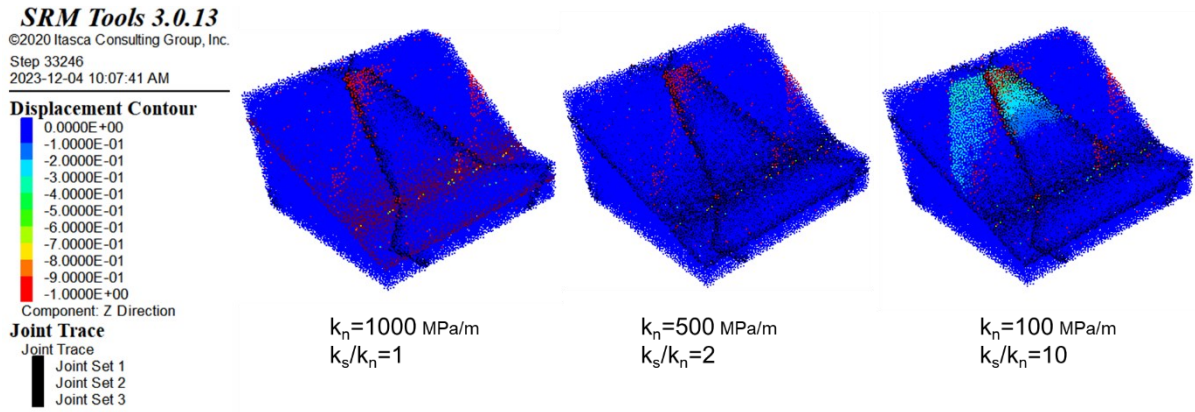


Figure 4-21: Vertical displacement contours for different fracture normal stiffness values.
 Case two

4.4.2 The effect of normal stiffness on Strength Reduction Factor (SRF)

4.4.2.1 Continuum model: Case one

Figure 4-22 shows the calculated SRF for each fracture normal stiffness value. It can be seen a clear drop in the calculated SRF by decreasing the fracture normal stiffness. At a fracture normal stiffness of 1000 MPa/m the calculated SRF (1.45) reflects a stable condition, however this stable condition transitions towards a critical condition when adopting a fracture normal stiffness of 100 MPa/m, leading to a significant decrease of approximately 40% in the calculated SRF (0.85).

Moreover, the SRF values obtained at a fracture normal stiffness greater than 500 MPa/m can meet typical open pit slope Design Acceptance Criteria (DAC) with Factor of Safety (FoS) of 1.3, or at stiffnesses of 167 MPa/m would meet more aggressive criteria (FoS of 1.2), depending on the slope design criteria adopted (e.g. the DAC proposed by Read and Stacey, 2009; or the Reliability-Based Design Acceptance Criteria (RBDAC) proposed by Maccitotta et al. in 2020, 2021). Whereas at lower fracture normal stiffnesses, the SRF values drop to unacceptable safety levels. These results can substantially impact the slope design process.

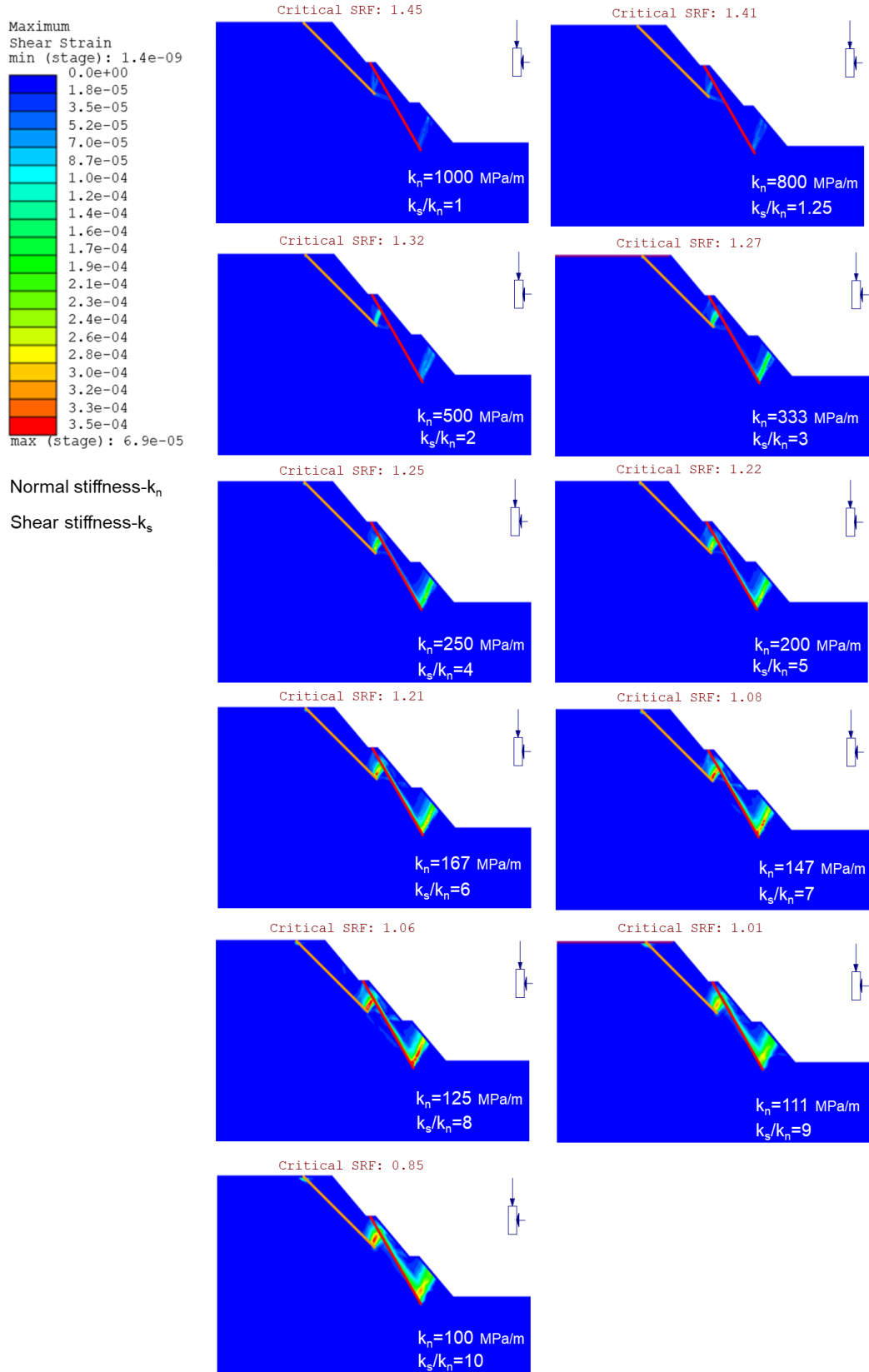


Figure 4-22: Calculated Strength Reduction Factor at different discontinuity normal stiffness values. Continuum model results in RS2

The results in Figure 4-22 also show that the internal shearing increases as the fracture normal stiffness decreases. The failure surface is represented by sliding along the fractures and shear failure of rock mass bridges, which is attributed to the internal shearing expressed as the maximum shear strain zones. The failure surface becomes more defined with the decrease of fracture normal stiffness. Table 4-5 summarizes the calculated SRF obtained from each scenario. The results obtained highlight the variability and the impact of fracture normal stiffness on the calculated SRF.

Table 4-5: Results of calculated Strength Reduction Factor (SRF) for variations of fracture normal stiffness. Continuum model results in RS2

Fracture Normal Stiffness, k_n (MPa/m)	Fracture Shear Stiffness, k_s (MPa/m)	k_s/k_n	Strength Reduction Factor, SRF
1000.00	1000	1.00	1.45
800.00	1000	1.25	1.41
500.00	1000	2.00	1.32
333.33	1000	3.00	1.27
250.00	1000	4.00	1.25
200.00	1000	5.00	1.22
166.67	1000	6.00	1.21
142.86	1000	7.00	1.08
125.00	1000	8.00	1.06
111.11	1000	9.00	1.01
100.00	1000	10.00	0.85

The variation of calculated SRF as fracture normal stiffness is reduced is shown in Figure 4-23. If DAC were defined by a FoS of 1.3, it can be seen that only 30% of the results fall within acceptable values, while the remaining 70% would require redesign. Additionally, the percentage of points in a critical condition, close to the limit of equilibrium, is 36%. These plots also suggest that SRF decreases as fracture normal stiffness decreases following a logarithmic trendline, in our case with a goodness of fit, R-squared, of 0.86. Figure 4-24 shows the ratio between fracture shear stiffness and normal stiffness

against the calculated SRF. The relationship between fracture stiffness ratio and SRF is linear with a goodness of fit, R-squared, of 0.95.

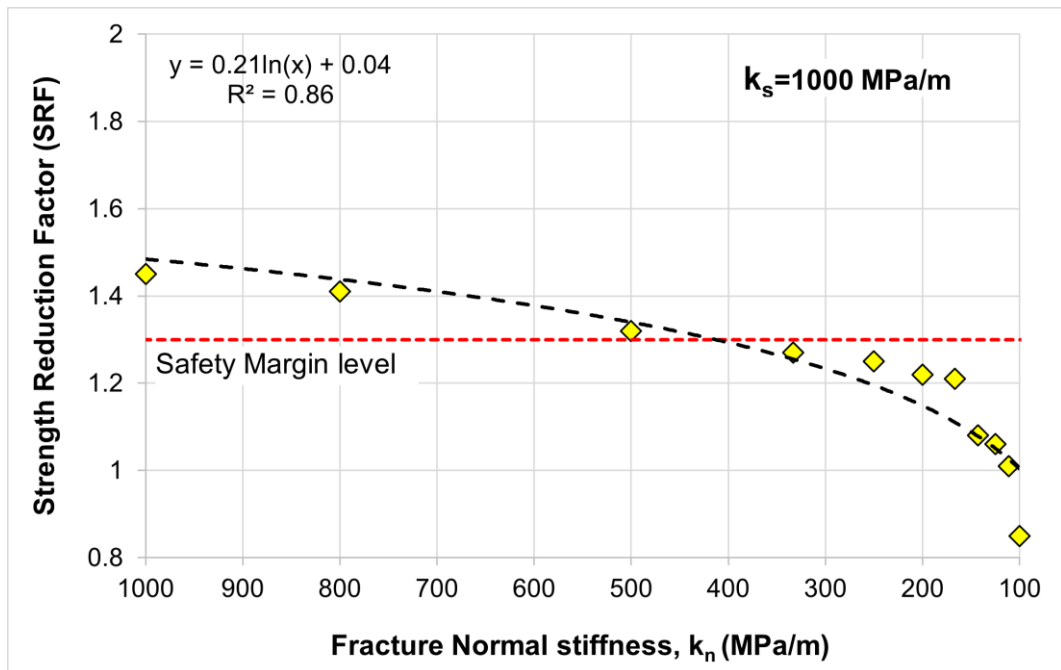


Figure 4-23: Variation of calculated SRF with fracture normal stiffness

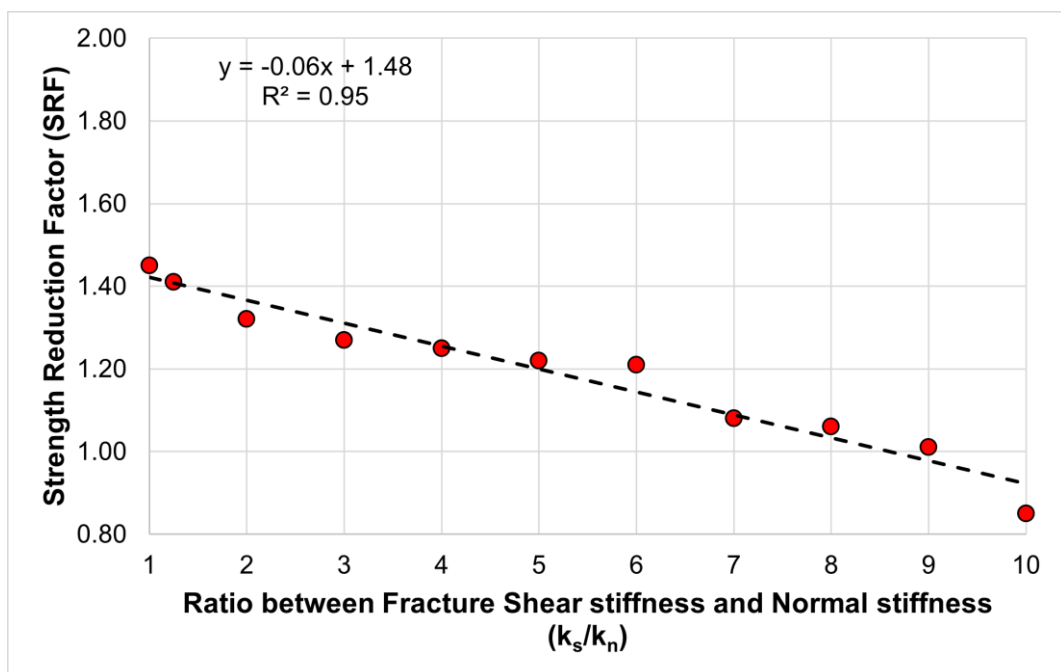


Figure 4-24: Variation of SRF with the ratio between fracture shear to normal stiffness

4.4.2.2 Discontinuum model: Case one

Slope Model also utilizes the strength reduction method (Bastola et al., 2020) to calculate values of reported FoS, however the nomenclature in the software is FoS as opposed to SRF in RS2. The FoS was calculated at the end of the excavation sequence and the calculation is done for each element in the model, as opposed to an overall calculation. The modelling results shown in Figure 4-25 illustrate the decrease in FoS while decreasing the normal stiffness value. This is consistent with the results of the continuum model. It can be noticed that the contours of FoS change from a stable condition (over 1.0 in greens and colder colours) to a critical condition (red scale colours) as the normal stiffness is reduced. Furthermore, at a normal stiffness value between 1000 MPa/m and 200 MPa/m, some relatively small unstable zones are localized in the upper ISA. Below this range, the unstable zone becomes localized in the middle ISA. The results obtained using a discontinuum model confirm the importance of the normal stiffness in the calculated FoS, and importantly, the mode of failure.

Joint Trace

Joint Trace
 Joint Set 1

Factor of Safety Contour

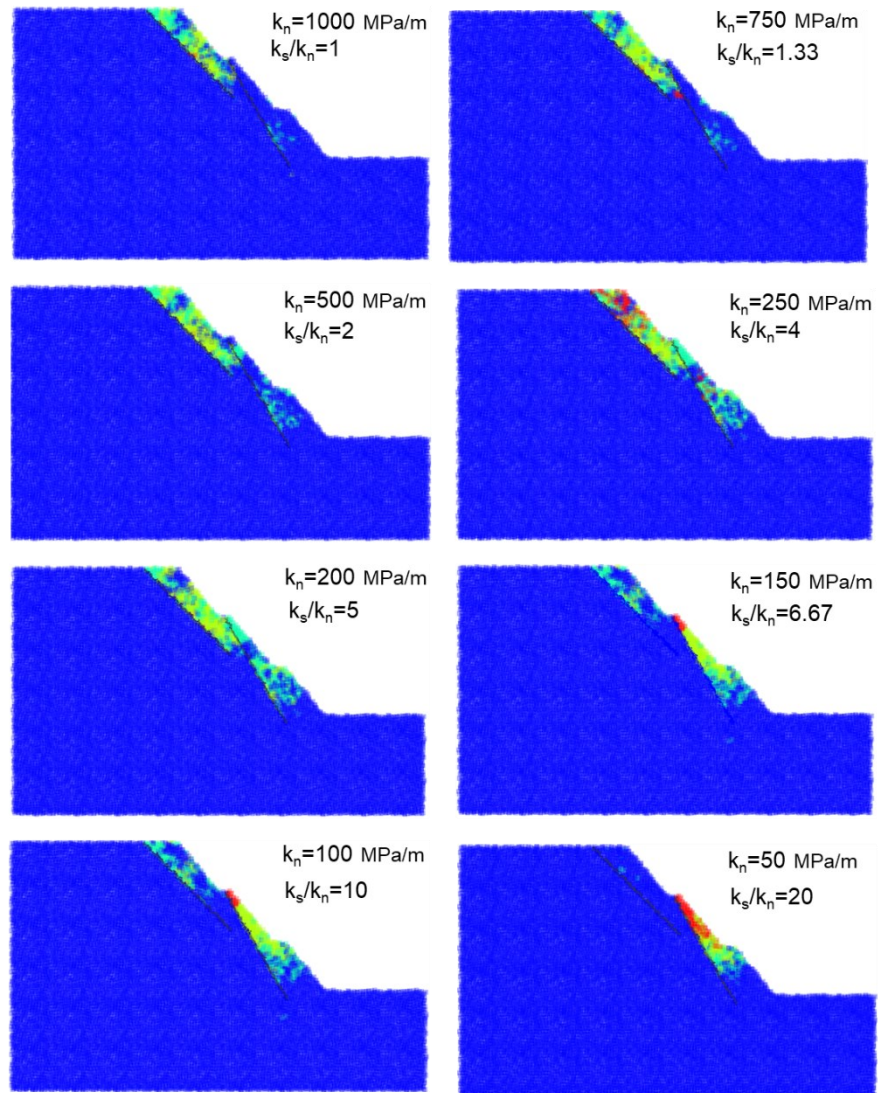
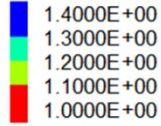


Figure 4-25: Contours of Factor of Safety for the different models analyzed at different fracture normal stiffness. Discontinuum model for Case one

Slope Model allows tracking the development of rock mass shearing, and Figure 4-26 shows the potential failure mechanisms that include the development of rock breakage through the course of the excavation sequence. In this figure, the rock breakage pattern, represented by the shaded areas in dark red, varies as fracture normal stiffness is reduced. This figure shows the development of shallow tension cracks behind the crest. The level of crack initiation and connectivity in all plots is more pronounced along the fracture A than fracture B, creating a vertical crack pattern that propagates and intersects both the slope surface and the toe of the upper ISA. Also, it can be seen that the extension of the rock breakage zone at the toe of the middle ISA decreases with the decreasing of fracture normal stiffness.

At a fracture normal stiffness between 1000 MPa/m and 500 MPa/m, the breakage of rock bridges suggests that slope instability can involve the upper and middle ISA. At a fracture normal stiffness between 1000 MPa/m and 100 MPa/m, no coalescence of the two fractures and rock bridge breakage through the toe of excavation is observed. However, at a fracture normal stiffness of 50 MPa/m, rock bridge breakage allows the development of a failure zone that combines coalescence of the two discontinuities and breakage at the toe of excavation. This can suggest a slope instability of the overall slope excavation. These results show the impact that the fracture normal stiffness can have on the slope failure mechanism even though the major fractures do not daylight at the slope face.

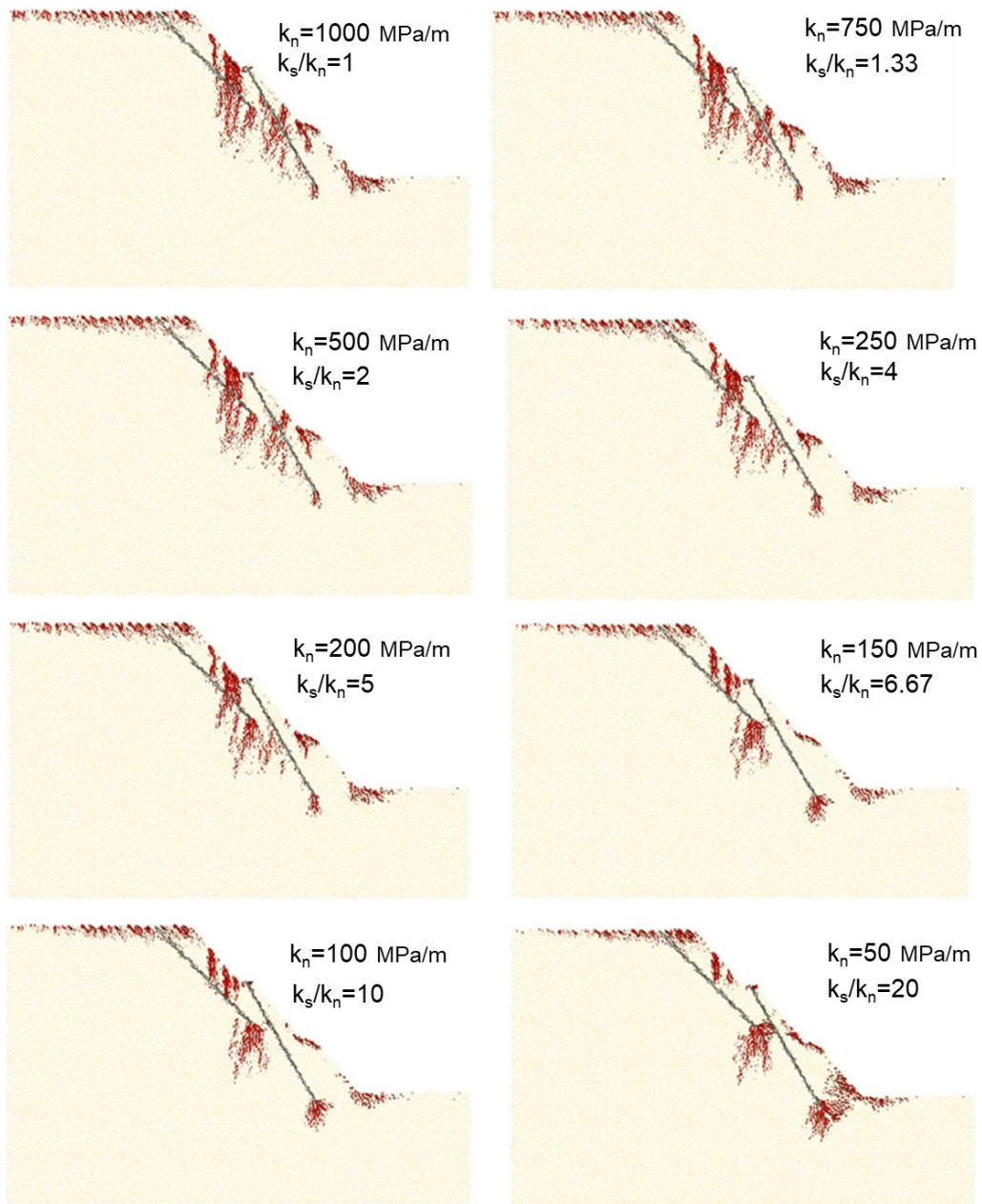


Figure 4-26: Rock breakage generated through the course of excavation sequence.

Discontinuum model for Case one

A representative FoS value was chosen based on the FoS contours and the scale of instability from Figure 4-25 (visually selected based on the most common values for failure that would involve inter-ramp or overall scales). This aimed to make a comparison between the results from the continuum and discontinuum models. Figure 4-27 shows variations of calculated SRF with Slope Model as fracture normal stiffness is reduced and compared against the results obtained with the continuum model (RS2) in terms of SRF. Although the results from the discontinuum model are lower than those obtained with

the continuum model, this figure indicates a clear consistency in the trend of results and suggests this response is not an artifact of the modelling approach employed.

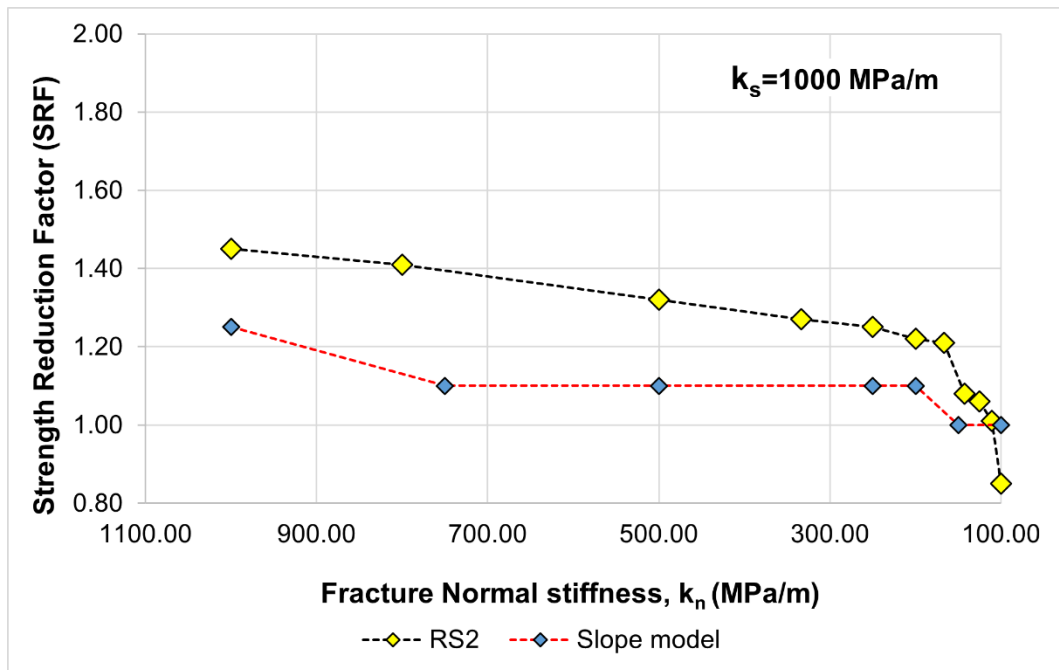


Figure 4-27: SRF results using RS2 and Slope Model at different fracture normal stiffness

4.4.2.3 Discontinuum model: Case 2

The corresponding FoS was calculated at the end of the excavation sequence for each model. The modelling results shown in Figure 4-28 display the contoured FoS while decreasing the fracture normal stiffness value. The effect on the calculated FoS is in general quite similar than those obtained in the Case 1, even though they are 2-dimensional models representing a distinct general configuration. At a normal stiffness value of 1000 MPa/m and 500 MPa/m, the contoured FoS at the verge of equilibrium is localized in small blocks. In contrast, at a normal stiffness of 100 MPa/m, the FoS at the verge of equilibrium is observed at a greater scale. This is significant for decision-making, as the volume of material involved in a potential failure can be substantially different depending on the fracture normal stiffness values.

SRM Tools 3.0.13
 ©2020 Itasca Consulting Group, Inc.
 Step 33246
 2023-12-04 11:15:56 AM

Materials
 Mark Type: cube
 Test Rock
 Scale: 54.3939

Joint Trace
 Joint Trace
 Joint Set 1
 Joint Set 2
 Joint Set 3

Factor of Safety Contour
 1.5500E+00
 1.5000E+00
 1.4500E+00
 1.4000E+00
 1.3500E+00
 1.3000E+00
 1.2500E+00
 1.2000E+00
 1.1500E+00
 1.1000E+00
 1.0500E+00
 1.0000E+00

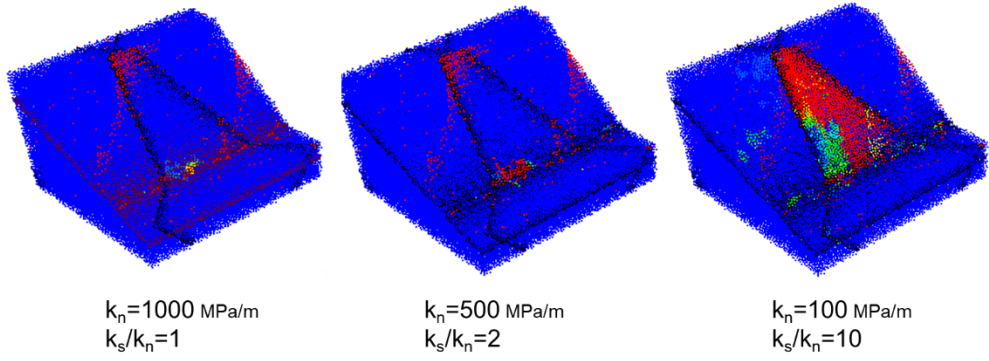


Figure 4-28: Contours of Factor of Safety for the different models analyzed at different fracture normal stiffness. Discontinuum model for Case two

Furthermore, along with the computed FoS, the breakage of rock bridges is also evaluated (Figure 4-29). At a fracture normal stiffness of 1000 MPa/m and 500 MPa/m, no coalescence of the two faults and rock bridge breakage through the toe of excavation is observed. However, at a fracture normal stiffness of 100 MPa/m, rock bridge breakage is concentrated close to the toe of the slope allowing to the development of a deep-seated slope failure.

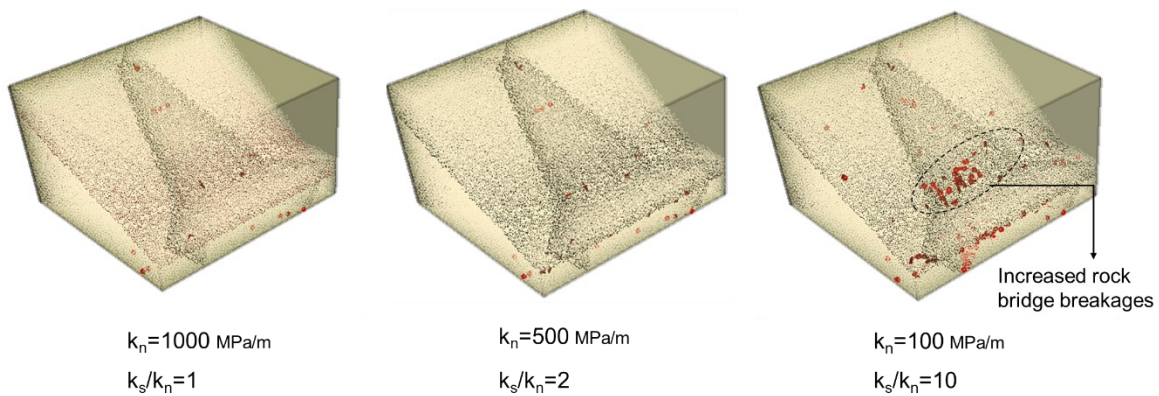


Figure 4-29: Rock breakage generated through the course of excavation sequence. Discontinuum model for Case two

4.5 Conclusions

This chapter has evaluated the influence of the fracture normal stiffness on slope deformation and stability as excavation progresses. 2-dimensional and 3-dimensional numerical modelling approaches adopted included a continuum Finite Element Method approach (RS2) and a discontinuum approach (Slope Model) to represent the mechanical response of the rock mass and major fractures subjected to initial conditions and to excavation sequence.

The two cases analyzed that represent two typical pit slope configurations include specific fracture networks modelled explicitly. The fracture normal stiffness was decreased gradually while the fracture shear stiffness was kept constant throughout the models. The results of the models showed that the decrease of fracture normal stiffness led to a reduction in the resultant Strength Reduction Factor. Also, it is generally seen that the fracture normal stiffness causes an increase in displacement and in shear strain that defines the failure mechanism and volume of slope failure. The results of the discontinuum and continuum approaches are consistent, which indicates the results are not an effect of the modelling technique. Additionally, it was observed that the rock breakage pattern is sensitive to the fracture normal stiffness.

From the results it is apparent that selecting an adequate fracture normal stiffness can be a critical component in the slope design process. In this regard, combining monitoring data with numerical modelling can provide a full slope-scale fracture normal stiffness aiming to reduce the epistemic uncertainty associated with pit slope design. As such, it is concluded that the fracture normal stiffness must be taken into account to provide better slope design evaluation studies, risk assessments and must be assessed using stress-strain analyses. However, it is important to note that as fracture normal stiffness is characterized by a non-linear behaviour, normal stiffnesses estimated from conventional laboratory tests would not be representative of the mobilized fracture normal stiffness; and calculated SRF could overestimate the stability of excavated slopes as the excavation face approaches major fractures.

5.0 General conclusions and future research work

5.1 Conclusion

Specific conclusions have been outlined in Chapter 3 and Chapter 4 of this thesis. These findings demonstrate the significance of understanding, incorporating, and recognizing uncertainties and its limits in open pit slope design. Furthermore, the tools for handling uncertainties such as probabilistic and sensitivity analysis, along with adopting a robust acceptability criteria such as the 2020 RBDAC can potentially enhance the slope design process. This improvement can lead to increased business rewards by implementing a slope design that meets adequate reliability, economic, and safety aspects.

The parametric study conducted in this thesis demonstrates the practicality of characterizing parametric uncertainty through the COV. The reduction of uncertainty, seen as an increase in valuable information, offers two key advantages: it can establish a defensible framework to increase site-specific information and provides insights into increasing reliability levels. Furthermore, the use of COV to characterize input parameters, which are propagated in the slope design process using 2-dimensional slope stability analysis, is reflected in the COV of the output parameter, specifically the calculated FoS. Additionally, it was observed that the variability of structural parameters, often quite limited at the initial stages of the project, plays an important role in slope stability analysis by introducing anisotropy. In this regard, it was demonstrated that stereographic projections are a valuable tool for defining potential ranges to introduce anisotropy. In general, the results have shown that the absence of large-scale structures does not yield to Inter-ramp and/or Overall slope failure. Thus, it is crucial their evaluation in terms of location, geometry, and strength parameters.

The probabilistic analysis conducted, which considered various sources of uncertainty, proves to be a powerful tool for assessing uncertainties. The three levels of reliability tested demonstrated that the outcomes, such as FoS, PoF, and COV, align well with the ranges proposed in the 2020 RBDAC and the assumptions behind its mathematical construct. On this basis, the practicality and flexibility of the 2020

RBDAC were compared with the current DAC (from the 2009 guidelines). The results of this comparison indicate that implementing the 2020 RBDAC in slope design could lead to a reduction in the volume of excavation for the next pushback in an open pit. This reduction would result in decreased costs therefore increased profitability of the open pit mine.

In the second part of the thesis, another source of uncertainty identified is the fracture normal stiffness. This parameter cannot be assessed through traditional methods such as the LE. A literature review of this stress-dependent parameter reveals its highly variable nature, often reported in wide ranges. Consequently, the stiffness parameter introduces a significant epistemic uncertainty. While different recommendations for adopting a particular value are provided, it is crucial to acknowledge its limitations and associated impacts. The sensitivity analysis conducted in Chapter 4 demonstrates that a reduction in normal stiffness increases displacement and decreases the calculated FoS. The effect on displacement is in line with previous investigations. Importantly, adopting different fracture normal stiffnesses can lead to significantly different FoS which could lead to different decisions regarding acceptability of a slope design when evaluated against the 2009 DAC or the 2020 RBDAC matrix.

Utilizing a probabilistic approach and conducting sensitivity analyses through both LE and stress-strain analysis, along with adopting the 2020 RBDAC, can lead to more robust open pit slope design. This integrated approach has the potential to reduce epistemic uncertainty, resulting in a more comprehensive slope design that aligns with operational requirements in terms of both economic and safety considerations.

5.2 Recommended Future Research Work

The recommended future work is the following:

- Adopting probabilistic analysis in 3-dimensional analysis, where the locations of geological features can be more robustly evaluated.

- Incorporating a Discrete Fracture Network (DFN) approach, which can enhance our understanding of the natural variability of fractures at both smaller scales, such as joints, and larger scales, such as faults, thereby providing greater design reliability.
- The approach developed in this thesis can be extended to other geological environments, whether they share similar characteristics or present distinct features. Importantly, considering that the behaviors of hard rocks and weak rocks differ significantly, assessing uncertainties in weak rock environments is recommended to extend the applicability and flexibility of the 2020 RBDAC.
- Finally, the stress-strain analysis conducted in this thesis should be subjected to testing using site-specific displacement information and to validate the obtained results under the adequate stress levels and confirm the hypothesis that low mobilized normal fracture stiffness could be a major contributing factor to observed pit slope failures.

6.0 References

- Abramson, L.W., Lee, T. S., Sharma, S., and Boyce, G. M. (2002). Slope stability and stabilization methods (2nd ed.). John Wiley & Sons Inc.
- Adams, B. M. (2015). Slope Stability Acceptance Criteria for Opencast Mine Design. G. Ramsay (Ed.), Proceedings of the 12th Australia New Zealand Conference on Geomechanics (pp. 8), Wellington, New Zealand.
- Al-E'Bayat, M., Sherizadeh, T., and Guner, D. (2023). Laboratory-Scale Investigation on Shear Behavior of Non-Persistent Joints and Joint Infill Using Lattice-Spring-Based Synthetic Rock Mass Model. *Geosciences*, 13(2), 23. <https://doi.org/10.3390/geosciences13020023>
- Alzoubi, A. M. (2009). The effect of tensile strength on the stability of rock slopes. PhD thesis. Department of Civil and Environmental Engineering. University of Alberta. <https://doi.org/10.7939/R32J68F7S>
- Baecher, G. B., and Christian, J. T. (2003). Reliability and statistics in geotechnical engineering. John Wiley & Sons Inc.
- Bandis, S. C. (1993). Engineering properties and characterization of rock discontinuities. *Comprehensive rock engineering*, 1, 155-183.
- Bandis, S. C., Lumsden, A. C., and Barton, N. R. (1983). Fundamentals of rock joint deformation. In *International Journal of Rock Mechanics and Mining Sciences & Geomechanics Abstracts* 20 (6), 249-268. [https://doi.org/10.1016/0148-9062\(83\)90595-8](https://doi.org/10.1016/0148-9062(83)90595-8)
- Barton, N. (1982). Shear strength investigations for surface mining. In *Proceedings of the 23rd US Rock Mechanics Symposium* (pp. 178-180).
- Bastola, S., Cai, M., and Damjanac, B. (2020). Slope stability assessment of an open pit using lattice-spring-based synthetic rock mass (LS-SRM) modeling approach. *Journal of Rock Mechanics and Geotechnical Engineering*, 12(5), 927-942. <https://doi.org/10.1016/j.jrmge.2019.12.019>
- Baynes, F. J. (2010). Sources of geotechnical risk. *Quarterly Journal of Engineering Geology and Hydrogeology*, 43, 321-331. <https://doi.org/10.1144/1470-9236/08-00>

- Bedi, A. and Harrison, J. (2013). Characterisation and propagation of epistemic uncertainty in rock engineering: A slope stability example. In Proceedings of the ISRM International Symposium-EUROCK 2013, October 23–26, 2013, Wroclaw, Poland.
- Bewick, R., Amann, F., Kaiser, P. and Martin, C. (2015). Interpretation of UCS test results for engineering design. In proceedings of the 13th ISRM International Congress of Rock Mechanics, May 10–13, 2015, Montreal, Canada.
- Brady, B. H., and Brown, E. T. (2006). Rock mechanics: for underground mining. Springer science & business media.
- Cancino, CF., Silva, R. and Giraud, C. (2021). Numerical assessment of an overall instability at Bajode la Alumbreira mine. In: P. M. Dight (ed.), Second International Slope Stability in Mining, Australian Centre for Geomechanics, Perth, pp. 27-36, https://doi.org/10.36487/ACG_repo/2135_0.03
- Carvalho, J., Castro, L. and Elmo, D. (2010). Geomechanical Numerical Modelling Workflow for Large Open Pits Applied to Retro-Analysis of the East Wall of Toquepala Mine. In Proceedings of the 44th US Rock Mechanics Symposium - 5th US/Canada Rock Mechanics Symposium, June 27–30, 2010, Salt Lake City, Utah.
- Ceryan, N., Kesimal, A., and Ceryan, S. (2018). Probabilistic analysis applied to rock slope stability: a case study from Northeast Turkey. In Integrating Disaster Science and Management (pp. 221-261). Elsevier.
- Conte, E., Silvestri, F., and Troncone, A. (2010). Stability analysis of slopes in soils with strain-softening behaviour. Computers and Geotechnics, 37(5), 710-722. <https://doi.org/10.1016/j.compgeo.2010.04.010>
- Creighton, A., Bixley, M., Elmoultie, M., Hassall, M., Macciotta, R. (2022). A reliability-based design acceptance criteria approach for inter-ramp and overall open pit slopes. In Proceedings of the 2022 Slope Stability conference in civil and mining, October 17-20, Tucson, AZ, US.
- Cundall, P. Damjanac, B. and Varun. (2016). Considerations on slope stability in a jointed rock mass. American Rock Mechanics Association. In Proceedings of the 50th US Rock Mechanics/Geomechanics Symposium, June 26–29, 2016, Houston, Texas.

- Dawson, E. M., Roth, W. H., and Drescher, A. (1999). Slope stability analysis by strength reduction. *Géotechnique*, 49(6), 835-840. <https://doi.org/10.1680/geot.1999.49.6.835>
- Day, J. J., Diederichs, M. S., and Hutchinson, D. J. (2017). New direct shear testing protocols and analyses for fractures and healed intrablock rockmass discontinuities. *Engineering Geology*, 229, 53-72. <https://doi.org/10.1016/j.enggeo.2017.08.027>
- Der Kiureghian A, and Ditlevsen, O. (2009). Aleatory or epistemic? Does it matter? *Structural Safety*, 31:105-112. <https://doi.org/10.1016/j.strusafe.2008.06.020>
- Department of Minerals and Energy (1999). *Geotechnical Considerations in Open Pit Mines, Guideline (Version 1.0)*, Perth, Western Australia.
- Duncan, J. M., Wright, S. G., and Brandon, T. L. (2014). *Soil Strength and slope stability*. (2nd ed.). Wiley.
- El-Ramly, H. (2001). *Probabilistic Analyses of Landslide Hazards and Risks: Bridging Theory and Practice*. PhD thesis. Department of Civil and Environmental Engineering. University of Alberta. <https://doi.org/10.7939/R3GH9BK6F>
- Evans, K.F., Kohl, T, Rybach, L, and Hopkirk, R.J. (1992). The effects of fracture normal compliance on the long term circulation behavior of a hot dry rock reservoir: a parameter study using the new fully-coupled code fracture. *Geothermal Resources Council Transactions*, 16, 449-456.
- Ferson, S. and Ginzburg, L. R. (1996). Different methods are needed to propagate ignorance and variability. *Reliability Engineering & System Safety*, 54(2-3), 133-144. [https://doi.org/10.1016/S0951-8320\(96\)00071-3](https://doi.org/10.1016/S0951-8320(96)00071-3)
- Flores, G. and Karzulovic, A. (2000). The role of the Geotechnical group in an Open Pit: Chuquicamata mine, Chile. In: W. A. Hustrulid, M. K. McCarter, and D. J. A. Van Zyl (Eds.), *Slope stability in Surface Mining* (pp. 141-152). SME.
- Foley, J., Cami, B., Ma, T., Javankhoshdel, S., Cremeens, J., and Carvalho, J. (2023). The Importance of Cross-Correlation in Probabilistic Analyses of Rock Slopes Using Generalized Hoek-Brown Criterion. In *Proceedings of the Geo-Risk 2023* (pp. 131-137). <https://doi.org/10.1061/9780784484982.014>

- Fookes, P. G., Baynes, F. J., and Hutchinson, J. N. (2000). Total geological history: a model approach to the anticipation, observation and understanding of site conditions. Proceedings of the ISRM International Symposium, Melbourne, Australia.
- Fossen, H. (2016). Structural geology. Cambridge university press.
- Gaida, M., Cambio, D., Robotham, M., and Pere, V. (2021). Development and application of a reliability-based approach to slope design acceptance criteria at Bingham Canyon Mine. P. M. Dight (Ed.), In Proceedings of the second International Slope Stability in Mining Conference, 83-94, Perth, Australia. https://doi.org/10.36487/ACG_repo/2135_02
- Giani, G. P. (1992). Rock slope stability analysis. CRC Press.
- Gibson, W. (2011). Probabilistic methods for slope analysis and design. Australian Geomechanics Journal, 46(3), 29-39.
- Goodman, R. E. (1991). Introduction to rock mechanics. John Wiley & Sons.
- Goodman, R.E. (1993). Engineering Geology: Rock in Engineering Construction. John Wiley & Sons Inc.
- Goodman, R. E., and Dubois, J. (1972). Duplication of dilatant behavior in the analysis of jointed rocks.
- Griffiths, D. V., and Lane, P. A. (1999). Slope stability analysis by finite elements. Géotechnique. 49(3), 387-403. <https://doi.org/10.1680/geot.1999.49.3.387>
- Hadjigeorgiou, J. and Harrison, J. (2011). Uncertainty and sources of error in rock engineering. In Proceedings of the 12th ISRM International Congress on Rock Mechanics, October 16-21, Beijing, China.
- Havaej, M, Wolter, A., Stead, D., Tuckey, Z., Lorig, L. and Eberhardt, E. (2013). Incorporating Brittle fracture into three-dimensional modelling of rock slopes. In Slope Stability 2013: Proceedings of the 2013 International Symposium on Slope Stability in Open Pit Mining and Civil Engineering (pp. 625-638). Australian Centre for Geomechanics.
- Herget, G. (1977). Pit Slope Manual: Chapter 2 – Structural Geology; CANMET (Canada Centre for Mineral Technology, formerly Mines Branch, Energy, Mines and Resources Canada), CANMET REPORT77-41; 123 p; October 1977.

- Hoek, E. (1998). Reliability of Hoek-Brown estimates of Rock Mass properties and their impact on design. *International Journal of Rock Mechanics and Mining Sciences*, 35(1), 63-68. [https://doi.org/10.1016/S0148-9062\(97\)00314-8](https://doi.org/10.1016/S0148-9062(97)00314-8)
- Hoek, E. and Bray, J. (1981). *Rock slope engineering* (3rd ed.). The Institution of Mining and Metallurgy. CRC Press, London.
- Hoek, E., Carranza-Torres, C., and Corkum, B. (2002). Hoek–Brown failure criterion- 2002 edition. In: Hammah R et al (eds) *Proceedings of the 5th North American rock mechanics symposium*. University of Toronto, Toronto, pp 267–273.
- Hoek, E., Read, J., Karzulovic, A., and Chen, Z. Y. (2000). Rock slopes in civil and mining engineering. In *Proceedings of the ISRM International Symposium* (pp. ISRM-IS-2000-013), International Society of Rock Mechanics, November 19–24, 2000, Melbourne, Australia.
- Hormazabal, E., Rovira, F., Walker, M., and Carranza-Torres, C. (2009). Analysis and design of slopes for Rajo Sur, an Open Pit mine next to the subsidence crater of El Teniente mine in Chile. Available at: <https://www.kz.srk.com/files/File/papers/El%20Teniente%20hormazabalpaper.pdf>
- Hudson, J. A., and Feng, X. T. (2015). *Rock engineering risk* (Vol. 1). CRC Press.
- Hudson, J. A., and Harrison, J. P. (2000). *Engineering rock mechanics: an introduction to the principles*. Elsevier.
- Hungr, O., and Coates, D. F. (1978). Deformability of joints and its relation to rock foundation settlements. *Canadian Geotechnical Journal*, 15(2), 239-249. <https://doi.org/10.1139/t78-022>
- Hustrulid, W. A., McCarter, M. K., and Van Zyl, D. J. (2000). *Slope stability in surface mining*. SME.
- Infanti, N., and Kanji, A. K. (1978). In Situ Shear Strength, Normal and Shear Stiffnesses Determinations at Agua Vermelha Project. In *proceedings of the 3rd International congress of IAEG*, 2, 175-183, Madrid, Spain.
- Itasca Consulting Group, Inc. (2018). *Slope Model Version 3.0.13*. Itasca Consulting Group, Minneapolis, Minesota, USA.
- Kafash, M., Barham, T., Sheykhloo, P., Davidson, R., and Yenne, L. (2022). Performance based design- How does performance based design work?. *Tailings and mine waste 2022*, In *Proceedings of the 26th international conference on tailings and mine waste*, November 6–9, 2022, Denver, CO.

- Karzulovic, A. (1988). The use of keyblock theory in the design of linings and supports for tunnels. PhD thesis. University of California, Berkeley.
- Keyter, G. J., Ridgway, M., Varley, P. M., and Venture, B. C. J. (2008). Rock engineering aspects of the Ingula powerhouse caverns. In Proceedings of the 6th International Symposium on Ground Support in Mining and Civil Engineering Construction, SAIMM (pp. 409-445).
- Lana, M. S. (2014). Numerical modeling of failure mechanisms in phyllite mine slopes in Brazil. *International Journal of Mining Science and Technology*, 24(6), 777-782. <https://doi.org/10.1016/j.ijmst.2014.10.007>
- Lisle, R. (2020). Geological structures and maps: A practical guide. Butterworth-Heinemann.
- Lorig, L. J., Cundall, P. A., Damjanac, B. and Emam, SA (2010). Three-Dimensional Model for Rock Slopes Based on Micromechanics. In Proceedings of the 44th US Rock Mechanics Symposium - 5th US/Canada Rock Mechanics Symposium, June 27–30, 2010, Salt Lake City, Utah.
- Ludvig, B. (1981). Direct shear tests of filled and unfilled joints. In Proceedings of the Conference on the Application of Rock Mechanics to Cut and Fill Mining, pp. 179-185. The Institution of Mining and Metallurgy, London.
- Macciotta, R. (2023). Slope risk management in light of uncertainty and environmental variability—2021 Canadian Geotechnical Colloquium. *Canadian Geotechnical Journal*, 60(12), 1777-1791.
- Macciotta, R., Creighton, A., and Martin, D. (2020). Design acceptance criteria for operating open-pit slopes: An update. *CIM Journal*, 11(4), 248–265, <https://doi.org/10.1080/19236026.2020.1826830>
- Macciotta, R., Creighton, A., Martin, C.D. (2021). Design acceptance criteria and risk tolerance for inter-ramp and overall open pit slopes. *Canadian Geotechnique* 2(3), 48-51
- Macciotta, R., Creighton, A., Martin, C.D. (2022). Reliability Based Design Acceptance Criteria for inter-ramp and overall pit slopes - fundamental considerations and mathematical background. In Proceedings of the Slope Stability conference in civil and mining 2022, October 17-20, Tucson, AZ, US.
- Macciotta, R. and Martin, C.D. (2016). Influence of joint stiffness in back analysis of rock tensile strength using Slope Model. In P. Gómez, C. Detournay, R. Hart and M. Nelson (Eds.),

Proceedings of the 4th Itasca Symposium on Applied Numerical Modeling, pp. 111-120, Lima, Peru.

- MacDonald, N. R., Packulak, T. R., and Day, J. J. (2023). A Critical Review of Current States of Practice in Direct Shear Testing of Unfilled Rock Fractures Focused on Multi-Stage and Boundary Conditions. *Geosciences*, 13(6), 172. <https://doi.org/10.3390/geosciences13060172>
- Makurat, A., Barton, N., Tunbridge, L., and Vik, G. (1991). The measurement of the mechanical and hydraulic properties of rock joints at different scales in the Stripa project. *Publikasjon-Norges Geotekniske Institutt*, 182, 1-8.
- Martin, C. D., Davison, C. C., and Kozak, E. T. (1990). Characterizing normal stiffness and hydraulic conductivity of a major shear zone in granite. In: Barton N, Stephansson O (Eds.), *Proceedings of the International symposium on rock joints*, Balkema, Rotterdam, pp 549–556.
- Martin, C.D. and Kaiser, P. K. (1984). Analysis of a rock slope with internal dilation. *Canadian Geotechnical Journal*, 21(4), 605-620. <https://doi.org/10.1139/t84-068>
- Martin, C.D., Rafiei Renani, H., Stevenson, G., and Watson, A. (2022). Constraining Joint Stiffness and In-situ Stress in a Slope Deformation Model. In *Proceedings of the 2022 Slope Stability conference in civil and mining*, October 17-20, Tucson, AZ, US.
- Martin, D. and Stacey, P. (2018). *Guidelines for open pit slope design in weak rocks*. Clayton South, VIC: CSIRO Publishing
- McMahon, B. (1985). Australian Geomechanics Society E.H. Davis Memorial Lecture: Geotechnical Design in the face of uncertainty. *Australian Geomechanics*, 10, 7-19.
- Nagendran, S. K., and Mohamad Ismail, M. A. (2021). Probabilistic and Sensitivity Analysis of Rock Slope Using Anisotropic Material Models for Planar Failures. *Geotech. Geol. Eng.*, 39:1979-1995. <https://doi.org/10.1007/s10706-020-01600-2>
- Packulak, T.R.M. (2018). Laboratory investigation of shear behaviour in rock joints under varying boundary conditions. M.A.Sc. thesis. Queen's University at Kingston, Kingston, ON. Available at: <http://hdl.handle.net/1974/24827>
- Padilla, R., Titley, S. and Pimentel, F. (2001). Geology of the Escondida porphyry copper deposit, Antofagasta region, Chile. *Economic Geology*, 96(2), 307-324. <https://doi.org/10.2113/gsecongeo.96.2.307>

- Passchier, C. W., and Trouw, R. A. (2005). *Microtectonics*. Springer Science & Business Media.
- Phoon, K. K., and Ching, J. (Eds.). (2015). *Risk and reliability in geotechnical engineering*. CRC Press.
- Phoon, K. K., and Retief, J. V. (Eds.). (2016). *Reliability of geotechnical structures in ISO2394*. CRC Press.
- Priest, S. D. (1993). *Discontinuity analysis for rock engineering*. Springer Science & Business Media.
- Priest, S. D., and Brown, E. T. (1983). Probabilistic stability analysis of variable rock slopes. *Transactions of the Institution of Mining and Metallurgy*, 92, A1-A12.
- Rafiei Renani, H. and Martin, C. D. (2020a). Slope stability analysis using equivalent Mohr–Coulomb and Hoek–Brown criteria. *Rock Mechanics and Rock Engineering*, 53(1), 13-21. <https://doi.org/10.1007/s00603-019-01889-3>
- Rafiei Renani, H. and Martin, C. D. (2020b). Factor of safety of strain-softening slopes. *Journal of Rock Mechanics and Geotechnical Engineering*, 12(3), 473-483. <https://doi.org/10.1016/j.jrmge.2019.11.004>
- Rafiei Renani, H., Martin, C. D., Varona, P., and Lorig, L. (2019). Stability analysis of slopes with spatially variable strength properties. *Rock Mechanics and Rock Engineering*, 52(10), 3791-3808. <https://doi.org/10.1007/s00603-019-01828-2>
- Ramsay, J. G., Huber, M. I., and Lisle, R. J. (1983). *The techniques of modern structural geology: Folds and fractures (Vol. 2)*. Academic press.
- Rapiman, M., and Sepulveda, R. (2006). Slope optimization at Escondida Norte Open Pit. Available at: https://www.saimm.co.za/Conferences/RockSlopes/265-278_Sepulveda.pdf.
- Read, J. and Stacey, P. (2009). *Guidelines for open pit slope design*. Collingwood, Vic.: CSIRO Publishing.
- Ridley, J. (2013). *Ore deposit geology*. Cambridge University Press.
- Rocscience Inc (2022). *DIPS-Graphical and statistical analysis of orientation data, Version 8.0*, Toronto, Canada.
- Rocscience Inc (2023). *RS2-2D Geotechnical finite Element Analysis, Version 11.02*, Toronto, Canada.
- Rocscience Inc (2023). *SLIDE2-2D limit equilibrium analysis for slopes, Version 9.0*, Toronto, Canada.

- Rode, N., Homand-Etienne, F., Hadadou, R., and Soukatchoff, V. (1990). Mechanical behaviour of joints of cliff and open pit. In Proceedings of the International symposium on rock joints (pp. 693-699).
- Rosenblueth, E. (1975). Point estimates for probability moments. Proceedings of the National Academy of Sciences, 72(10), 3812-3814. <https://doi.org/10.1073/pnas.72.10.3812>
- Ruffolo, R. M., and Shakoor, A. (2009). Variability of unconfined compressive strength in relation to number of test samples. Engineering Geology, 108(1-2), 16-23. <https://doi.org/10.1016/j.enggeo.2009.05.011>
- Rutqvist, J., and Stephansson, O. (2003). The role of hydromechanical coupling in fractured rock engineering. Hydrogeology Journal, 11, 7-40.
- Sjöberg, J. (1996). Large scale slope stability in open pit mining: a review. Technical Report, Lulea University of Technology, Division of Rock Mechanics, Lulea, Sweden, 229.
- Sharon, R. and Eberhardt, E. (2020). Guideline for Slope Performance Monitoring. CRC Press/Balkema.
- Shen, J. and Karakus, M. (2014). Simplified method for estimating the Hoek-Brown constant for intact rocks. Journal of Geotechnical and Geoenvironmental Engineering, 140(6), 04014025. [https://doi.org/10.1061/\(ASCE\)GT.1943-5606.0001116](https://doi.org/10.1061/(ASCE)GT.1943-5606.0001116)
- Steffen, O. K. H., Contreras, L. F., Terbrugge, P. J., and Venter, J. (2008). A risk evaluation approach for pit slope design. In Proceedings 42nd US Rock Mechanics Symposium (ARMA-08-231), June 29–July 2, 2008, San Francisco.
- Sullivan, T. D. (2006). Pit slope design and risk—A view of the current state of the art. In Proceeding of the International Symposium on Stability of Rock Slopes in Open Pit Mining and Civil Engineering.
- Swan, G. and Sepulveda, R. (2000). Slope stability at Collahuasi. In: W. A. Hustrulid, M. K. McCarter, and D. J. A. Van Zyl (Eds.), Slope stability in Surface Mining (pp. 163-170). SME.
- Tamimi, S., Amadei, B., and Frangopol, D. M. (1989). Monte Carlo simulation of rock slope reliability. Computers & structures, 33(6), 1495-1505. [https://doi.org/10.1016/0045-7949\(89\)90489-6](https://doi.org/10.1016/0045-7949(89)90489-6)
- Valdivia, C. and Lorig, L. (2000). Slope stability at Escondida Mine. In: W. A. Hustrulid, M. K. McCarter, and D. J. A. Van Zyl (Eds.), Slope stability in Surface Mining (pp. 153-162). SME.

- Vásárhelyi, B., Kovács, L., and Török, Á. (2016). Analysing the modified Hoek–Brown failure criteria using Hungarian granitic rocks. *Geomechanics and Geophysics for Geo-Energy and Geo-Resources*, 2, 131-136.
- Wenner, D., and Harrison, J. P. (1996). Techniques to cope with uncertain parameters in geomechanics on different levels of information. In *Proceedings of the ISRM International Symposium - EUROCK 96*, September 2–5, 1996, Turin, Italy.
- Wesseloo, J., and Read, J. (2009). Acceptance criteria. In: J. Read and P. Stacey (Eds.), *Guidelines for open pit slope design* (pp. 221-236). CRC Press/Balkema.
- Whitman, R. V. (2000). Organizing and evaluating uncertainty in geotechnical engineering. *Journal of Geotechnical and Geoenvironmental Engineering*, 126(7), 583-593.
- Wittke, W. (1990). *Rock Mechanics, Theory and Applications with case histories*. Springer Verlag, Berlin, Heidelberg, New York, London.
- Wittke, W. (2014). *Rock mechanics based on an anisotropic jointed rock model (AJRM)*. John Wiley & Sons.
- Wyllie, D. C., and Mah, C. (2004). *Rock slope engineering*. CRC Press.
- Zangerl, C., Evans, K. F., Eberhardt, E., and Loew, S. (2008). Normal stiffness of fractures in granitic rock: A compilation of laboratory and in-situ experiments. *International Journal of Rock Mechanics and Mining Sciences*, 45(8), 1500-1507. <https://doi.org/10.1016/j.ijrmms.2008.02.001>
- Zienkiewicz, O. C., Humpheson, C. and Lewis, R. W. (1975). Associated and non-associated and viscoplasticity and plasticity in soil mechanics. *Géotechnique*, 25(4), 671-689. <https://doi.org/10.1680/geot.1975.25.4.671>
- Zimmermann, H. J. (2000). An application-oriented view of modeling uncertainty. *European Journal of operational research*, 122(2), 190-198. [https://doi.org/10.1016/S0377-2217\(99\)00228-3](https://doi.org/10.1016/S0377-2217(99)00228-3)